D-q impedance identification in three phase systems using multi-tone perturbation

Bo Zhou

Thesis submitted to the Faculty of the Virginia Polytechnic Institute and State University in partial fulfillment of the requirements for the degree of

Master of Science
in
Electrical Engineering

Paolo Mattavelli, Co-Chair
Dushan Boroyevich, Co-Chair
Rolando Burgos

Jan 30, 2013
Blacksburg, Virginia

Keywords: AC stability, *d-q* impedances, multi-tone, diode bridge rectifier

D-q impedance identification in three phase systems using multi-tone perturbation

Bo Zhou

Abstract

In electric power systems, the existence of constant power loads such as output-regulated power converters may bring instability problem to AC or DC distributed systems. Impedance based stability criteria has been proven a good tool for small-signal stability analysis.

This works focuses on the developing of a comprehensive software tool which can extract DC or three phase AC impedances, and apply stability analysis. An algorithm is designed to select FFT window and adjust perturbation frequencies. This feature enables the software to accurately measure impedances even in existence of system line harmonics. Furthermore, multi-tone approach is developed to improve simulation time. The complete software tool is tested with simulation models and experiment results, to show the effectiveness.

When multi-tone approach is applied on nonlinear loads, it gives incorrect results. The reason is that perturbation frequency will have overlapping with side-band harmonics. An algorithm is designed to avoid this problem. The algorithm is tested with 12-pulse diode rectifier simulation model, and 6-pulse diode rectifier simulation model and experimental test bed. Both simulation and experiment results verifies the concept.

Acknowledgements[1]

First of all, I would like to express my sincere gratitude to my advisor, Dr Paolo Mattavelli, for his patient guidance and kind help throughout all my years at Virginia Tech. It is him who leads me step by step into the world of power electronics. He is generous to answer my numerous questions and give me suggestions, which push me forward to progress. I still keep all the notes he wrote for me during our personal meetings, which encourage me to dig into unknown problems. His rigorous attitude to the science will always be my best example to learn from. I would like to wish him all the best in his life.

I am also grateful to my committee members Dr Dushan Boroyevich and Dr Rolando Burgos, for all the discussions during the weekly meetings and their valuable suggestions. I gained a lot from Dr Boroyevich's overview of the research and his humorous personality. Dr Burgos' research habits also helped me a lot.

I would like also to thank all the CPES team members: Ms. Teresa Shaw, Ms. Marianne Hawthorne, Ms. Linda Gallagher, Ms. Teresa Rose, Ms. Linda Long, Mr. Bob Martin and Mr David Gilham. Their support helps me to achieve my academic goal.

I would likt also to thank my CPES friends and colleagues. It is my honor to know you and work together with you: Mr. Zhiyu Shen, Mr. Bo Wen, Mr. Marko Jaksic, Mr. Igor Cvetkovic, Dr. Sara Ahmad, Dr. Qiang Li, Dr. Fang Luo, Dr. Pengju Kong, Dr. Dong Dong, Dr. Ruxi Wang, Mr. Doug Sterk, Mr. David Reusch, Mr. Xiao Cao, Mr. Shu Ji, Mr. Pengjie Lai, Mr. Qian Li, Mr. Daocheng Huang, Mr. Zijian Wang, Mr. Zheng Chen, Mr. Haoran Wu, Mr. Mingkai Mu, Mr. Feng Yu, Mr. Yingyi Yan, Mr. Chanwit Prasantanakorn, Ms. Yiying Yao, Mr. Yipeng Su, Mr. Milisav Danilovic, Mr. Hemant Bishnoi, Mr. Weiyi Feng, Mr. Wei Zhang, Mr. Shuilin Tian, Mr. Li Jiang (F.C.Lee), Mr. Li Jiang (K.Ngo), Mr Xuning Zhang, Mr. Jin Li, Mr. Pei-Hsin Liu, Mr. Yin Wang, Mr. Lingxiao Xue, Mr. Zhemin Zhang, Mr. Tao Tao, Mr. Di Xu, Mr. Hanguang Zheng, Mr. Zhiqiang Wang, Mr. Xiucheng Huang, Mr. Yang Jiao, Mr. Zhengyang Liu, Mr. Yucheng Yang, Mr Dongbing Hou, Miss. Han Cui, Mr. Jun Wang, Mr. Qiong Wang, Mr. Xuebing Chen, Mr. Chi Li, Mr. Chao Fei, Mr. Fang Chen, Miss. Yincan Mao, Mr Ming Lv. Without your help, this thesis would be impossible.

[1] This work was sponsored by the Boeing Company.

Last but most importantly, I would like to express my deepest gratitude to my parents Jian Zhou, Qiulin Gao, and my girlfriend Xiaoxiao Li. Their selfless love and support encourage me to overcome all the problems in my life and create a better future.

Thank you all,

Bo

TABLE OF CONTENTS

LIST OF FIGURES

LIST OF TABLES

Chapter 1. INTRODUCTION

1.1. Background and motivation

The application of power electronic technology enables high-quality power conversion. In many cases there are requirements of output power regulation. As described in [1-4], the constant power loads show negative incremental input impedance characteristic. For ideal source systems like grids, the effect of constant power loads is very small. However there are some smaller systems like aircraft systems, electric vehicles, ships and renewable energy systems. When these systems operate in islanding mode, constant power loads may bring unstable issues.

As these systems become more and more widely applied, it is important to guarantee safe operation. It is shown that the stability of DC systems can be analyzed and predicted by studying the return ratio of source output impedance and load input impedance [5][6]. A few stability criteria have also been proposed to define stability margin of DC systems [7-9].

Like DC systems, the stability of 3 phase AC systems can be also analyzed by studying the source and load impedances. General Nyquist Criterion (GNC) [10] is applied in multi-variable systems like 3 phase AC systems. In [11], stability criteria for three phase system can be derived by studying the eigenvalue loci of the multi-variable return ratio matrix. Moreover in some specific applications when the power factor of load converter is high, the GNC can be simplified [12] by only studying the return ratio of Z_{dd} impedances.

It is shown that source and load impedances play a very important role in system stability prediction. Therefore there is a need to identify the source and load impedances of power system at DC or AC interfaces. A lot of work has been devoted to measuring the impedance of DC systems [13-15]. There are also attempts to identify impedance of AC systems [16-20]. However most methods have been tested and verified for passive components. Few are verified for switching converters. Even for software simulation, there are few available tools for AC impedance identification.

1.2. Synchronous rotating coordinate of 3 phase systems and impedance in d-q coordinate

Electrical source and load systems can be unstable when they are interconnected. The stability can be analyzed by studying the source and load impedance at the interface. For DC systems that is straight forward because it is easy to find the steady state operation point and identify impedances. However for 3 phase AC system, it is not that easy to find a steady state operation point. A typical 3 phase power system is shown in Fig. 1-1.

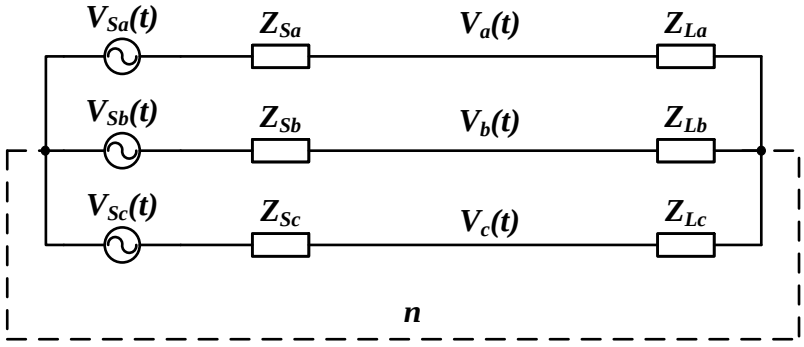

System voltages are with respect to neutral point n

Fig. 1-1 Three phase AC system diagram

The voltages at the AC interface are given by (1-1).The interface voltages and currents are time-varying, which means there is no way to find steady state operation point.

$$\begin{aligned} v_a(t) &= V_m\cos(\omega t), \\ v_b(t) &= V_m\cos(\omega t - 2\pi/3), \\ v_c(t) &= V_m\cos(\omega t + 2\pi/3), \end{aligned} \tag{1-1}$$

The system is non-stationary with periodic tendencies. The three voltages could be represented as a voltage vector, rotating in a three-dimensional space. If all the voltages follows the expression (1-1), the vector will be rotating in a circle with an angular speed of ω. In order to transform the system to stationary, a rotating coordinate can be defined with the same angular speed. The transformation matrices between two coordinates are defined by (1-2):

$$T_{dq0/abc}(\omega) = \sqrt{\frac{2}{3}}\begin{bmatrix} \cos(\omega t) & \cos(\omega t - 2\pi/3) & \cos(\omega t + 2\pi/3) \\ -\sin(\omega t) & -\sin(\omega t - 2\pi/3) & -\sin(\omega t + 2\pi/3) \\ 1/\sqrt{2} & 1/\sqrt{2} & 1/\sqrt{2} \end{bmatrix}, \quad (1\text{-}2)$$

$$T_{abc/dq0}(\omega) = T^{-1}{}_{dq0/abc}(\omega), \quad (1\text{-}3)$$

This alignment will be applied for all the impedance extraction in this work.

Applying the transformation to the voltages, we get:

$$\begin{bmatrix} v_d(t) \\ v_q(t) \\ v_0(t) \end{bmatrix} = T_{dq0/abc}\begin{bmatrix} v_a(t) \\ v_b(t) \\ v_c(t) \end{bmatrix} = \sqrt{\frac{2}{3}}\begin{bmatrix} 3/2 \\ 0 \\ 0 \end{bmatrix} V_m, \quad (1\text{-}4)$$

By doing this, we could transform the non-stationary 3-phase system in abc coordinates to stationary system in *d*-*q*0 coordinates. For balanced system, the 0-axis variables are always 0, which could be ignored. The *d*-*q* system diagram is shown in Fig. 1-2:

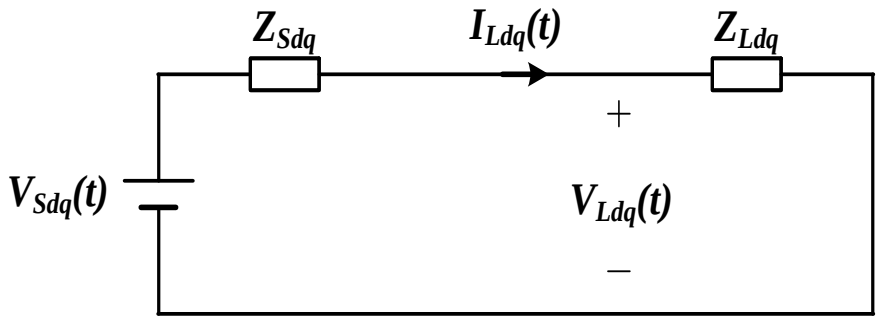

Fig. 1-2 Three phase system diagram in *d*-*q* coordinate

By transforming the three phase system into *d*-*q* coordinate, a steady state operation point can be found. Thus the impedance measurement techniques can be applied also in three phase systems.

The load impedance in *d*-*q* coordinate can be defined:

$$\begin{bmatrix} v_{Ld}(s) \\ v_{Lq}(s) \end{bmatrix} = \begin{bmatrix} Z_{Ldd}(s) & Z_{Ldq}(s) \\ Z_{Lqd}(s) & Z_{Lqq}(s) \end{bmatrix}\begin{bmatrix} i_{Ld}(s) \\ i_{Lq}(s) \end{bmatrix} \quad (1\text{-}5)$$

The source impedance in *d*-*q* coordinate can be defined in the same way.

1.3. Stability criteria for three phase systems

Constant power loads such as power converters with regulated output voltage have negative small-signal input impedance. In DC distributed systems, this phenomenon may result in small-signal instability at the DC interface.

$$v_{DC\_interface}(s) = \frac{1}{1 + Z_S(s)/Z_L(s)} v_{DC\_source}(s) \tag{1-6}$$

The transfer function between DC source voltage and interface voltage is given by (1-6). It is proposed in [5] that Nyquist criterion could be applied on the DC interface stability by studying the return ratio $Z_S(s)/Z_L(s)$, where $Z_S(s)$ stands for the source impedance and $Z_L(s)$ stands for the load impedance.

On the other hand, three phase AC system is a multi-input multi-output (MIMO) system. Generalized Nyquist Criterion is proposed to extend the frequency response methods in single-input single-output systems to MIMO systems.

A multi-variable feedback system is shown in Fig. 1-3.

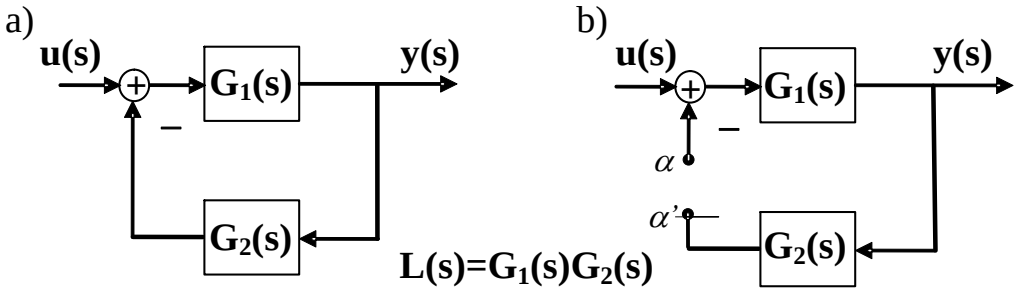

Fig. 1-3 Multi-variable feedback configuration: a) closed-loop and b) open-loop.

Theorem: The Generalized Nyquist Stability Criterion [10].

Let the multivariable feedback system shown in Fig. 1-3 have no open-loop unobservable or uncontrollable modes whose corresponding characteristic frequencies lie in the right half plane. Then this configuration will be closed-loop stable if and only if the net sum of anticlockwise encirclements of the critical point ($-1+j0$) by the set of characteristic loci of $\mathbf{L}(s)$ is equal to the total number of right-half plane poles of $\mathbf{G}_1(s)$ and $\mathbf{G}_2(s)$.

As duality, the AC interface stability could be addressed similarly as DC interface stability problem, with the application of Generalized Nyquist Stability Criterion. The AC interface voltage transfer function is given by:

$$v_{dq\_interface}(s) = \left(I + Z_{Sdq}(s)Y_{Ldq}(s)\right)^{-1} v_{dq\_source}(s) \quad (1\text{-}7)$$

where $Z_{Sdq}(s)$ stands for *d-q* source impedance and $Y_{Ldq}(s)$ stands for *d-q* load admittance, which is the inverse of *d-q* load impedance.

The return ratio for three phase AC systems is defined [11]:

$$L(s) = Z_{Sdq}(s)Y_{Ldq}(s) = \begin{bmatrix} Z_{Sdd}(s) & Z_{Sdq}(s) \\ Z_{Sqd}(s) & Z_{Sqq}(s) \end{bmatrix} \begin{bmatrix} Y_{Ldd}(s) & Y_{Ldq}(s) \\ Y_{Lqd}(s) & Y_{Lqq}(s) \end{bmatrix} \quad (1\text{-}8)$$

According to Generalized Nyquist Stability Criterion, the characteristic loci of $L(s)$ could indicate the stability at the AC interface. This approach has been experimentally verified in [31].

In the specific application of high power-factor rectifiers, the cross coupled input admittance terms $Y_{Ldq}(s)$ and $Y_{Lqd}(s)$ is negligible due to the *d-q* vector current control. In this case, the return ratio could be rewritten as:

$$L(s) = Z_{Sdq}(s)Y_{Ldq}(s) = \begin{bmatrix} Z_{Sdd}(s) & Z_{Sdq}(s) \\ Z_{Sqd}(s) & Z_{Sqq}(s) \end{bmatrix} \begin{bmatrix} Y_{Ldd}(s) & 0 \\ 0 & Y_{Lqq}(s) \end{bmatrix} \quad (1\text{-}9)$$

In this case, the eigenvalues of the return ratio can be derived [12]:

$$\begin{aligned} \lambda_1 &= L_{dd(s)} = Z_{Sdd}(s)Y_{Ldd}(s) \\ \lambda_2 &= L_{qq(s)} = Z_{Sqq}(s)Y_{Lqq}(s) \end{aligned} \quad (1\text{-}10)$$

The Generalized Nyquist Stability Criterion may be applied by counting the net clockwise encirclements around $-1 + j0$.

In sum, the stability of AC distributed could be addressed by studying the source and load *d-q* impedance at the AC interface, with the utilization of Generalized Nyquist Stability Criterion. Therefore, how to measure *d-q* impedances becomes the key point for stability analysis. In this work, this issue will be addressed.

1.4. Contents

In chapter 2, impedance measurement algorithm and a few previous attempts on impedance identification for AC systems are reviewed. A software tool for stability analysis is designed. The tool is tested with a few application examples and the results are compared with analytical expressions to verify the effectiveness.

In chapter 3, based on the impedance measurement system architecture in [16], some efforts are made to extend the system capability.

In chapter 4, a new perturbation method is proposed to increase measurement time. An algorithm is developed to enable the application of this method on nonlinear loads.

In chapter 5, all the completed work is summarized and future work is discussed.

Chapter 2. STABILITY ANALYSIS SOFTWARE SUITE

2.1. Impedance measurement algorithm

The basic idea to measure small signal impedance is to collect the time-domain voltage and current information at certain frequency range of interest, at the system interface, and analyze frequency responses to calculate impedance.

To measure the small signal impedance of three phase AC systems, perturbation signals should be created and injected into the system, to identify the frequency-domain information of the system. If the perturbation is injected as shunt current, a three phase AC system diagram is shown in Fig. 2-1:

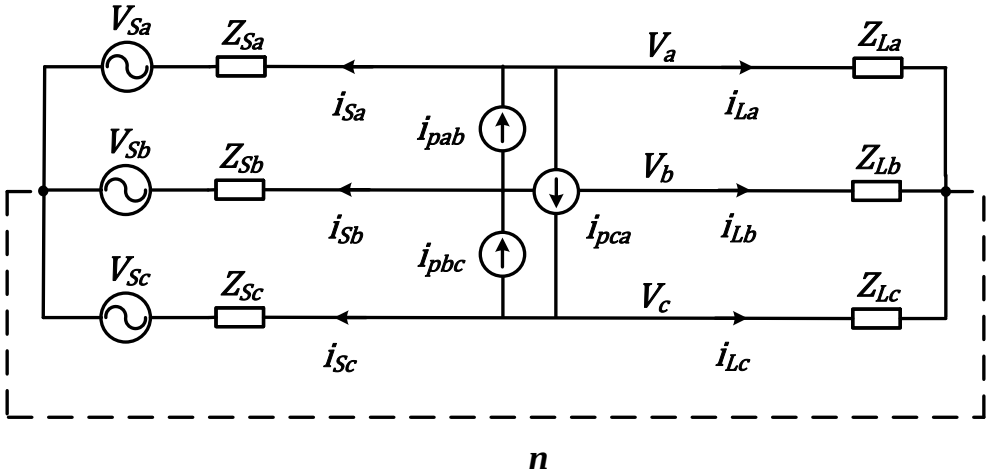

Fig. 2-1 Three phase system diagram in abc coordinates with shunt current perturbation

The small-signal impedance of three-phase AC systems can be studied by transforming the system to a synchronous rotating *d-q* coordinates, because steady state operation point only existing in *d-q* coordinates. To measure the impedance, small signal perturbations are injected between source impedance and load impedance. The voltage and current responses can be

collected and used for impedance calculation. Taking shunt current injection as an example, the three phase AC system diagram in *d-q* coordinates is shown in Fig. 2-2.

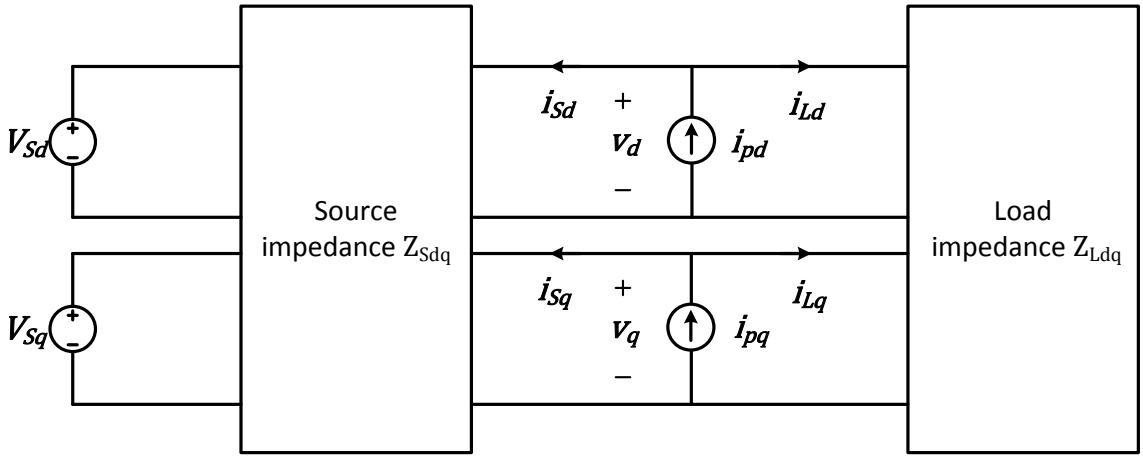

Fig. 2-2 Three phase system diagram in *d-q* coordinates with shunt current perturbation

The perturbation signals are injected into the system at steady state operation point. Since the source and load *d-q* impedances are both 2 by 2 matrices, 2 sets of linearly independent equations are required, which means 2 linearly independent injections are required. Assuming the system impedances do not change in the 2 measurements and considering the load impedance for example, the system equation during the first measurement is shown in (2-1):

$$\begin{bmatrix} v_{d1}(s) \\ v_{q1}(s) \end{bmatrix} = \begin{bmatrix} Z_{Ldd}(s) & Z_{Ldq}(s) \\ Z_{Lqd}(s) & Z_{Lqq}(s) \end{bmatrix} \begin{bmatrix} i_{Ld1}(s) \\ i_{Lq1}(s) \end{bmatrix} \tag{2-1}$$

During the second measurement, the system equation is shown in (2-2):

$$\begin{bmatrix} v_{d2}(s) \\ v_{q2}(s) \end{bmatrix} = \begin{bmatrix} Z_{Ldd}(s) & Z_{Ldq}(s) \\ Z_{Lqd}(s) & Z_{Lqq}(s) \end{bmatrix} \begin{bmatrix} i_{Ld2}(s) \\ i_{Lq2}(s) \end{bmatrix} \tag{2-2}$$

Combining the 2 equations, the load impedance can be solved in (2-3):

$$\begin{bmatrix} Z_{Ldd}(s) & Z_{Ldq}(s) \\ Z_{Lqd}(s) & Z_{Lqq}(s) \end{bmatrix} = \begin{bmatrix} v_{d1}(s) & v_{d2}(s) \\ v_{q1}(s) & v_{q2}(s) \end{bmatrix} \begin{bmatrix} i_{Ld1}(s) & i_{Ld2}(s) \\ i_{Lq1}(s) & i_{Lq2}(s) \end{bmatrix}^{-1} \tag{2-3}$$

Similarly, given the current and voltage responses at the source side, the source impedance can be solved in (2-4):

$$\begin{bmatrix} Z_{Sdd}(s) & Z_{Sdq}(s) \\ Z_{Sqd}(s) & Z_{Sqq}(s) \end{bmatrix} = \begin{bmatrix} v_{d1}(s) & v_{d2}(s) \\ v_{q1}(s) & v_{q2}(s) \end{bmatrix} \begin{bmatrix} i_{Sd1}(s) & i_{Sd2}(s) \\ i_{Sq1}(s) & i_{Sq2}(s) \end{bmatrix}^{-1} \quad (2\text{-}4)$$

2.2. Perturbation methods review

2.2.1. Perturbation in steady state operation point

The perturbation source must be electrically connected to the system to generate perturbation signals. Depending on the objective of measurement, the perturbation source could be controlled voltage source, current source, power source or impedances.

2.2.1.1. *Shunt current injection and series voltage injection*

To be electrically connected into the system, the perturbation source could be connected either as shunt current source or series voltage source. The system diagram of two injection connections is shown in Fig. 2-3:

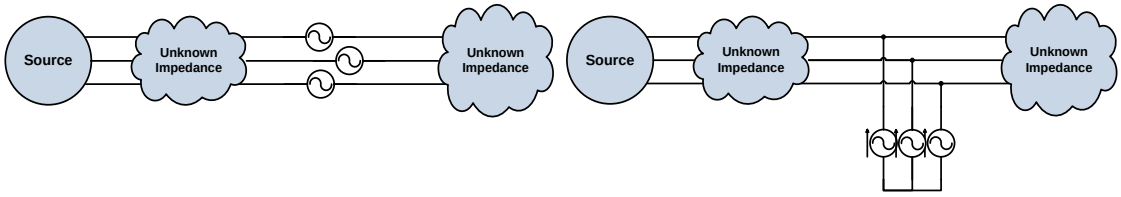

(a) Series voltage injection (b) Shunt current injection

Fig. 2-3: Injection connections

In most electrical systems, source impedances are much smaller than load impedance because power is delivered to the load. Thus shunt current injection will make more perturbation currents go to source side. Considering the noises of the system and numerical errors of measurement, the source impedance will be more accurate compared with load impedances. On the other hand, series voltage injection will get more accurate load impedance information.

2.2.1.2. ***Single phase injection***

In most of the cases, the three phase AC systems are balanced, and perturbation sources are connected to all the three phases to make it a balanced perturbation. In [17], a method of single phase injection is proposed in which a perturbation current source is connected between phase B and phase C. The system diagram is shown in Fig. 2-4:

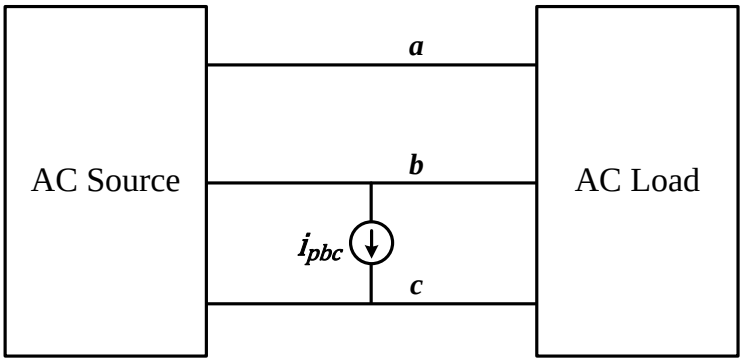

Fig. 2-4 Single phase injection diagram

Suppose the frequency point of interest is ω_e and the supply voltage frequency is ω_s, in the first measurement the frequency component $\omega_s+\omega_e$ is injected as square wave. Voltage responses and current responses $v_{d1}, v_{q1}, i_{d1}, i_{q1}$ in *d-q* coordinate can be extracted. In the second measurement the frequency component $\omega_s-\omega_e$ is injected as square wave. Voltage responses and current responses $v_{d2}, v_{q2}, i_{d2}, i_{q2}$ in *d-q* coordinate can be extracted. Therefore *d-q* impedances could be calculated using the equation (2-4).

It is shown in [17] that this method could get accurate measurement results. Compared with three phase injection, single phase injection is simpler to implement and could save power electronics components. In medium or high power applications, this may be cost-saving.

However, the unbalanced injection may bring other frequency components into the system in addition to the interested ones. Moreover, the injected perturbation power is also small compared to the balanced three phase injection.

2.2.2. Perturbation based on transient response

2.2.2.1. ***Step response***

In [20], a model identification approach based on step response in *d-q* coordinates is proposed and validated. The system diagram is shown in Fig. 2-5.

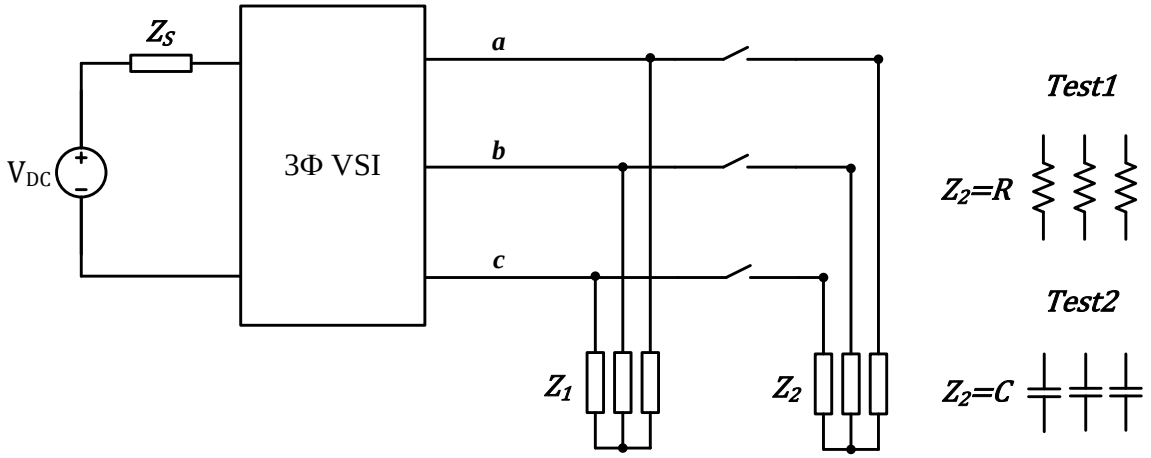

Fig. 2-5 Current step test diagram

In this paper, the d-q coordinates in this work is aligned with abc supply voltage ($V_q = 0$). In test 1, by connecting or disconnecting resistive load Z_2 from the system, step variation on the active power is created, which is equivalent to a current step in d axis. In test 2, by connecting or disconnecting capacitive load Z_2 from the system, reactive power step is created, which is equivalent to a current step in q axis. The *d-q* output impedance and input current to output current transfer function of voltage source inverter are identified by collecting the input and output voltage and current waveforms.

2.3. STability Analysis Software sUite(STASU)

In most common simulation software for three phase systems, such as Matlab, Saber, PSIM, there is not a suite to measure *d-q* impedance and analyze small-signal stability. In this work, a comprehensive software suite is developed to calculate the source and load *d-q* impedance of DC system and three phase AC system, and apply small-signal stability analysis based on impedance data either from simulation or from measurement.

2.3.1. Review of existing software tools for d-q impedance extraction

In this part, the software tools for frequency response analysis will be reviewed.

2.3.1.1. ***Saber***

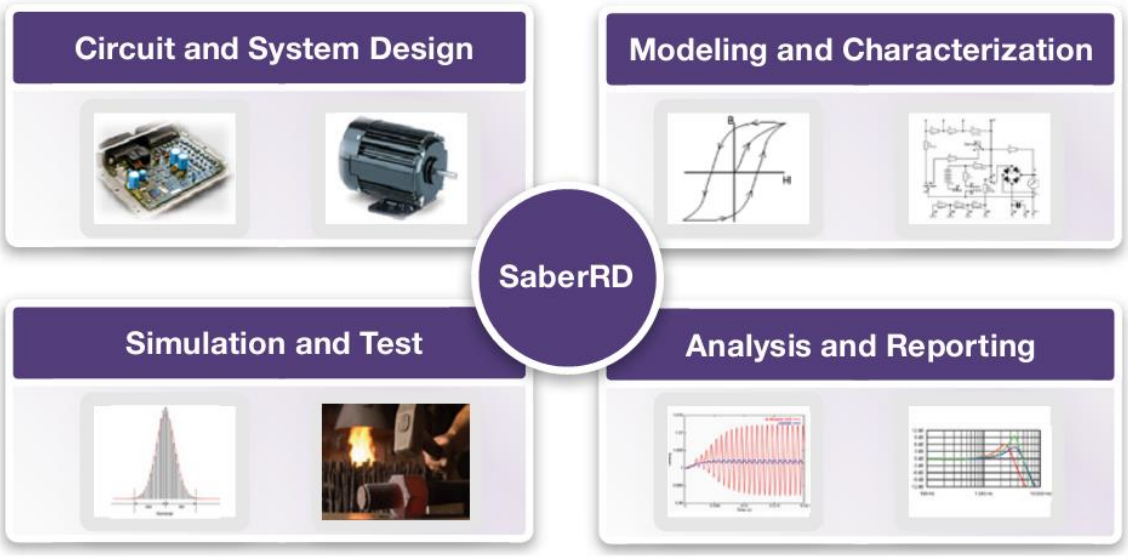

Fig. 2-6 Saber simulation tool

Saber [21] is a physical system simulation and design software tool developed by Synopsys. It is capable to simulate averaged model and switching converter model. It also provides frequency response analysis: for averaged model, linearization can be applied to extract the frequency-domain information. For switching converter models, Saber provides time domain system analyzer (tdsa) block to apply AC analysis.

In tdsa, the user could specify the steady state operation point or search for the operation point automatically by running a simulation before AC sweeping. The starting frequency point, stopping frequency point, number of frequency points and frequency incremental type (linear or logic) are also defined by the user. The software provides fixed-step and variable-step simulation option.

Tdsa could be used to extract impedance of DC-DC converters. However, tdsa cannot be directly used for three-phase system impedance analysis, because the system voltages and currents are time-varying. Moreover, the simulation could generate large result file.

2.3.1.2. ***Powersim***

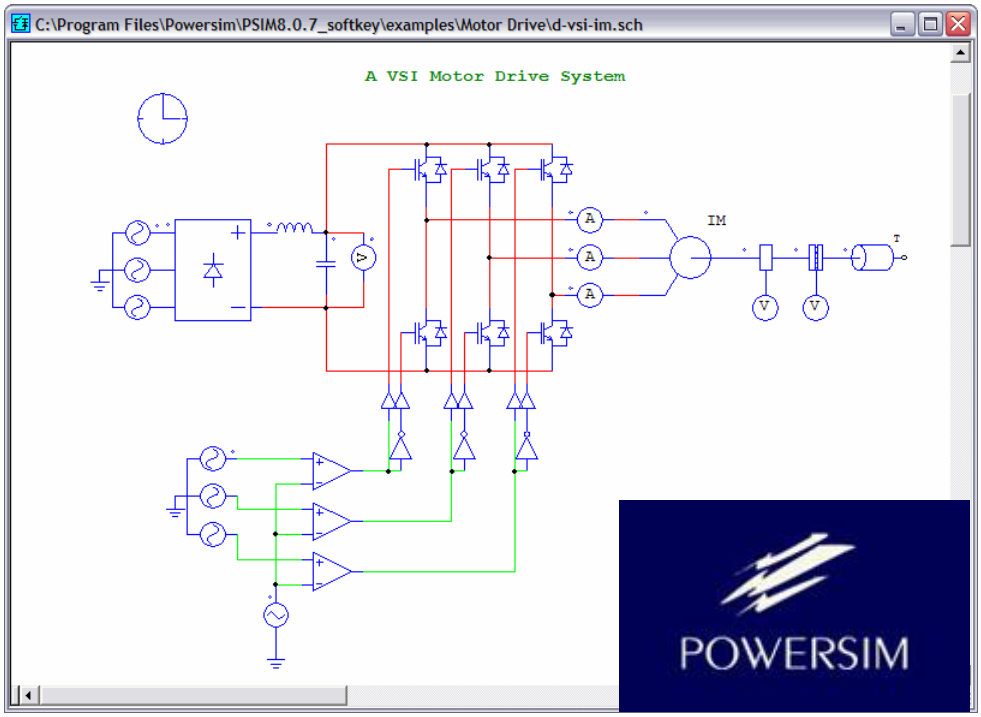

Fig. 2-7 Powersim software tool

Powersim [22] is a simulation software tool especially designed for power electronics and motor control. It can simulate both averaged model and switching model. For averaged model, it can get the frequency domain information from linearization. For switching model, it provides an AC sweep block to extract the small signal model.

The software could save and load simulation states with a '.ssf' file. This feature can be used to inject perturbation around steady state operation point. The software provides only fixed step simulation. Moreover in the AC analysis, the user could specify start frequency, stop frequency, number of frequency points, frequency incremental type, amplitude of start frequency, amplitude of stop frequency and additional frequency points of user's interest.

Like saber, powersim could not be directly used to extract impedance of three phase AC systems.

2.3.1.3. ***Plecs***

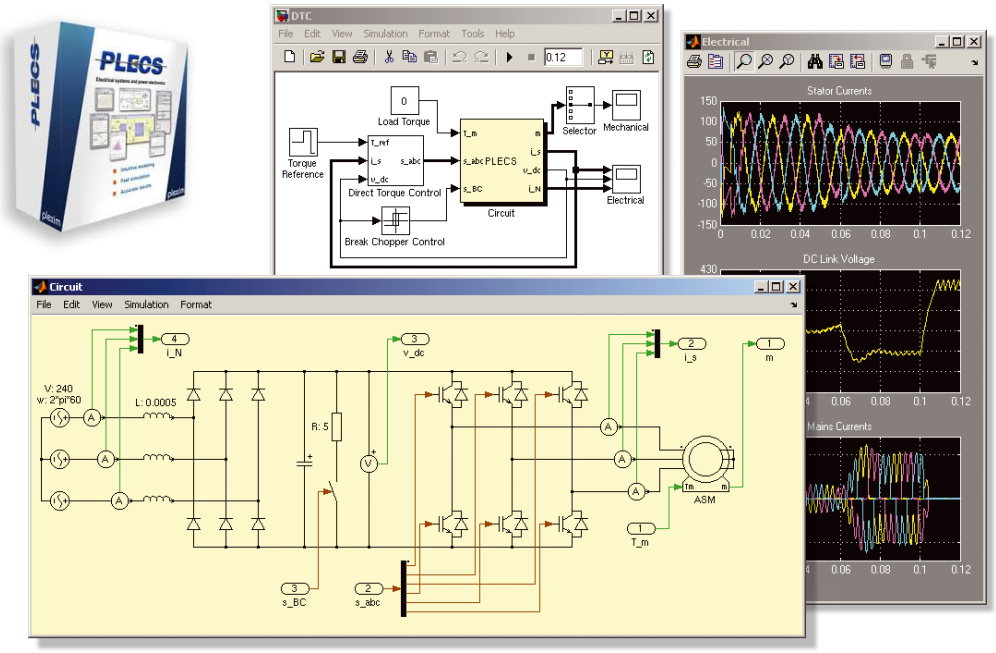

Fig. 2-8 Plecs software tool

Plecs [23] is a circuit simulator for electrical system modeling and control. It has two different versions: Matlab/Simulink [24] block set and standalone version. It can simulate both averaged model and switching converter model. It could linearize averaged model to get frequency domain information. For switching model, it provides AC analysis block and impulse response block to do small signal analysis.

In the AC analysis block, sinusoidal perturbation signal is injected in the steady state operation point, and AC sweeping is used. In the impulse response block, an impulse is made in the steady state operation point. In both blocks, the user could specify the time period for the system to reach steady state, start frequency, stop frequency, number of frequency points, frequency incremental type and perturbation amplitude. All these features are similar with the AC sweeping block of Saber and Powersim.

Like Saber and Powersim, Plecs cannot automatically find the steady state operation point of three phase AC systems. It needs modification to extract *d-q* impedances.

2.3.1.4. ***Simplis***

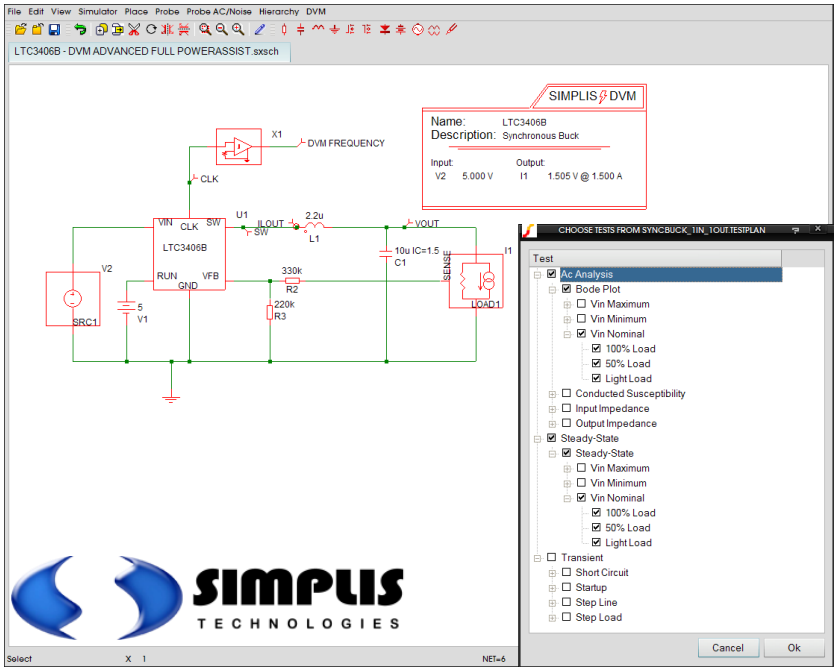

Fig. 2-9 SIMPLIS software tool

SIMPLIS [25] is a circuit simulator designed for rapid modeling of switching power systems. It provides AC analysis block for frequency domain information extraction.

In the AC analysis block, SIMPLIS would run one simulation to automatically find steady state. User could specify start frequency, stop frequency, frequency incremental type, points per decade, and amplitude of perturbation.

AC sweeping simulation in SIMPLIS is much faster compared with other software tools. It can even detect the steady state operation point of AC system, by sampling and comparing the variable values at a given line frequency. However, the block still needs modification to be able to extract *d-q* impedances of three phase systems.

2.3.1.5. ***SimPowerSystems***

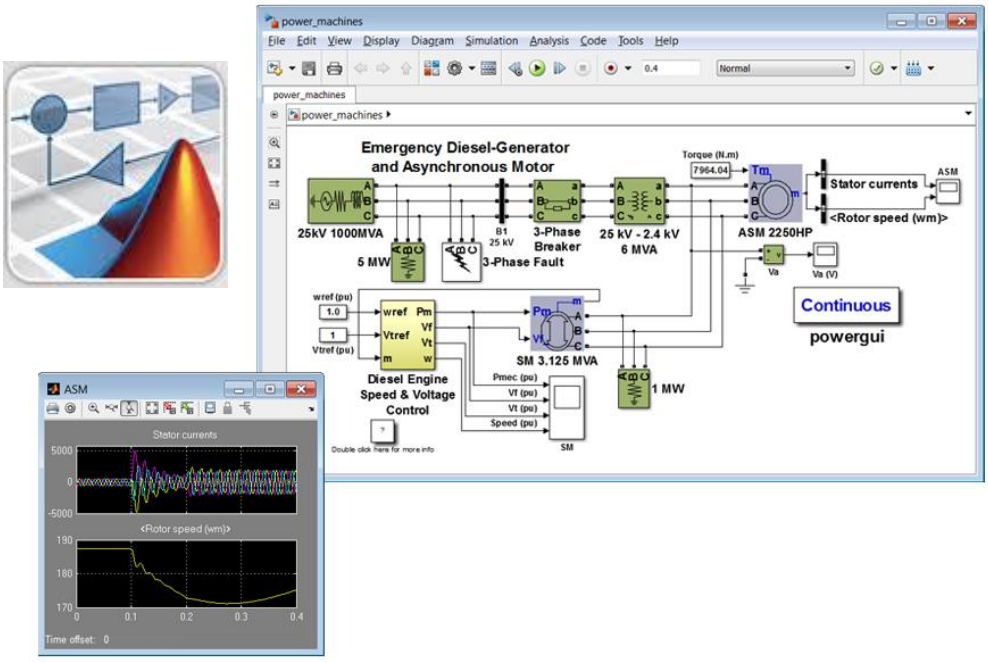

Fig. 2-10 Simpowersystems software tool

SimPowerSystems is a toolbox of Matlab/Simlulink. It provides components library and analysis tools for electric power system modeling and simulating. It can linearize averaged model to get frequency domain information. For switching models, it does not provide AC analysis block. It has variable step and fixed step solvers.

SimPowerSystems provides interface with other simulation software tools such as Saber, Powersim and Plecs.

2.3.1.6. ***Conclusion***

Among the common software tools for frequency domain analysis, there is no such tool that can automatically extract *d-q* impedances from three phase AC systems. It is useful to stability research to develop a comprehensive stability analysis software tool, which could extract *d-q* and DC impedances from switching converter models, and apply stability analysis based on the impedance information.

SimPowerSystems/Matlab is suitable for developing such a tool, because it provides different powerful simulation solvers and a user-friendly environment, and it is commonly used software tool for time-domain simulations of different switching power converter circuits.

2.3.2. Introduction to STASU

STASU has been implemented in Simulink\Matlab software with the use of SimPowerSystems toolbox. It is capable to do both impedance extraction and stability analysis.

The algorithm for the impedance extraction by simulation is based on the fast Fourier transform (FFT), whose window is determined by a phase-locked loop (PLL) synchronized with the line frequency to minimize errors caused by unbalanced and harmonic components. Furthermore, two types of injection signal waveforms can be used for impedance identification; the pure sinusoidal signal (single-tone signal) and the multi-tone signal, which is a superposition of multiple frequency components of sinusoidal signals. The multi-tone approach significantly reduces the computational time needed for impedance identification. The perturbation signals are injected into the system either by shunt current injection or by series voltage injection. The two different injection methods provide accurate measurement whether the impedance is low or high.

The stability analysis is based on impedance data, which can be either from a simulation tool or from impedance analyzer measurement. The resulting form is unified for both simulation and experiment. Given the impedance of the source side and the load side, the software can apply stability analysis for both AC (Generalized Nyquist Criterion or simplified GNC) and DC systems (Nyquist Criterion).

The flowchart for STASU is shown in Fig. 2-11, and it consists of three parts:

1) Impedance calculation of switching simulation models;

2) Small-signal stability analysis using impedance measurement data or simulation data obtained from the impedance calculation;

3) Graphical user interfaces (GUI).

The GUIs provides the user access to 1) and 2).

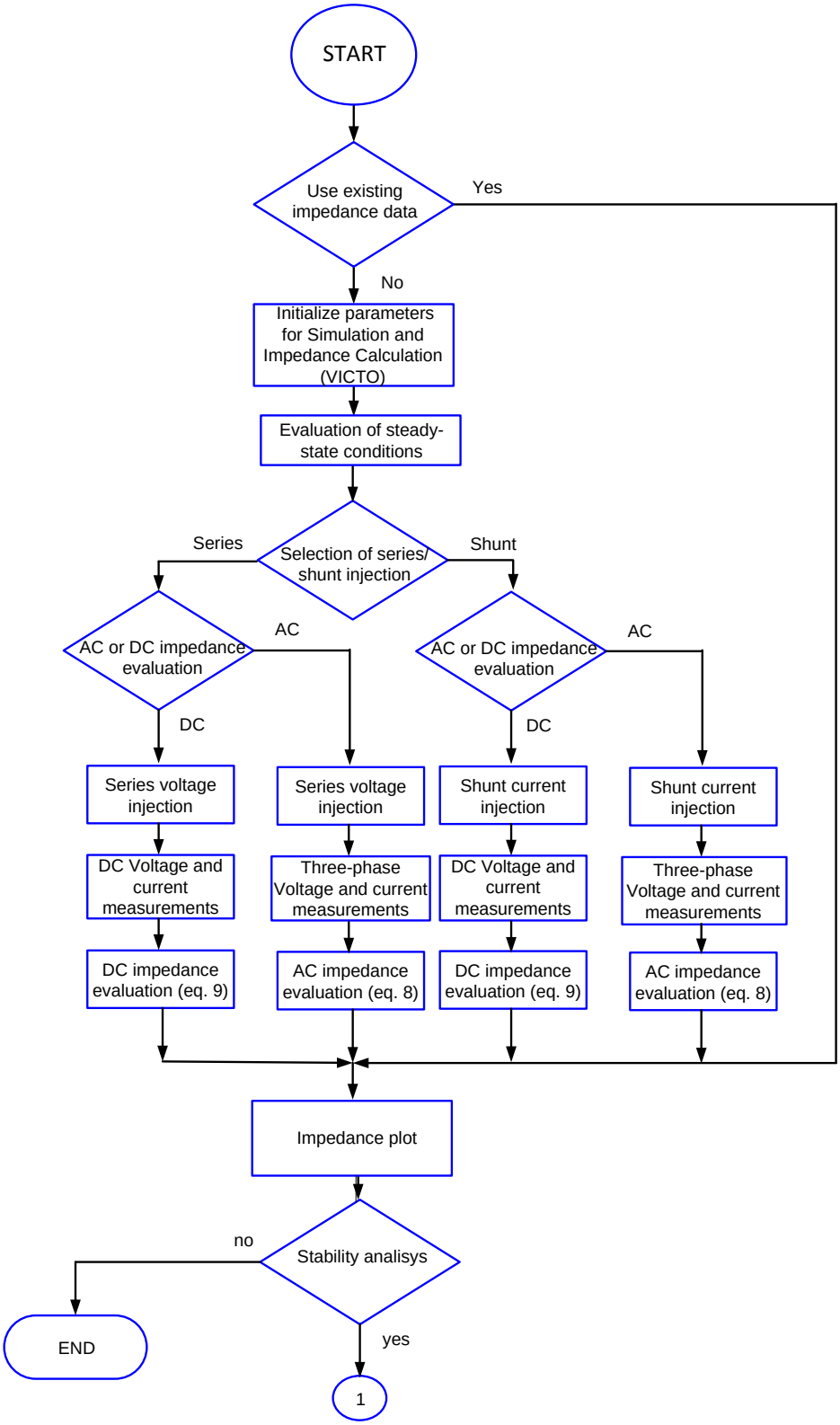

Fig. 2-11 (a) Flow chart for impedance calculation

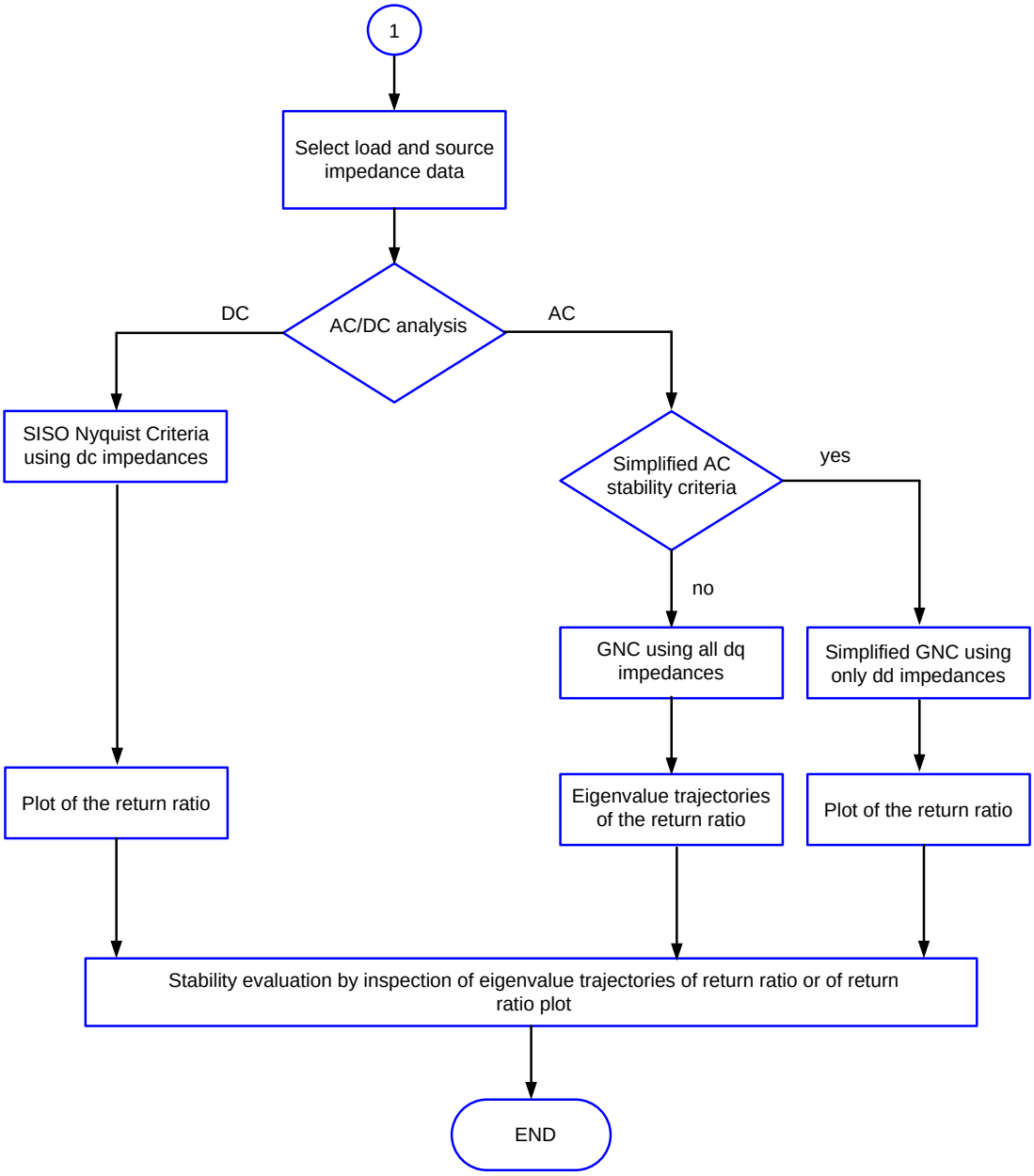

Fig. 2-11 (b) Flow chart for small-signal stability analysis using impedance measurement data or simulation data

2.3.3. Impedance calculation tool implementation

Several types of injection blocks, which inject perturbation signals, are built separately and put into the Simulink library. Two methods of injecting perturbation signals are provided: the shunt current injection method and the series voltage injection method.(a) (b)

Fig. 2-12 (a) shows the schematic of shunt current injection block, which is characterized by three-phase AC systems in *d-q* coordinates. In order to evaluate the *d-q* impedances, it is necessary to sense source and load currents in three-phase abc coordinate and sense the three phase abc voltage at the interface section. Currents and voltages are then transformed from abc coordinates to *d-q* coordinates. The characterization of *d-q* impedances requires two independent perturbations in *d-q* coordinates. The first perturbation is injected in the d-coordinate, while the second perturbation in the q-coordinate. The equations to calculate impedances have been provided from (2-1) to (2-4).

The *d-q* series voltage injection block is shown in (a) (b)

Fig. 2-12(b). After injecting two perturbations, as explained for the shunt current injection, source and load *d-q* impedance are evaluated using the same approach used for the shunt injection.

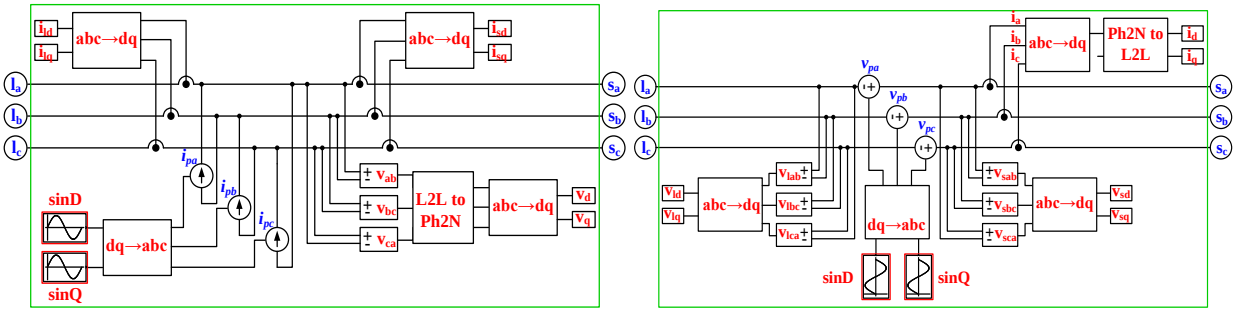

(a) (b)

Fig. 2-12 *d-q* Source and load impedance measurement blocks (a) shunt series injection, yielding phase to neutral *d-q* impedances (b) series voltage injection, yielding line to line *d-q* impedances

The injection blocks for DC impedance calculation are simple versions of three phase *d-q* injection blocks. We will not go into details here.

In order to perform *d-q* analysis, it is necessary to provide the phase information for the *d-q* transformation inside the impedance extraction blocks. The solution implemented in STASU is a synchronous reference frame Phase Looked Loop (PLL). As shown in Fig. 2-13, the basic block diagram of the PLL consists of phase detector, low-pass filter and integrator, providing phase at the output. In general terms, the PLL is used at the interface section. In order to minimize the interaction with the perturbation signal, the PLL bandwidth needs to be lower than the lowest injection frequency, slowing down the response of the complete simulation model. Since the phase information is sometimes available in the simulation model, PLL implementation is left optional in the tool, it can be either included into the block or phase can be generated in the model itself and then provided as input to the *d-q* impedance extraction block.

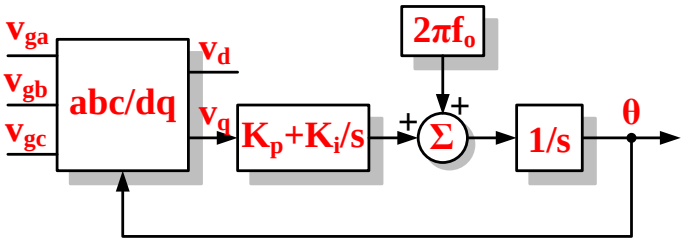

Fig. 2-13 Phase-Looked Loop in the Synchronous Reference Frame

The first function of PLL is to track the system phase angle, to apply dq0/abc and abc/dq0 transformation. The other function of PLL is that it detects system line frequency, which will be used to determine the perturbation frequencies and FFT window. This feature will be explained in 2.3.4.4.

All the developed blocks for the source and load impedance identification are included in the Simulink library. Thus, the developed blocks could be dragged into any power converter model and used to extract the source and load impedances.

2.3.4. Algorithm explanation

2.3.4.1. *Introduction*

This part explains impedance extraction algorithm and clarifies concepts used in the implementation of algorithm. The need of a settling time after perturbation injection is recalled in 2.3.3.2 of this chapter, while frequency aliasing and spectral leakage are explained in section 2.3.3.3 and 2.3.3.4 of this chapter, respectively. Section V explains multi-tone approach and compares it to sinusoidal (single-tone) approach. The focus of the chapter is on algorithm and problems that were solved to make impedance calculation tool working.

2.3.4.2. *Settling time after perturbation injection*

When the impedance is extracted, the data related to the transient response of the system need to be discarded. In fact, frequency domain response is obtained if FFT is applied to waveforms in steady-state. It is shown that besides the initial transient response of the system, there will be a second transient response when sinusoidal perturbation is injected due to the uncertainty of the initial phase. This is like a response to initial conditions of states of the circuit, it vanishes after some time. In order to clarify this aspect, a simple second-order RLC circuit, shown in Fig. 2-14, is taken as an example.

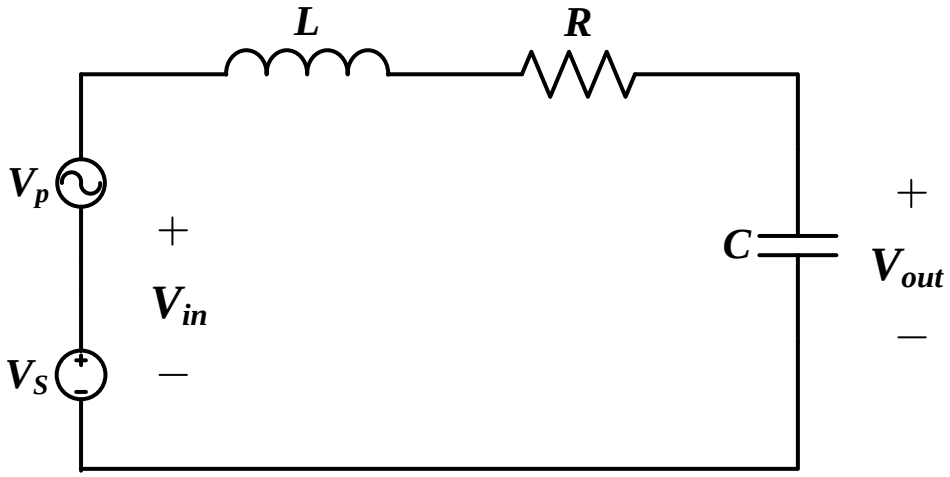

Fig. 2-14 Second-order RLC circuit

The parameters used in in Fig. 2-14 are: L = 1 mH, R= 10 Ω, C = 2 F, Vs = 5V DC and V_p is a 1V 350Hz sinusoidal voltage perturbation which is injected into the system at 2ms.

The input waveform voltage V_{in} is shown in Fig. 2-15.

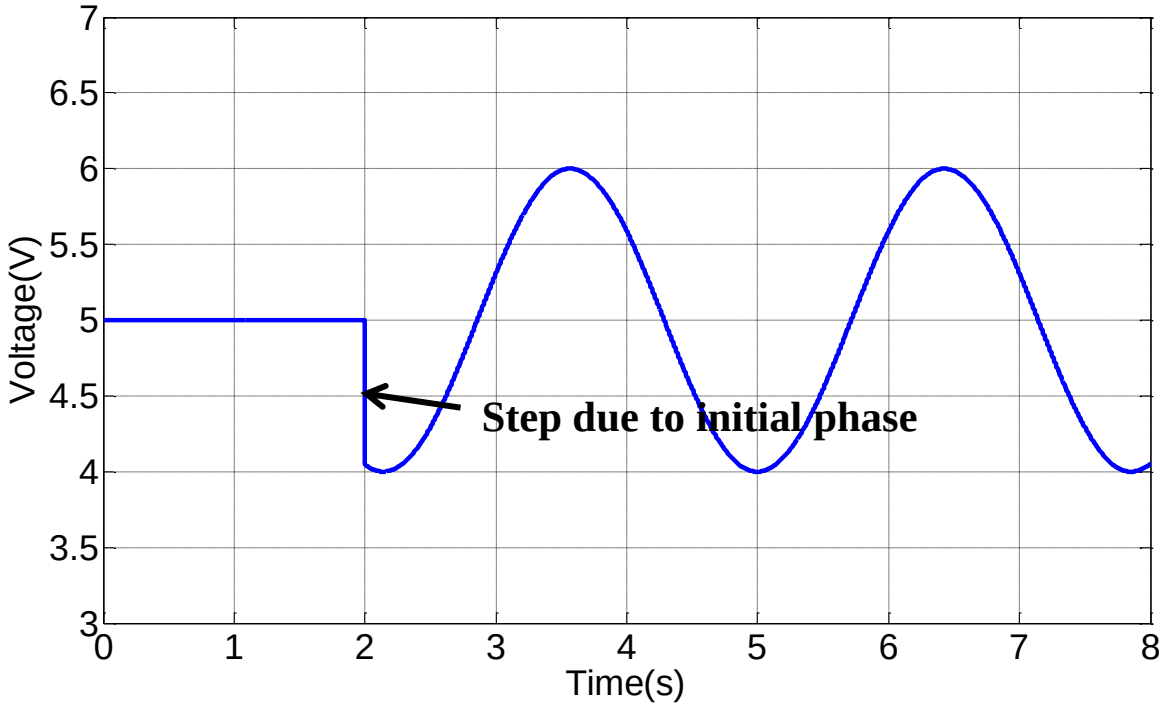

Fig. 2-15 Input voltage waveform

Then the corresponding output voltage waveform is shown in Fig. 2-16. As can be seen, there are two transient responses, practically with the same duration, one at the beginning of the simulation and the second after the injection of the perturbation signal. The information about duration of the settling time (T_{settle}) is selected by the user within the GUI.

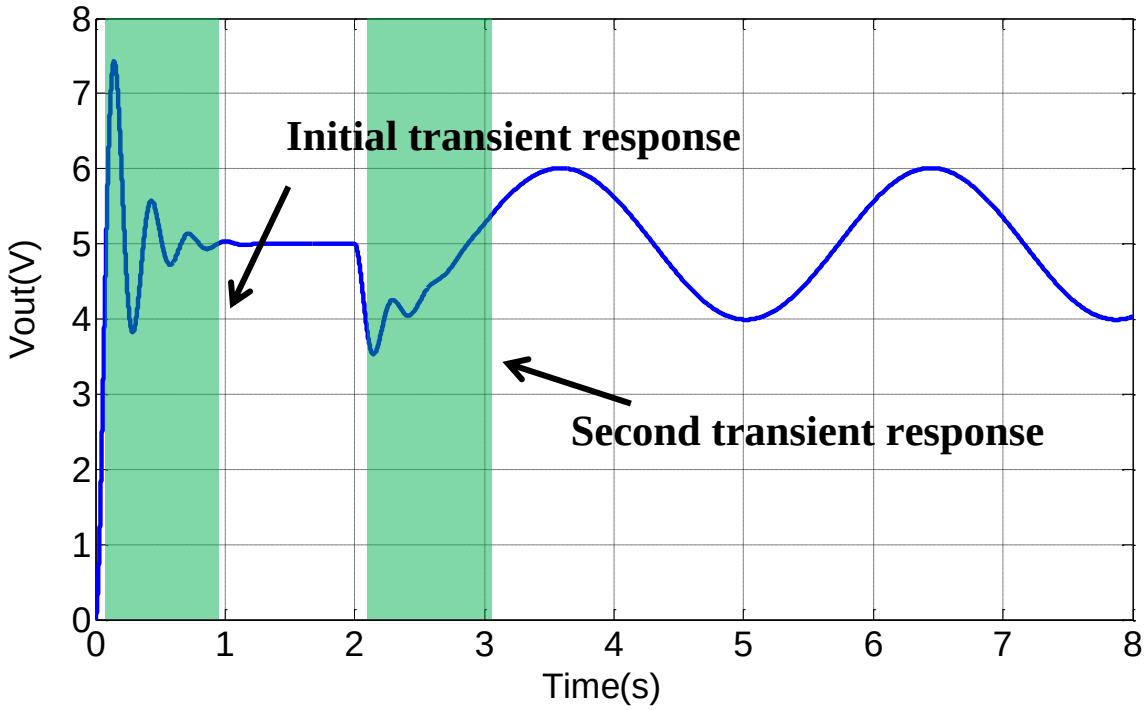

Fig. 2-16 Output voltage waveform

Once the simulation begins, the impedance analyzer will start a first simulation. The simulation time is T_{settle}, and in this simulation there will be no perturbation injected.

After this simulation, the system has reached steady state and then multiple simulations with perturbation are started. In each simulation, the sinusoidal perturbation of one specific frequency is injected. Because of the second transient response, the simulation time will consist of two parts: one is related to the second transient response; the other is the time of the FFT window. In STASU, the simulation time during perturbation is chosen to be $0.8 \cdot T_{settle} + T_{FFT\_window}$

2.3.4.3. *Frequency Aliasing*

There is a frequency-domain ambiguity associated with the discrete-time signal samples. We can understand this effect by looking at the example of a time-domain signal sampling [26]. Suppose there is a sinusoidal signal of 7kHz, which is shown in Fig. 2-17 (a), and we sample the signal at the frequency of 6kHz, which is shown in Fig. 2-17 (b).

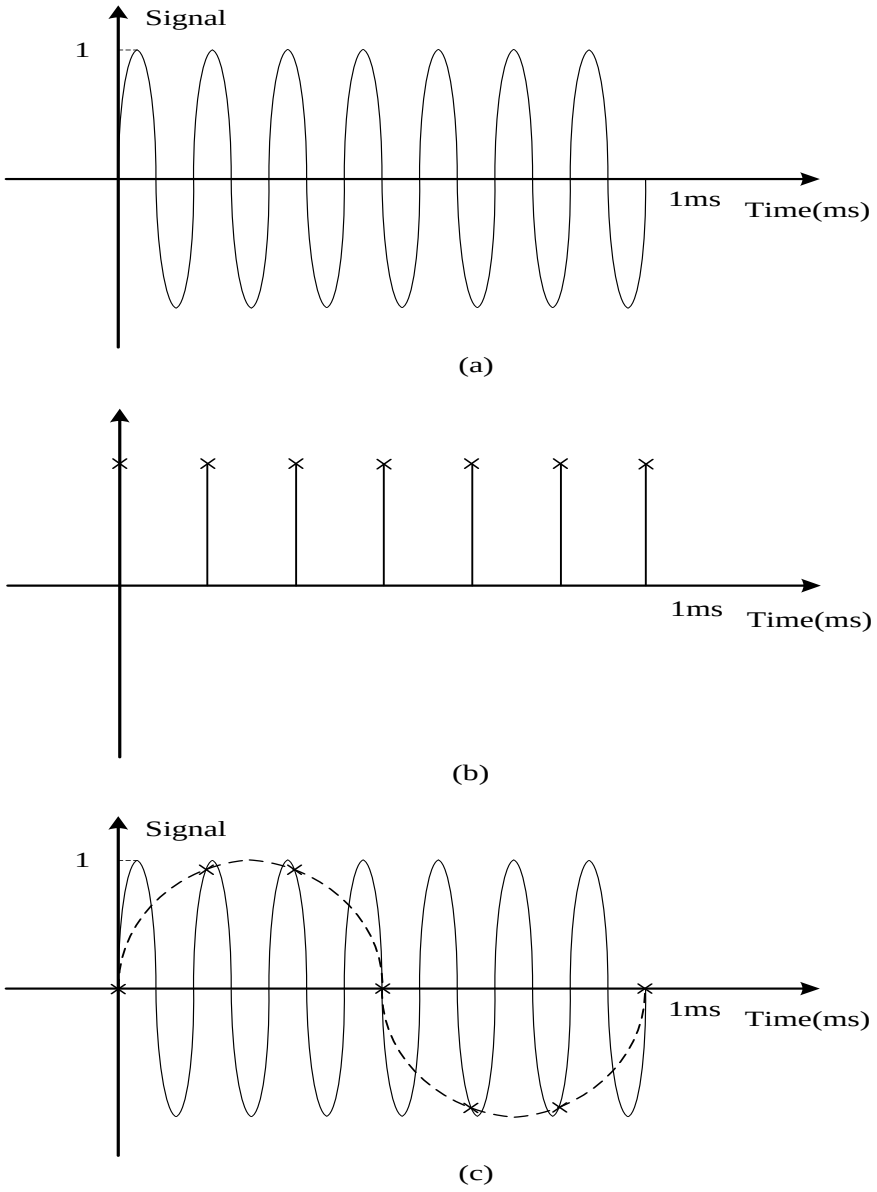

Fig. 2-17 Aliasing effect in time domain

As shown in Fig. 2-17 (c), from the discrete data sampled from the original 7kHz sine wave, we could also understand it as a 1kHz sine wave (dotted line). The effect of ambiguity is called aliasing.

In digital signal processing, we could always observe aliasing effect if Nyquist–Shannon sampling theorem is not satisfied. For example, if the bandwidth of a signal to be sampled is f_p, the sampling frequency is f_s, and $f_p > f_s$. The spectrum is shown in Fig. 2-18:

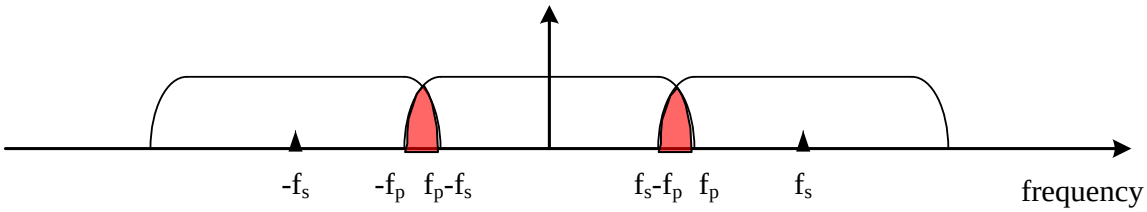

Fig. 2-18 Aliasing effect in frequency domain

As shown in Fig. 2-18, if $f_p > f_s$, there will be frequency aliasing in the shaded area.

In power converter systems, there will be high frequency components due to switching frequency. In order to avoid aliasing effect, a low-pass filter is placed before the input of sampling circuit whose cut-off frequency components is less than Nyquist frequency .

In STASU, for the concern of accuracy and calculation time, the default sampling frequency is selected as 1 MHz. A 4th order low-pass filter is used as anti-aliasing filter, and the cut-off frequency is chosen to be 2 times the maximum perturbation frequency. The idea of using band-pass filter was investigated, but it was dismissed due to the slow response of a narrow band-pass filter. The use of the band-pass filter would slow down the extraction of the impedances from simulation model.

2.3.4.4. ***Selection of perturbation frequencies***

To avoid spectral leakage effect, the FFT window should be periodical for all frequency components to be studied. Since there is usually line-frequency component at AC side, the FFT window should contain integer number of line periods and all the perturbation periods, which means $T_{FFT\_window} = m \cdot T_{line} = n \cdot T_{pert}$.

However if we want to make the FFT window periodical for the line frequency components and perturbation frequency components, the time for FFT window may be very long. For example, if one perturbation frequency is 121 Hz, and the line frequency is 60 Hz, in order to be periodical for both frequency components, the frequency of FFT window should be 1 Hz, which contains 121 perturbation periods and 60 line-frequency periods. Obviously a better option is to slightly move the perturbation frequency to 120 Hz and then the frequency for FFT window could be 60 Hz, which contains one line-frequency period and two perturbation periods. So perturbation frequencies are allowed to be shifted slightly from the original position. The

frequency resolution $f_{resolution}$ is defined as the smallest distance allowed for moving the perturbation frequencies from their original position.

In STASU, there is algorithm that imposes $T_{FFT\_window} = m \cdot T_{line} = n \cdot T_{pert}$, but shift the perturbation frequency (within the fresolution value) to keep FFT window to the smallest size, as described hereafter

Let us suppose to have line frequency component f_{line}, and perturbation frequencies $f_{pert1} < f_{pert2} \ldots < f_{pertn}$.

In practice, if $f_{line} > f_{pert1}$, the smallest possible FFT window is the period of f_{pert1}, considering FFT window should also contain integer number of line periods, we adjust f_{pert1} according to f_{line}. Let us define function round(x) as the nearest integer of x and choose $m = round\left(\frac{f_{line}}{f_{pert1}}\right)$, and $f_{FFT\_window} = \frac{f_{line}}{m}$. Then the fundamental frequency of FFT window is the first perturbation frequency. The next step is to shift all the perturbation frequencies to fit for the FFT window. Thus,

$$f_{pertn} = round\left(\frac{f_{pertn}}{f_{FFT\_window}}\right) \quad (2\text{-}5)$$

The example below shows the process:

$f_{line} = 250Hz$, $f_{pert1} = 100Hz$, $f_{pert2} = 600Hz$, $f_{pert3} = 3600Hz$;

then $m = 2$, $f_{FFT\_window} = 125Hz$;

and adjust the perturbation frequencies, $f_{pert1} = 125Hz$, $f_{pert2} = 625Hz$, $f_{pert3} = 3625Hz$;

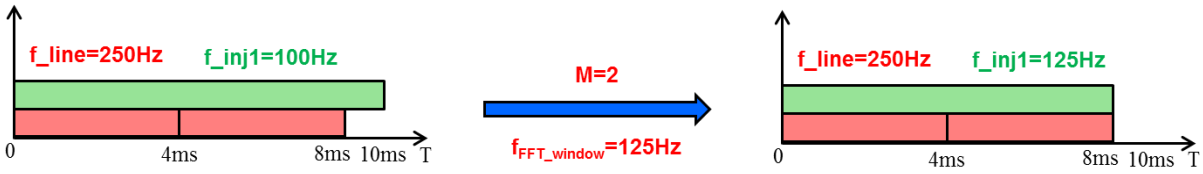

Fig. 2-19 Choosing FFT window when $f_{line} > f_{pert1}$

However if $f_{line} < f_{pert1}$, the smallest possible FFT window is the period of f_{line}. Thus, we choose $f_{FFT\_window} = f_{line}$. The next step is to shift all the perturbation frequencies to fit for the FFT window:

$$f_{pertn} = round\left(\frac{f_{pertn}}{f_{FFT\_window}}\right) \cdot f_{FFT\_window} \quad (2\text{-}6)$$

The example below shows the process:

$f_{line} = 110Hz$, $f_{pert1} = 200Hz$, $f_{pert2} = 400Hz$, $f_{pert3} = 800Hz$;

then $f_{FFT\_window} = 110Hz$;

and adjust the perturbation frequencies, $f_{pert1} = 220Hz$, $f_{pert2} = 440Hz$, $f_{pert3} = 770Hz$;

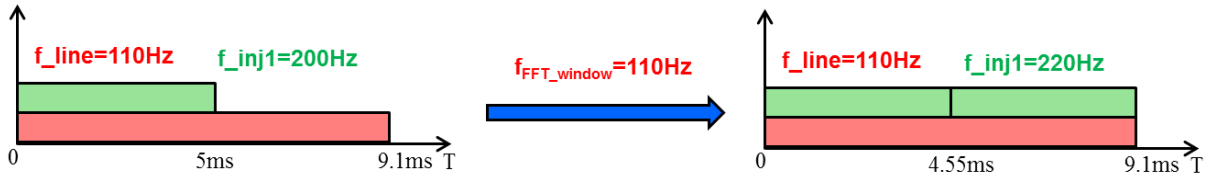

Fig. 2-20 Choosing FFT window when $f_{line} < f_{pert1}$

There is, of course, a trade-off between the length of FFT window and frequency resolution. Higher resolution leads to larger FFT window. The parameter frequency resolution (f_resolution_c) is used for handling with this trade-off. After the frequency of FFT window is determined by the line frequency and perturbation frequency, we will divide it by f_resolution_c. The default value of f_resolution_c is 1. If f_resolution_c is set to be n, the frequency for FFT window will be $\frac{f_{FFT\_window}}{n}$, thus we will have n times higher resolution.

Since the FFT window is adjusted according to the line frequency, the line harmonics will not affect the impedance measurement results. This algorithm makes STASU more widely useable. For example, let's consider a three phase system with unbalanced voltage source. The two times line frequency negative sequence component will not affect the measurement data with this algorithm.

2.3.4.5. ***Multi-tone approach***

Instead of injecting one sinusoidal perturbation per simulation, it is convenient to inject multi-sine perturbation (denoted as "multi-tone" perturbation) during one single simulation as shown for DC/DC power converters [27][28]. One example of multi-sine signal in time and frequency domain is shown in . There are two important issues to be considered for multi-tone injection:

1. Choice of phase of each tone: the crest factor C of signal x(t), defined as the ration between the peak value and the root-means-square (rms) value (i.e. $C = \frac{|x(t)|_{peak}}{x(t)_{rms}}$) of

the final multi-sine signal should be low enough to reduce the perturbation in the system [28, 29].

2. Choice of frequency of each tone: frequencies for each tone should be equidistantly distributed in frequency domain and fit in the FFT window. The same rounding method described in the previous section is applied here.

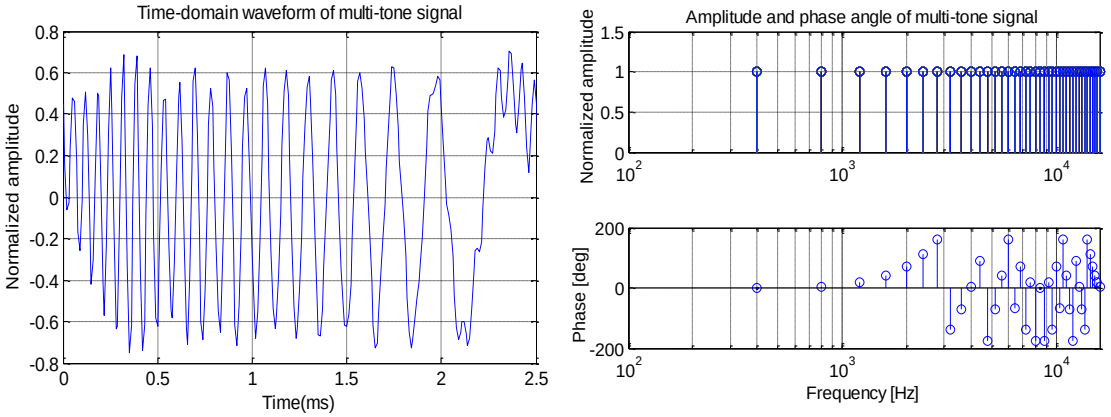

(a) (b)

Fig. 2-21 Multi-tone signal (a) time domain waveform (b) frequency components

For the first issue, the same method as in [30] is applied in STAISU. The algorithm is explained by an example where we assume to have 50 tones with the same amplitude equal to 1V and different frequencies 445Hz, 2*445Hz, 3*445Hz … 50*445Hz. If the phases for all the tones are equal, the multi-sine signal is shown in Fig. 2-22 (a), where the peak value is almost 16V, and if we apply the method proposed in [29] for the phases, the multi-sine signal is shown in Fig. 2-22 (b), where the peak value is slightly above 4V. Comparing both signals, it is obvious that the method explained in [29] effectively limits the crest factor of the multi-sine signal.

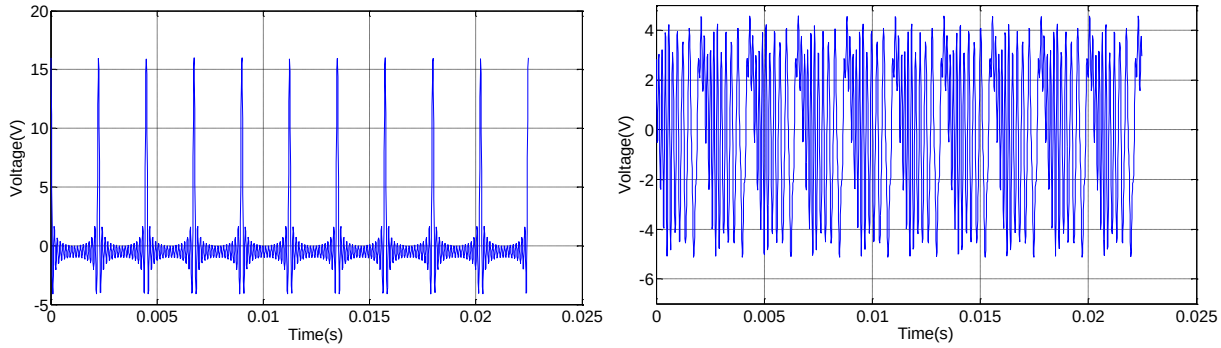

(a) (b)

Fig. 2-22 Time domain multi tone signal waveforms (a) without adjusting of phase (b) with phase adjusting using Newman phase approach

2.3.4.6. ***Time saving evaluation case study***

The main advantage of multi-tone over single-tone is that it is more time-saving. We will evaluate how much time multi-tone could save by studying a specific example.

Suppose the settling time for the system is T_{settle}, the number of frequency points of interest is N_{pert}, and the system line period is T_s. For the simplicity of analysis without losing generality, suppose the FFT window of measurement is the same as system line period T_s.

In single-tone measurement, the first simulation for the system to reach steady state will be T_{settle}. During perturbation, the time for a single perturbation frequency point will be $0.8T_{settle} + T_s$. Considering the total number of frequency points, and 2 perturbations (on d axis and on q axis), the simulation time during perturbation is $1.6N_{pert} \cdot T_{settle} + 2N_{pert} \cdot T_s$. Therefore, single tone method requires a total time $(1.6N_{pert} + 1) \cdot T_{settle} + 2N_{pert} \cdot T_s$.

In multi-tone measurement, the first simulation for the system to reach steady state will be T_{settle}. During perturbation, the time for all the perturbation frequency points will be $0.8T_{settle} + T_s$. Considering the 2 perturbations (on d axis and on q axis), the simulation time during perturbation is $1.6 \cdot T_{settle} + 2 \cdot T_s$. Therefore, single tone method requires a total time $(2.6) \cdot T_{settle} + 2 \cdot T_s$.

Let's further specific the numbers. Suppose in Simulink, using a max $1e^{-6}$ variable time step (default setting in STASU), the simulation time for T_{settle} is 3 minutes, and we want to measure 50 frequency points. Let's further suppose the line period is ignorable compared with system

settling time. Then for single tone, it takes $(1.6 \times 50 + 1) \times 5 \approx 400$ minutes, or 6.5 hours, to simulate. However in multi-tone, it takes only $2.6 \times 5 = 13$ minute for the whole simulation. Obviously multi-tone is much more time-saving than single-tone, especially when the number of perturbation frequency points is large.

2.3.5. Stability analysis

To make STASU a more comprehensive tool and provide stability analysis, a few new functions are included in the STASU project. In this chapter, the function of the Generalized Nyquist Criterion [10](GNC), simplified GNC [12], SISO Nyquist criterion, and impedance over-plot will be explained.

2.3.5.1. *GNC, simplified GNC, SISO Nyquist Criterion*

GNC provides stability analysis of AC systems using *d-q* impedance data. For unity-power-factor loads, the simplified stability criteria for AC systems can be also used. The SISO Nyquist criterion provides stability analysis of DC systems using DC impedance data. The stability analysis is performed by inspection of eigenvalue trajectories in the complex plane for AC systems, or on the trajectory of the return ratio for DC systems or for simplified criteria.

The flowchart of Matlab® codes for stability analysis is shown in Fig. 2-23. The transfer functions of the source and load impedances are extracted by curve fitting, then the return ratio is calculated and stability criteria can be checked.

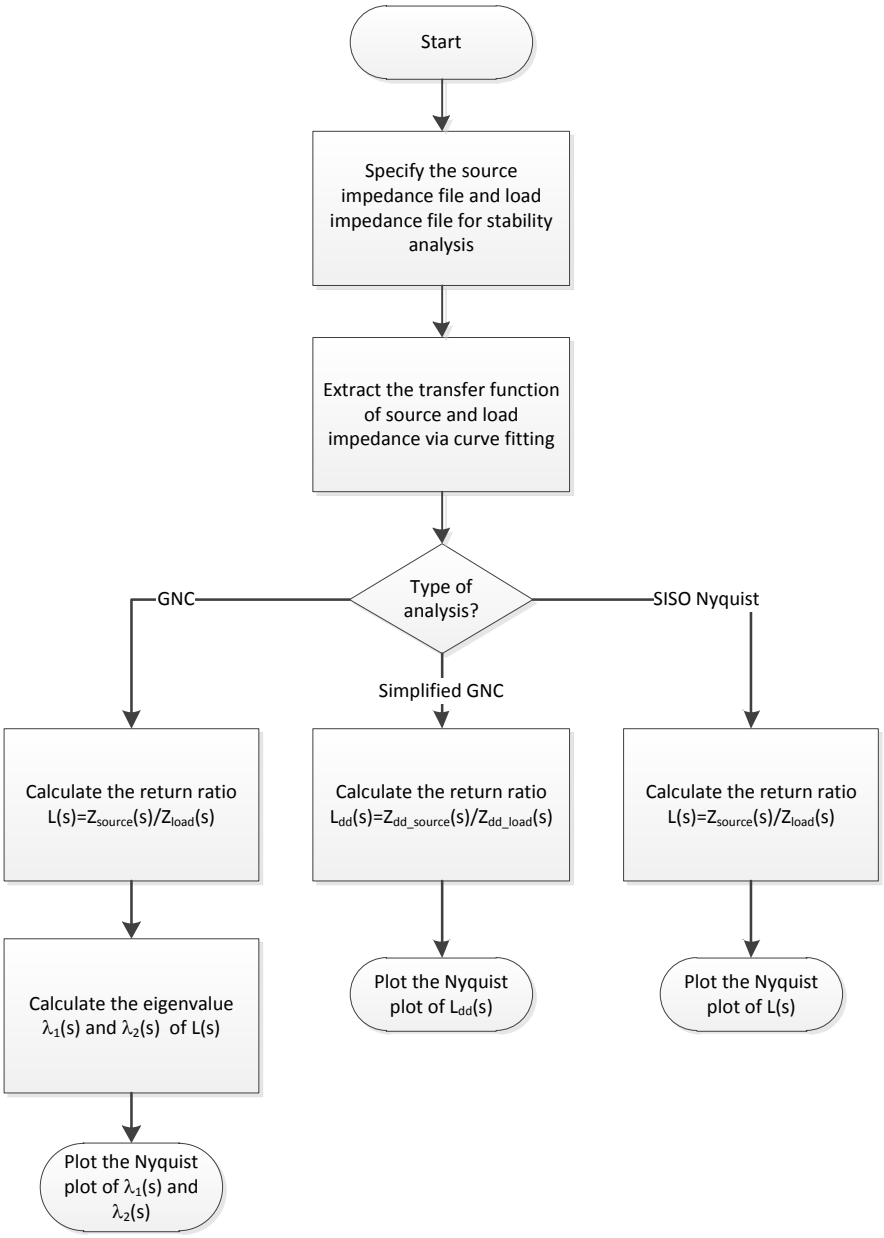

Fig. 2-23 Flow chart of Matlab codes for stability analysis

2.3.5.2. ***Impedance Over-plot***

The impedance over-plot function enables the user to view the impedance of different targets on the same figure. The user can check the impedance interactions of the source and the load, or check the impedance change of the same target under different conditions.

The flowchart of Matlab® codes for over-plot is shown in Fig. 2-24. There are two main parts: the first part is to save all the file names into first in first out (FIFO) stacks. The second part is to load those file names and plot them on the same figures one by one.

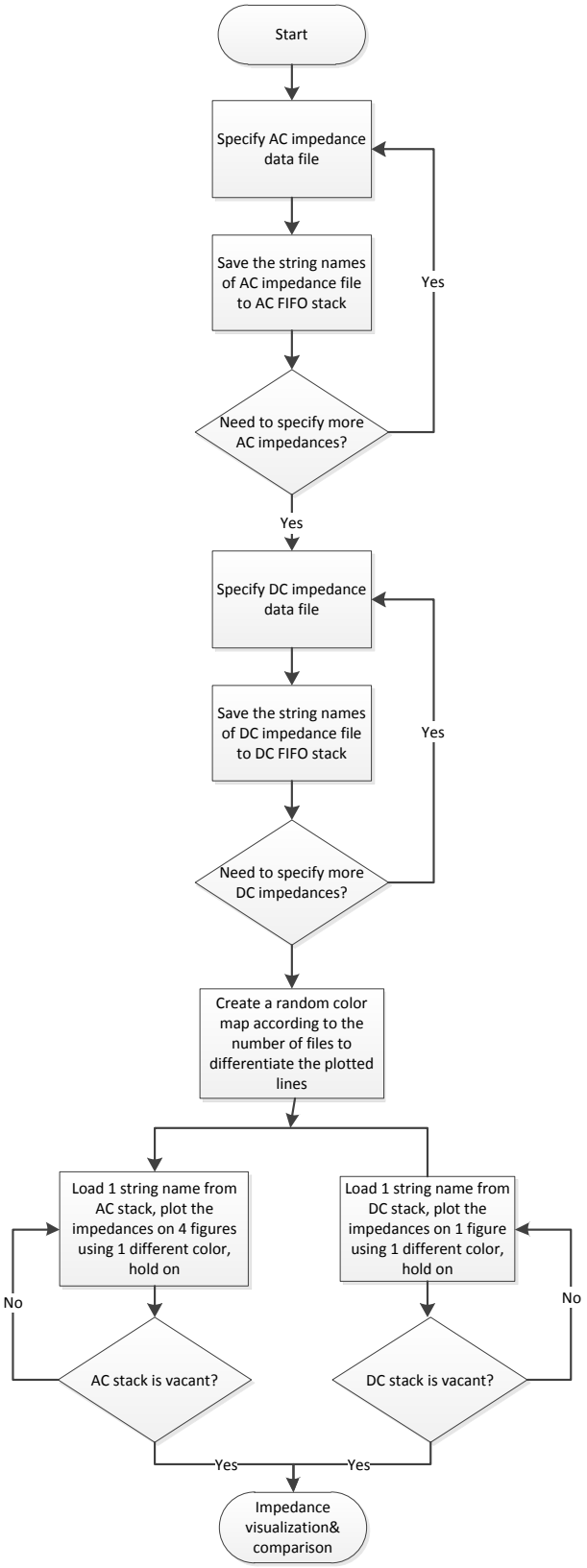

Fig. 2-24 Flow chart of impedance over-plot

2.3.6. Simulation results and application examples

2.3.6.1. ***Passive source and load under unbalanced voltage source***

In this example, resistors and inductors are used as load to test whether the virtual impedance calculation tool works well for unbalanced voltage source. The schematic of the model is shown in Fig. 2-25:

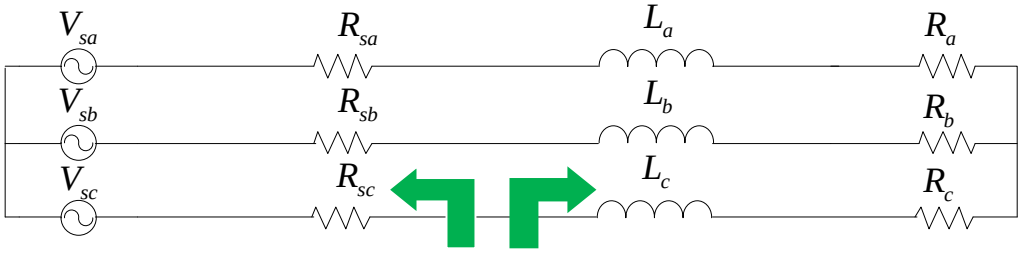

Fig. 2-25 Schematic of unbalanced voltage source example

The parameters of the test are shown below in Table 2-2.

Table 2-1 Parameters of passive components

Parameter	Value
ω_s(line frequency)	413*2*π(rad/s)
V_{sa}, V_{sc}	110 V
V_{sb}	99 V
R_{sa}, R_{sb}, R_{sc}	20 Ω
L_a, L_b, L_c	1 mH
R_a, R_b, R_c	100 Ω
Impedance measurement block	Three-phase mtone shunt current P2N
Frequency measurement range	10Hz~10kHz
Number of points	30
Perturbation amplitude	0.2A

The analytical expression of *d-q* load impedance is derived:

Note the AC interface voltages $v_{la}(t), v_{lb}(t), v_{lc}(t)$, and load currents $i_a(t), i_b(t), i_c(t)$.

The voltage and current relationship in abc coordinates is:

$$\begin{bmatrix} v_{la}(t) \\ v_{lb}(t) \\ v_{lc}(t) \end{bmatrix} = R \begin{bmatrix} i_a(t) \\ i_b(t) \\ i_c(t) \end{bmatrix} + L \frac{d}{dt} \begin{bmatrix} i_a(t) \\ i_b(t) \\ i_c(t) \end{bmatrix}$$

Using the dq0/abc transformation matrix T defined in (1-2), we get

$$T^{-1} \begin{bmatrix} v_d(t) \\ v_q(t) \\ v_0(t) \end{bmatrix} = RT^{-1} \begin{bmatrix} i_a(t) \\ i_b(t) \\ i_c(t) \end{bmatrix} + LT^{-1} \frac{d}{dt} \begin{bmatrix} i_a(t) \\ i_b(t) \\ i_c(t) \end{bmatrix} + L \left(\frac{d}{dt} T^{-1} \right) \begin{bmatrix} i_a(t) \\ i_b(t) \\ i_c(t) \end{bmatrix}$$

$$\rightarrow \begin{bmatrix} v_d(t) \\ v_q(t) \end{bmatrix} = R \begin{bmatrix} i_d(t) \\ i_q(t) \end{bmatrix} + L \frac{d}{dt} \begin{bmatrix} i_d(t) \\ i_q(t) \end{bmatrix} + \omega_s L \begin{bmatrix} -i_q(t) \\ i_d(t) \end{bmatrix}$$

Transforming the equation to frequency domain, we get:

$$\begin{bmatrix} v_d(s) \\ v_q(s) \end{bmatrix} = R \begin{bmatrix} i_d(s) \\ i_q(s) \end{bmatrix} + Ls \begin{bmatrix} i_d(s) \\ i_q(s) \end{bmatrix} + \omega_s L \begin{bmatrix} -i_q(s) \\ i_d(s) \end{bmatrix}$$

$$Z = \begin{bmatrix} R + sL & -\omega_s L \\ \omega_s L & R + sL \end{bmatrix}$$

The results from STASU are compared with analytical expression:

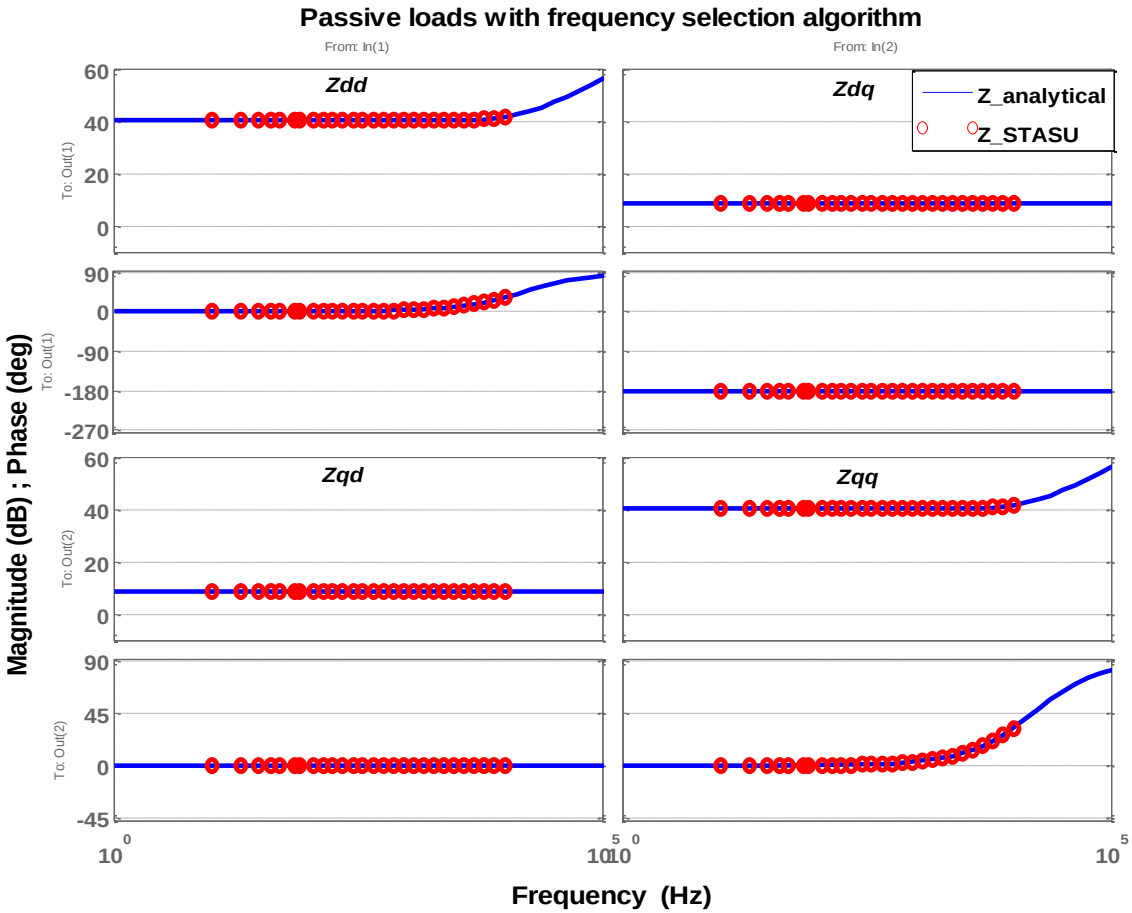

Fig. 2-26 *d-q* Impedance of unbalanced voltage source example

From Fig. 2-26, the solid line is analytical expression and the dots are results from STASU. It is shown that the result from STASU matches with analytical expression, which shows that STASU could accurately measure impedance of three phase AC systems Even in unbalanced case in which there exist system line-frequency harmonics, the perturbation frequency selection algorithm in STASU could avoid the affect.

To show the effectiveness of perturbation frequency selection algorithm, the model is simulated again, without the FFT window aligned with line frequency. The results are shown in .

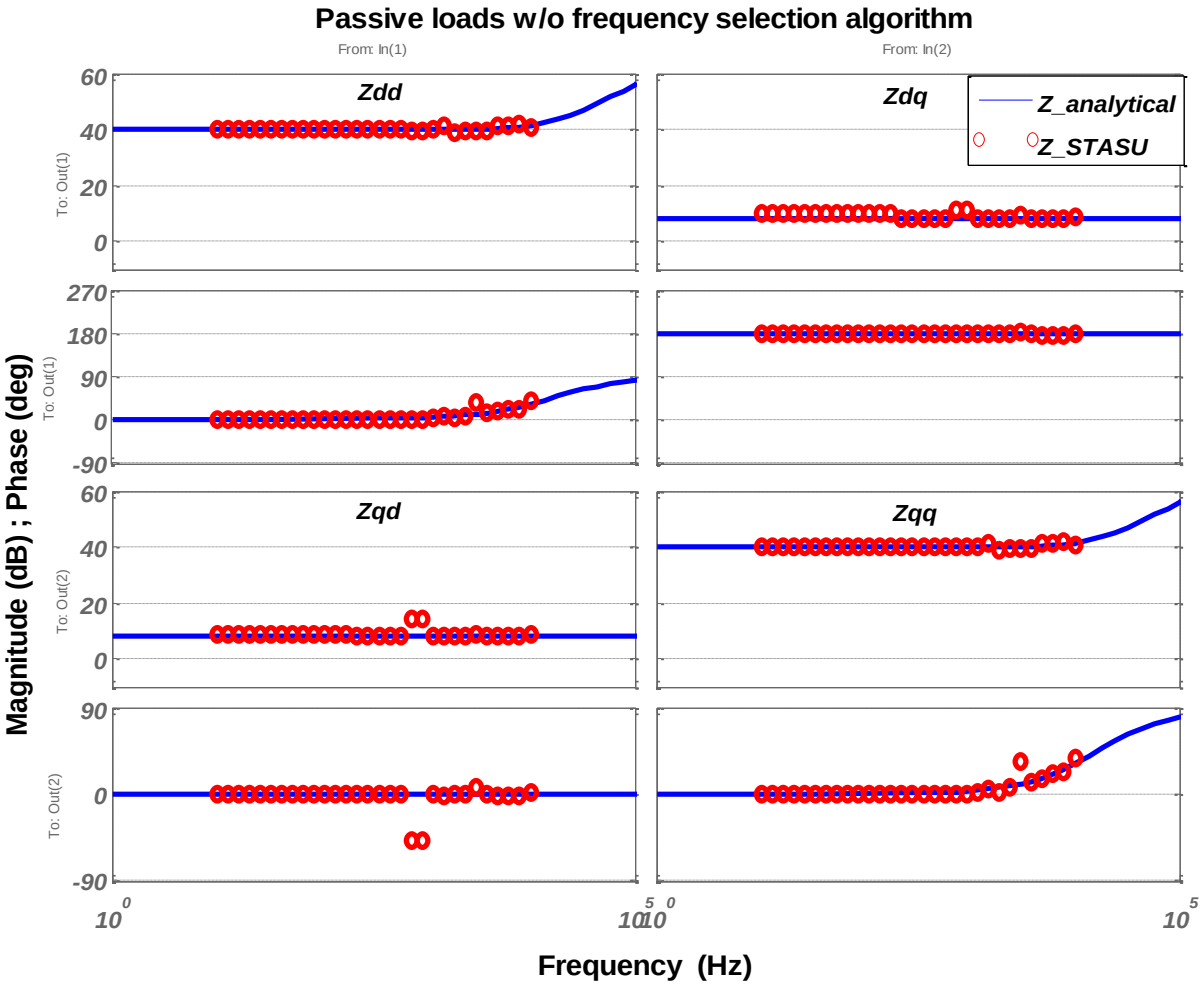

Fig. 2-27 *d-q* Impedance of unbalanced voltage source example

It is clearly shown that if FFT window is not aligned with line frequency, and perturbation frequencies are not adjusted according to the line frequency, the existence of line harmonics in the system will affect the accuracy of measurement results. The effectiveness of perturbation frequency selection algorithm is proved in this example.

2.3.6.2. ***DC/DC Converter***

This is a DC/DC buck converter with an input voltage of 24V and output voltage 5V. The schematic is shown below in Fig. 2-28.

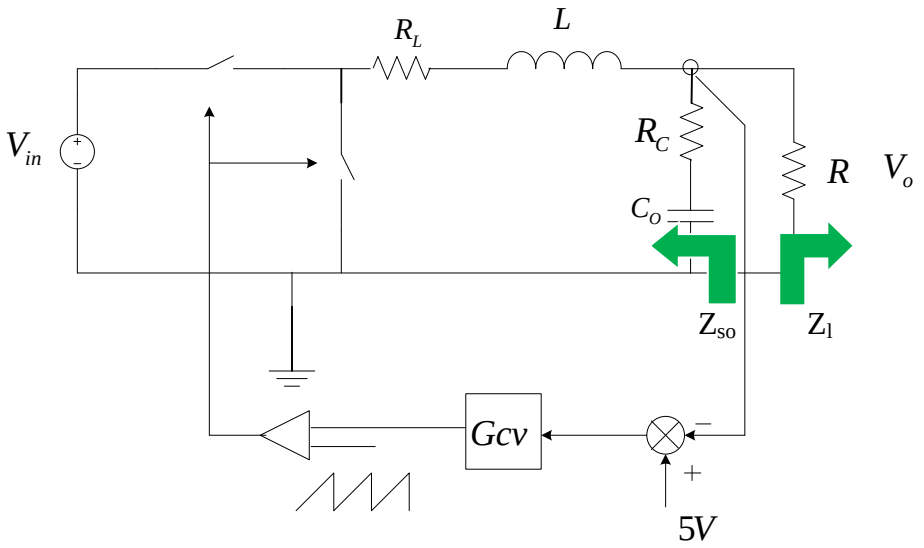

Fig. 2-28 Schematic of DC/DC converter

And the parameters are shown below in Table 2-2.

Table 2-2 Parameters of DC/DC converter

Parameter	Value
L	20μH
R_L	0.5 mΩ
C_O	100 μF
R_C	1.4mΩ
R	1Ω
V_{in}	24V
G_{cv} Bandwidth	1.5kHz
Switching frequency	50kHz
Impedance measurement block	DC stone shunt current
Frequency measurement range	100Hz~20kHz
Number of points	20
Perturbation amplitude	0.5A

The derivation of close-loop output impedance is shown below:

The open-loop output impedance could be expressed as:

$$Z_O = R_O \frac{(1 + s/s_{z1})(1 + s/s_{z2})}{1 + a_1 s + a_2 s^2} \tag{2-7}$$

Where

$$R_O = R_L || R = \frac{R_L R}{R_L + R} \tag{2-8}$$

$$s_{z1} = \frac{1}{R_C C_O} \tag{2-9}$$

$$s_{z2} = \frac{R_L}{L} \tag{2-10}$$

$$a_1 = \frac{L}{R_L + R} + C_O \left(R_C + \frac{R_L R}{R_L + R} \right) \tag{2-11}$$

$$a_2 = L C_O \frac{R_C + R}{R_L + R} \tag{2-12}$$

The open-loop control to output transfer function is:

$$G_{vd} = \frac{V_O(s)}{d(s)} = V_{in} \frac{(1 + s/s_{z1})}{1 + a_1 s + a_2 s^2} \tag{2-13}$$

The voltage-loop controller is designed as:

$$\begin{aligned} G_{cv} &= \frac{\omega_I}{F_M} \frac{(1 + s/\omega_{z1})(1 + s/\omega_{z2})}{s(1 + s/\omega_{p1})(1 + s/\omega_{p2})} \\ &= \frac{8.5712 \times 10^3}{s} \frac{\left(1 + \frac{s}{1.4\pi \times 10^3}\right)\left(1 + \frac{s}{1.46\pi \times 10^3}\right)}{\left(1 + \frac{s}{6.4\pi \times 10^3}\right)\left(1 + \frac{s}{4.548\pi \times 10^3}\right)} \end{aligned} \tag{2-14}$$

Closed-loop output impedance is derived:

$$Z_{o-cl} = \frac{Z_{o-op}}{1 + T_v} = \frac{Z_{o-op}}{1 + G_{vd} G_{cv}} \tag{2-15}$$

where T_v is the voltage loop gain of the converter, G_{vd} is control-to-output-voltage transfer function, and G_{cv} is the controller transfer function.

Then comparison of analytical expression and impedance extracted by STASU is shown in Fig. 2-29.

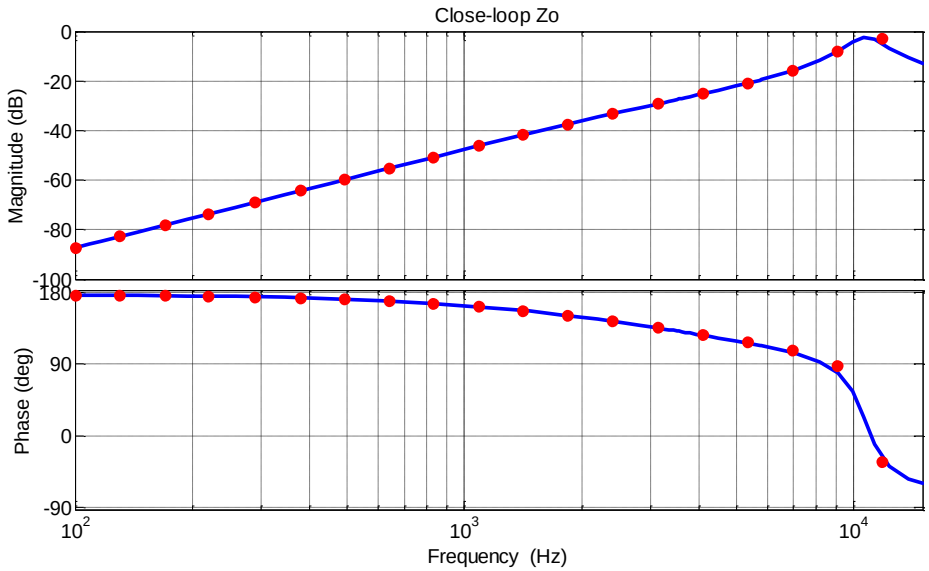

Fig. 2-29 Closed-loop output impedance of DC/DC converter (line: analytical; dots: STASU)

From Fig. 2-29, it is shown that the impedance calculated by STASU matches with the analytical expression, which means that STASU could accurately measure the DC impedance.

2.3.6.3. ***Conclusion***

There are 3 examples in total. In the first example, STASU is used to measure the input impedance of 3 phase passive loads under unbalanced voltage source. It is proved that STASU could accurately measure the *d-q* impedance of three phase simulation models. In the second one, STASU is used to measure output impedance of DC/DC buck converter. The result also proves that STASU could accurately measure DC impedance.

In the third example, STASU is used to measure VSI/AFE back to back setup. Both AC interface and DC interface are measured. The source impedance and load impedance are obtained at the same time and used for analysis. The result of stability analysis agrees with time-domain waveform. The stability analysis capability of STASU is verified.

Both single-tone approach and multi-tone approach are used, and both shunt current injection and series voltage injection are tested. It is shown that single-tone approach and multi-tone approach could accurately extract impedances from switching models.

2.4. Experimental verification of multi-tone approach

In this part, the experimental verification of multi-tone approach will be presented. The experimental test bed setup will be introduced. The experimental results from multi-tone will be compared with analytical expression to show the effectiveness.

2.4.1. System implementation

The system diagram for multi-tone method is shown in Fig. 2-30.

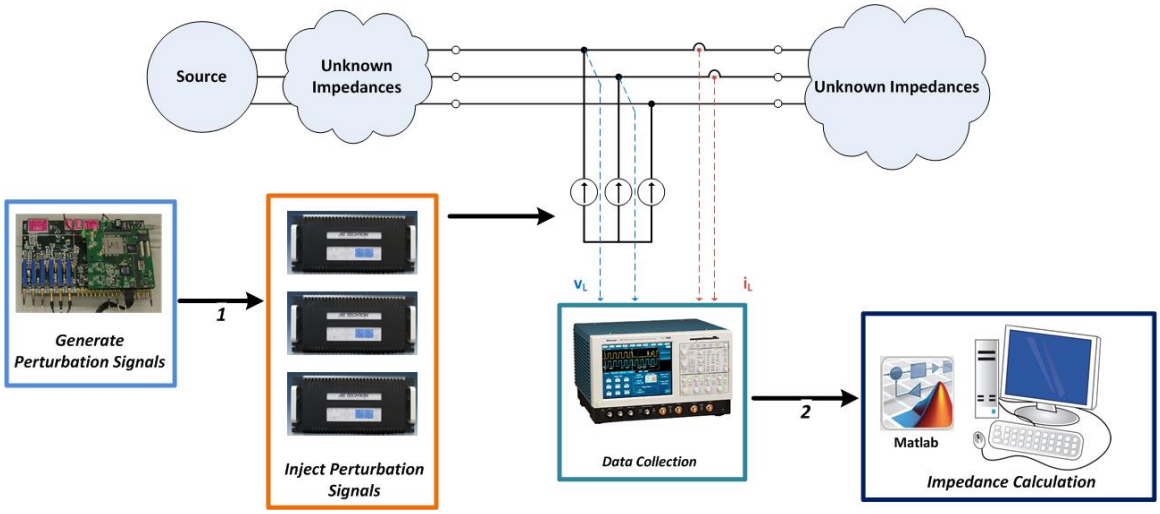

Fig. 2-30 System diagram for multi-tone approach verification

Universal controller is used to generate multi-tone perturbation signal and transform the perturbation from *d-q* coordinate to abc coordinate. Three power amplifiers are connected to the system and inject perturbation through transformers. After system reaches steady state under perturbation, voltage and current responses are collected by oscilloscope. The waveforms are transferred to the computer. All the data are saved and analyzed to calculate the impedance of the system.

In this implementation, all the data are transferred to the computer to extract the frequency-domain information, which is different from the impedance analyzer in Chapter 3. This is because network analyzer cannot calculate the frequency-domain response of all the frequency

points, from a single time-domain waveform. It is also not feasible to restore all the data in DSP and calculate impedances with DSP, because the data will be large and DSP does not have enough memory. However in Matlab, it is easy to apply FFT and extract frequency domain response of all the frequency points.

This structure could be improved in the future. First of all, the oscilloscope and computer could be replaced with a PXI platform or similar measurement and automation systems. Its high-performance data collection, processing and calculation will make it easy to automatically calculate impedance. Moreover, a higher-sampling-frequency DSP may be used to generate multi-tone signal, to increase the signal resolution at high frequency range.

2.4.2. Generating multi-tone signal

The flowchart for multi-tone signal generating is shown in Fig. 2-31.

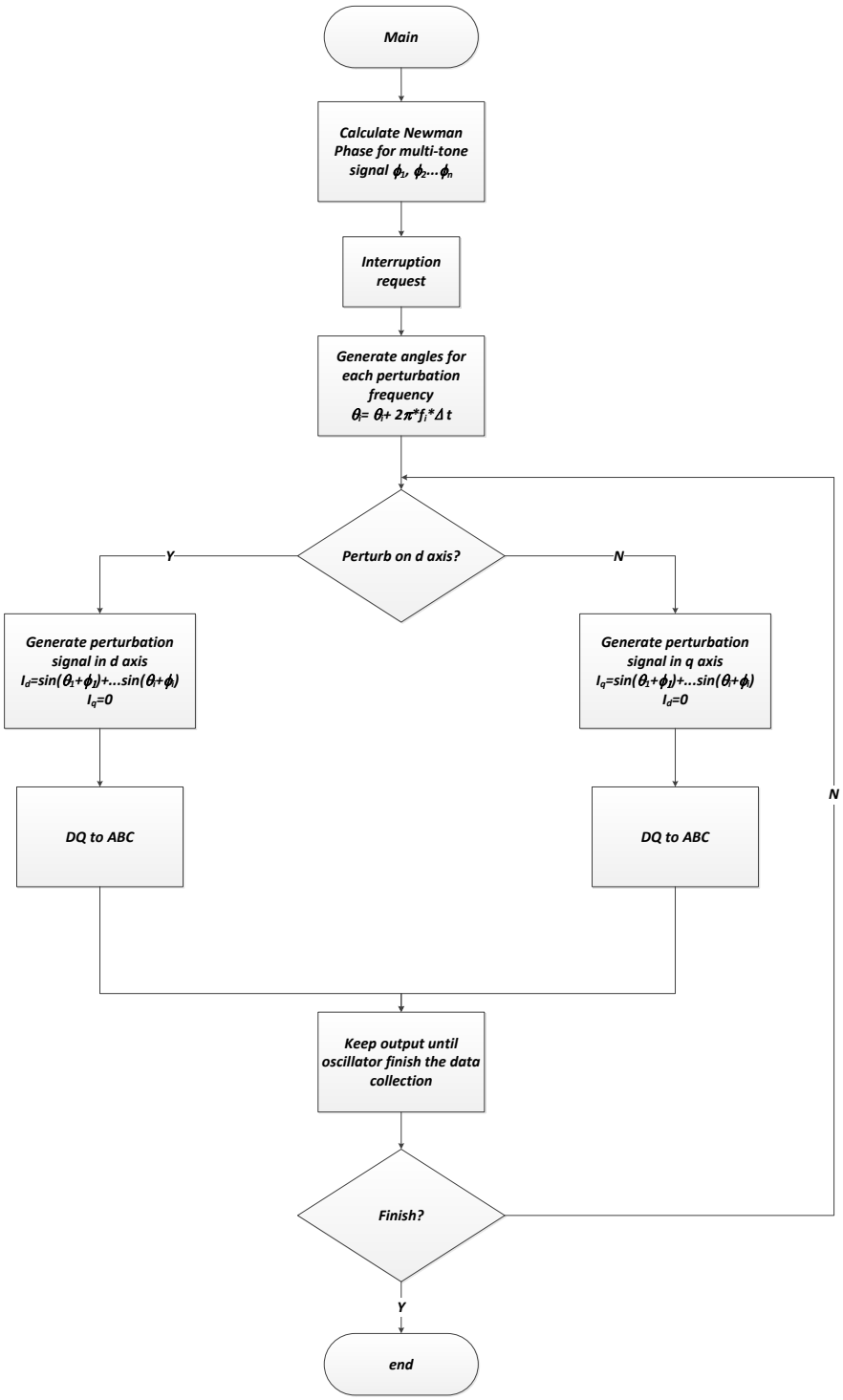

Fig. 2-31 Flowchart of multi-tone signal generation

System voltage signals are input to DSP. PLL is used to track the system voltage angle and align *d-q* coordinate. Before the DSP program enters main loop and wait for the interruption, all the multi-tone signals are pre-calculated and saved in DSP program memory. In this application,

the DSP is AD-21150 from analog devices. Available memory is 256K words of 16bit data. At most 20000 data points can be used to represent the multi-tone signal. Considering 60kHz sampling frequency, which is the DSP interruption frequency, if the maximum perturbation frequency is 6kHz, the 6kHz signal has a 10 points resolution. The minimum perturbation frequency is 3Hz because 20k data points are sampled at 60kHz. If perturbation frequency goes lower, not enough data points could represent a full period of perturbation signal.

2.4.3. Data acquisition

Tektronix MSO4054B oscilloscope is used for waveform collection, which is shown in Fig. 2-32.

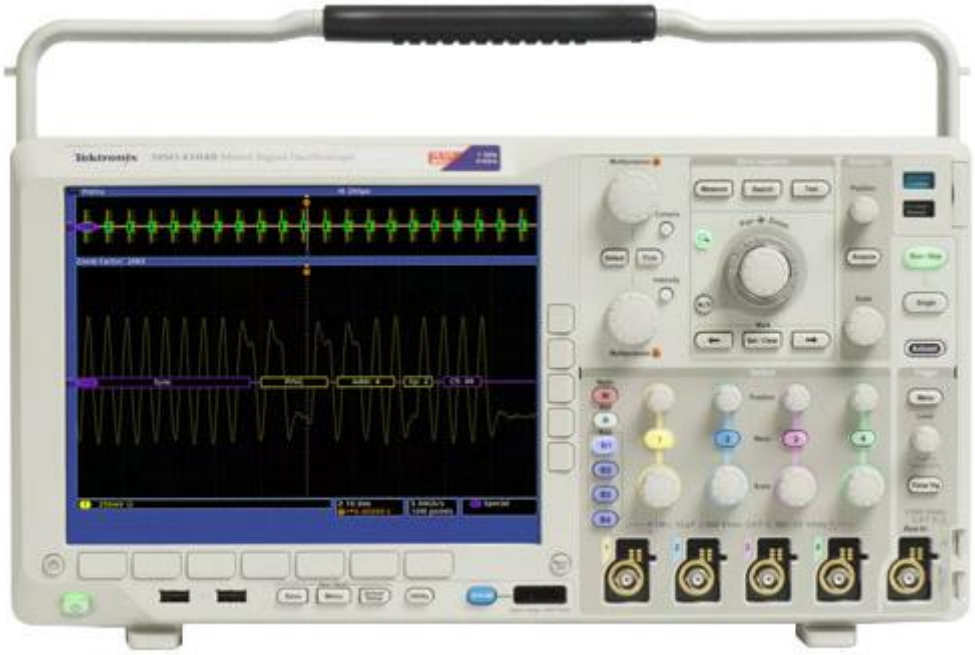

Fig. 2-32 MSO4054B oscilloscope

The bandwidth is 500MHz. The highest sample rate is 2.5GS/s. The max record length is 20M points. The oscilloscope could be configured to communicate with computer from LAN. The voltage and current waveforms could be automatically saved into Matlab data file.

In the verification experiments, the record length is chosen to be 20M points, and the sampling rate is chosen to be 1MHz. The over-qualified specs of oscilloscope could increase the accuracy of measurement for the purpose of method verification.

2.4.4. Data back-calculation

The data back calculation flowchart is shown in Fig. 2-33.

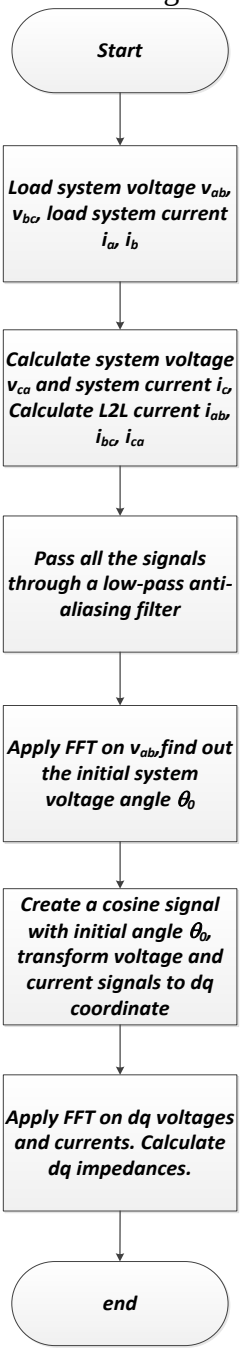

Fig. 2-33 Flowchart of multi-tone impedance calculation

Two voltage waveforms and two current waveforms are obtained by 4-channel oscilloscope. The data is loaded. All the voltage and current signals in abc coordinate are calculated. Then all the waveforms are passed through a low-pass filter, whose cut-off frequency is chosen to be 10

times maximum perturbation frequency (much lower than half of the sampling frequency 500kHz). The initial system angle is found through FFT. FFT window is chosen to be periodic for both line frequency and perturbation frequencies, according to the same algorithm in 2.3.4.4. Then the voltage and current responses are transformed to *d-q* coordinates. *d-q* impedances are calculated.

2.4.5. Experiment results on passive components

2.4.5.1. ***Resistive load***

The test diagram is shown in Fig. 2-34.

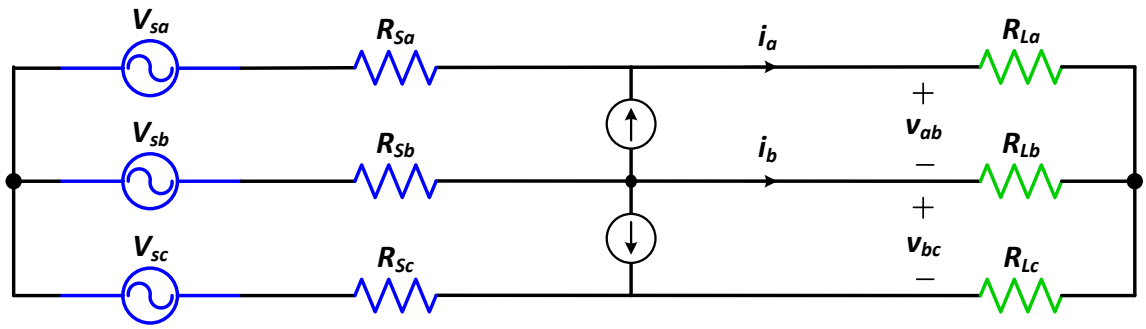

Fig. 2-34 Resistive load multi-tone test diagram

The parameters are shown in Table 2-3.

Table 2-3 Parameters for resistive load test

Description	Symbol	Value
System voltage	V_{Sa}, V_{Sb}, V_{Sc}	50V, 400Hz
Source impedance	R_{Sa}, R_{Sb}, R_{Sc}	2Ω
Load resistor	R_{La}, R_{Lb}, R_{Lc}	10Ω
Perturbation amplitude	I_{pert}	0.8A

The load resistors are measured. The analytical expression of line-to-line *d-q* impedance for three- phase balanced resistors is:

$$\begin{bmatrix} Z_{Sdd}(s) & Z_{Sdq}(s) \\ Z_{Sqd}(s) & Z_{Sqq}(s) \end{bmatrix} = \begin{bmatrix} 3R_L & 0 \\ 0 & 3R_L \end{bmatrix} \quad (2\text{-}16)$$

The injected frequency components are shown in Table 2-4.

Table 2-4 Perturbation frequencies

f_{pert}(HZ)	80	160	250	350	500	650	800	1000	1300	1600

The measurement result is shown in and compared with analytical expression, as shown in Fig. 2-35.

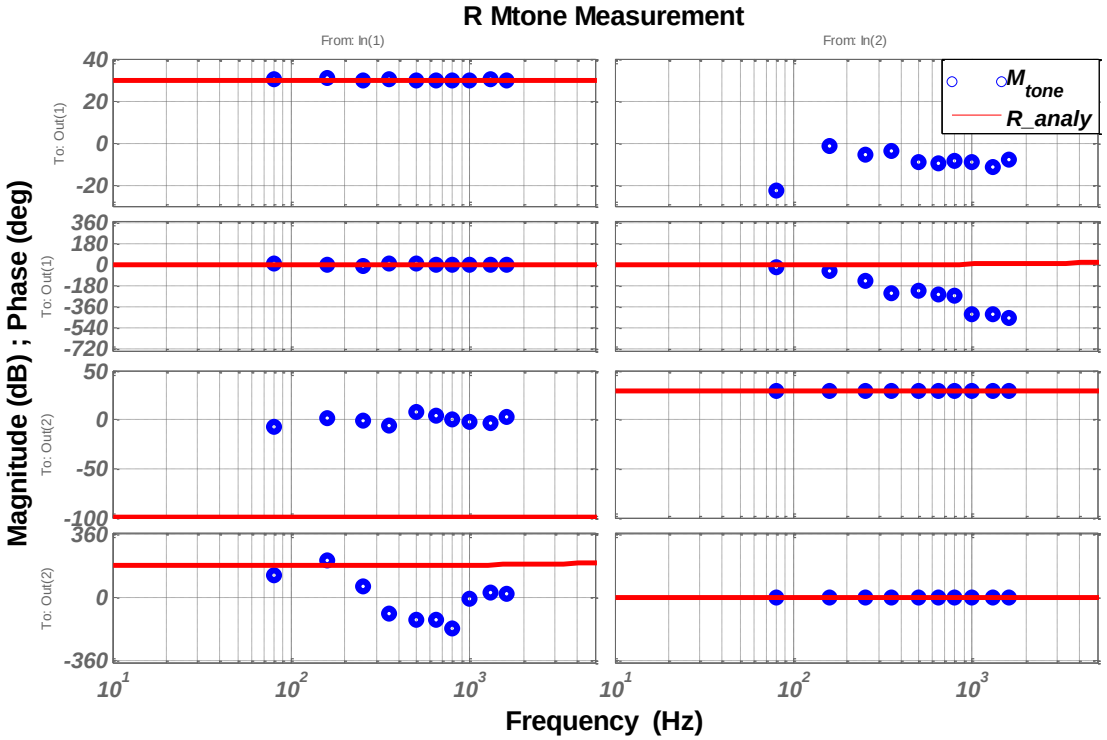

Fig. 2-35 Resistive load multi-tone measurement

The magnitude of $Z_{d\text{-}q}$ and Z_{qd} is 20dB lower than Z_{dd} and Z_{qq}, which shows that the multi-tone measurement results could well match the analytical expression.

2.4.5.2. ***RL load***

The test diagram is shown in Fig. 2-36.

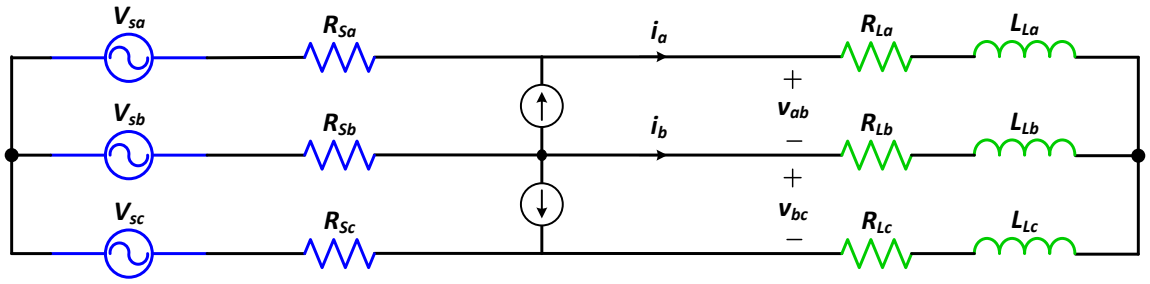

Fig. 2-36 RL multi-tone test diagram

The parameters are shown in Table 2-5.

Table 2-5 Parameters for RL load test

Description	Symbol	Value
System voltage	V_{Sa}, V_{Sb}, V_{Sc}	50V, 400Hz
Source impedance	R_{Sa}, R_{Sb}, R_{Sc}	2Ω
Load resistor	R_{La}, R_{Lb}, R_{Lc}	10Ω
Load inductor	L_{La}, L_{Lb}, L_{Lc}	470μH

The load resistors are measured. The analytical expression of line-to-line *d-q* impedance for three- phase balanced RL loads is:

$$\begin{bmatrix} Z_{Sdd}(s) & Z_{Sdq}(s) \\ Z_{Sqd}(s) & Z_{Sqq}(s) \end{bmatrix} = \begin{bmatrix} 3R_L + 3sL & -3\omega L \\ 3\omega L & 3R_L + 3sL \end{bmatrix} \quad (2\text{-}17)$$

The injected frequency components are shown in Table 2-6.

Table 2-6 Perturbation frequencies

f_{pert}(HZ)	100	200	300	600	900	1400	2200	3800	5800	7800

The measurement result is shown in and compared with analytical expression, as shown in Fig. 2-37.

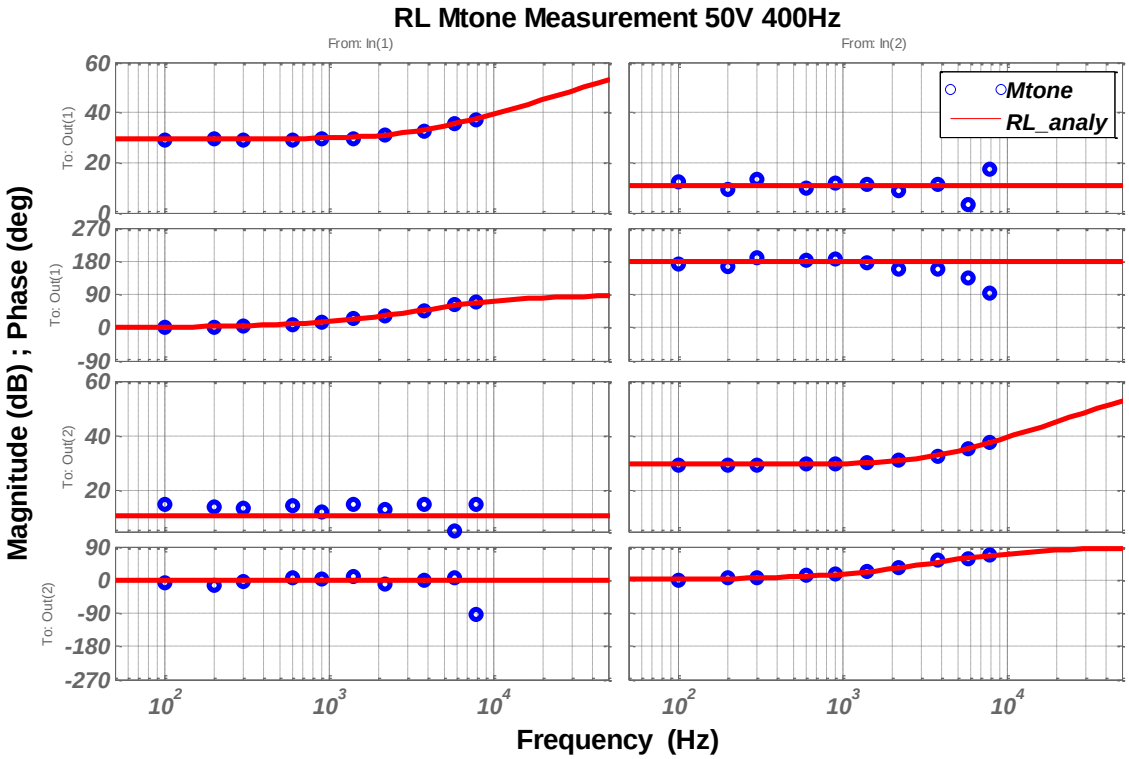

Fig. 2-37 RL load multi-tone measurement

It is shown that the multi-tone measurement results could well match the analytical expression.

2.5. Summary

In this chapter, the algorithm for *d-q* impedance calculation is introduced. Several methods to inject perturbation into three phase systems are reviewed. Based on this, STASU is developed and tested with several cases. The results show that STASU is a qualified tool to extract impedance of simulation models, and apply stability analysis based on impedance data.

Chapter 3. LOW POWER IMPEDANCE ANALYZER

3.1. Introduction

A three-phase impedance analyzer has been implemented in [16]. In that design, single-tone AC sweeping is used for impedance measurement. Controlled shunt current source are connected to the system through transformers to inject perturbation signals. In this work, the impedance analyzer is further extended to be capable to inject series voltage perturbation.

3.2. System implementation

The system diagram of three phase impedance analyzer is shown in Fig. 3-1.

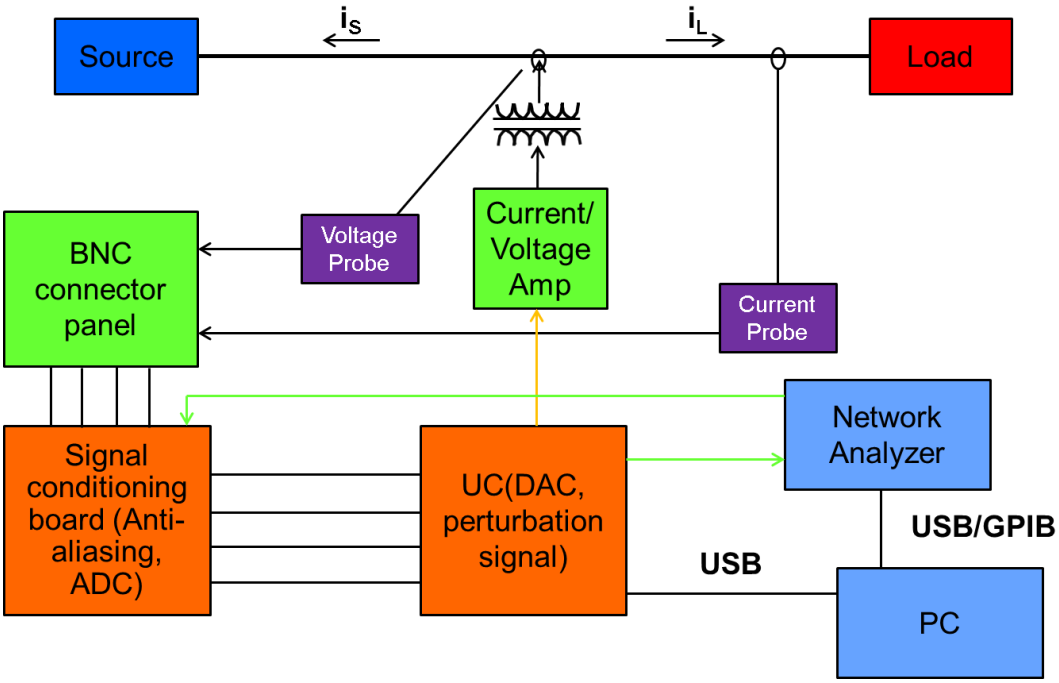

Fig. 3-1 System diagram of three phase impedance analyzer

Including series voltage injection, the power stage diagram of impedance analyzer is shown in Fig. 3-2.

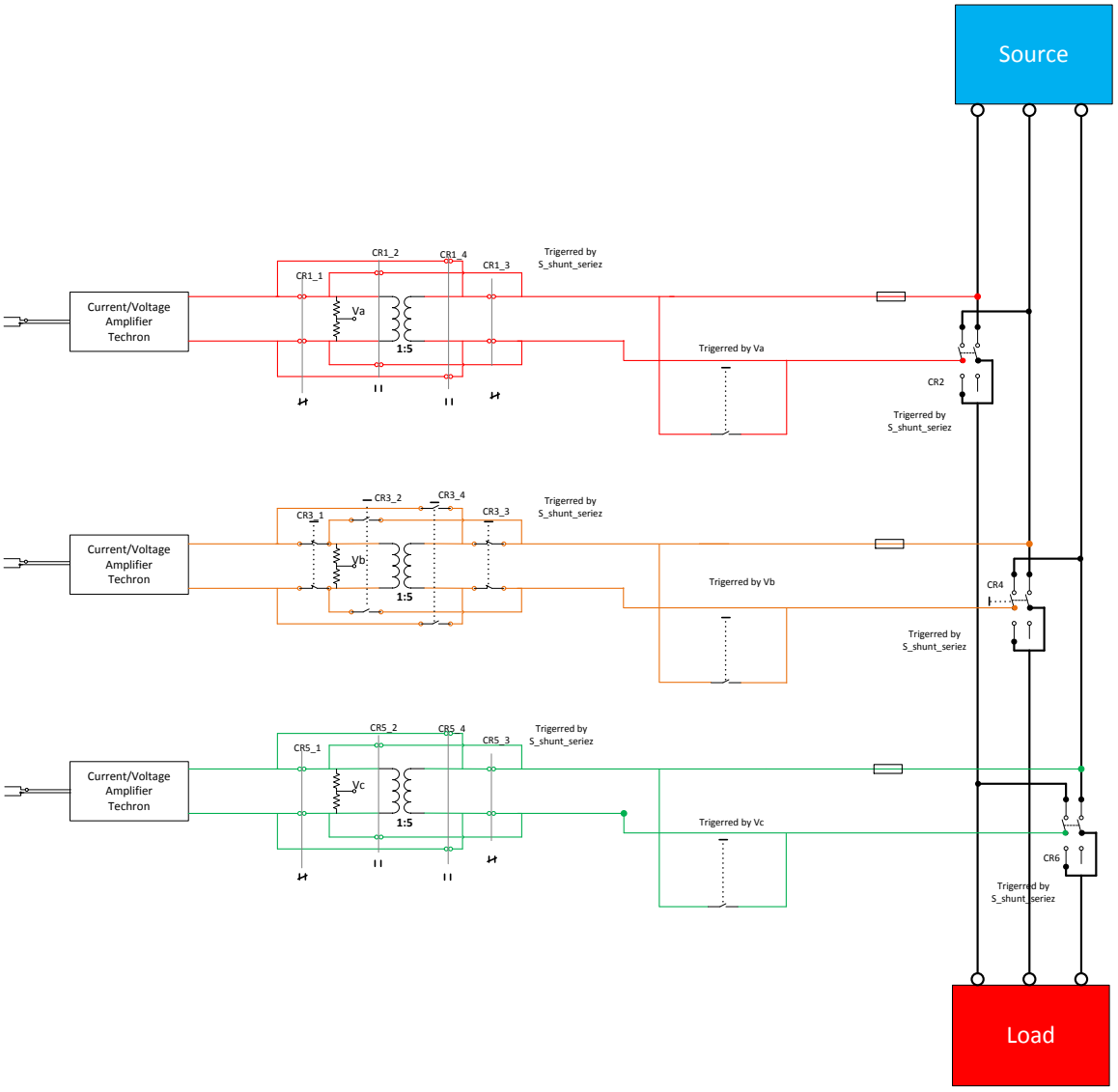

Fig. 3-2 Switch of shunt current injection and series voltage injection

Two major changes need to be made to switch from shunt current injection to series voltage injection. One is that the controlled perturbation source connection needs to be changed from shunt connection to series connection.

The other is that the transformer needs to be turned around: during shunt current injection, the current amplifier is connected to the low-voltage side of the transformer, such that the high-voltage side of transformer is connected to the bus to sustain the system line-to-line voltage; during series voltage injection, the voltage amplifier is connected to the high-voltage side of the

transformer, such that the low-voltage side of transformer is connected to the bus to sustain the system phase current.

A relay board is made to implement the switch from shunt current to series voltage. The connection is shown in Fig. 3-3.

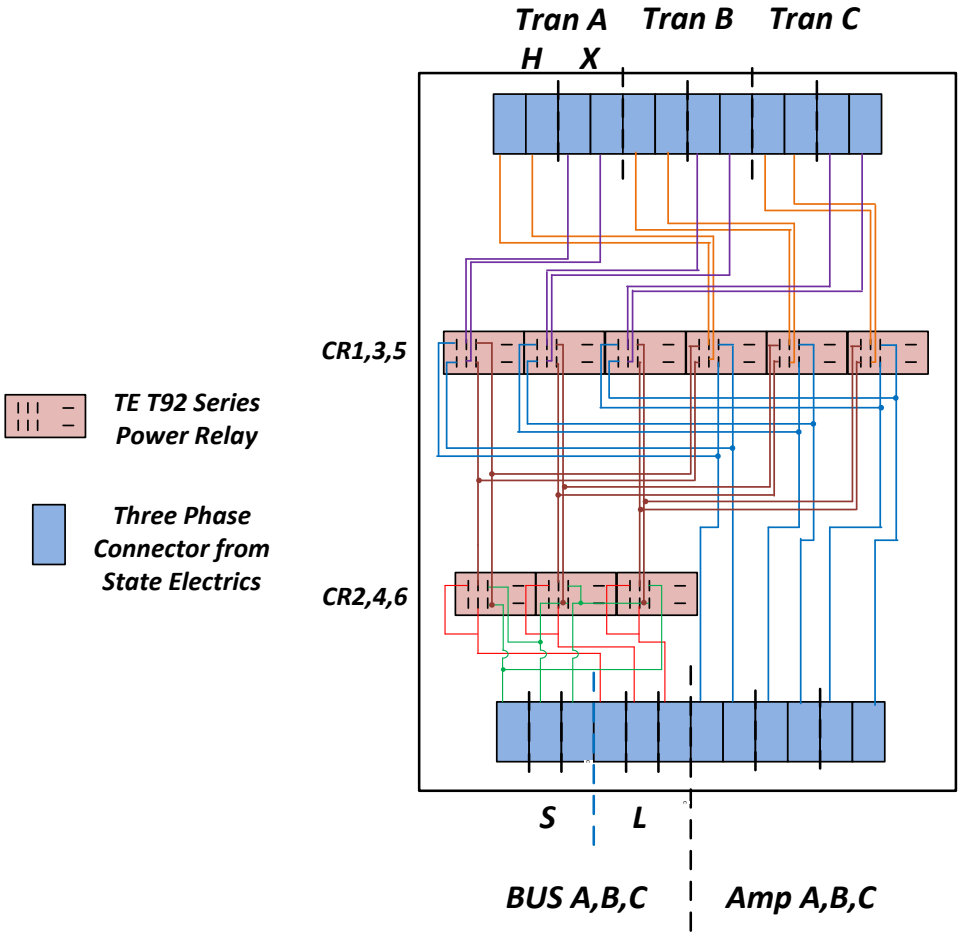

Fig. 3-3 Relay connection for shunt/series switch

3.3. System protection

3.3.1. Grounding fault in series voltage

The diagram of overvoltage protection is shown in Fig. 3-4.

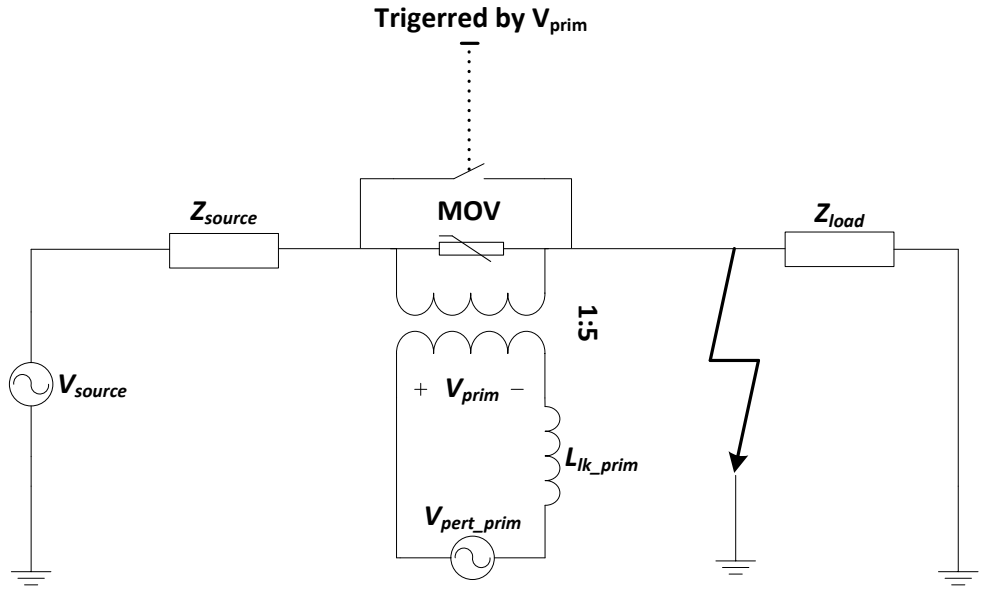

Fig. 3-4 Overvoltage protection

As shown in Fig. 3-4, if grounding fault happens at load side, the system voltage will drop on source impedance and the amplifier. Since the transformer turn ratio is 1:5, the voltage across the amplifier may damage the amplifier.

Crowbar relay is designed for the overvoltage protection. The voltage across the transformer is monitored. If this voltage is larger than the allowed voltage for the amplifier, the relay will close to short the transformer, such that the system voltage will never drop on the amplifier.

Three phase solid state relay is T53tp50d. It is a SCR relay with DC control voltage 3V~32V. The rated output current is 50A. It is a random turn on version. The max turn on time is 20μs.

To make sure that before the protection relay is triggered, the transient voltage will not go beyond the voltage limit of the amplifier, metal oxide varistor (MOV) should be connected in parallel with the relay. The varistor voltage is chosen to be 100V, less than the amplifier voltage limitation 125V.

The schematic of overvoltage protection board is shown in Fig. 3-5.

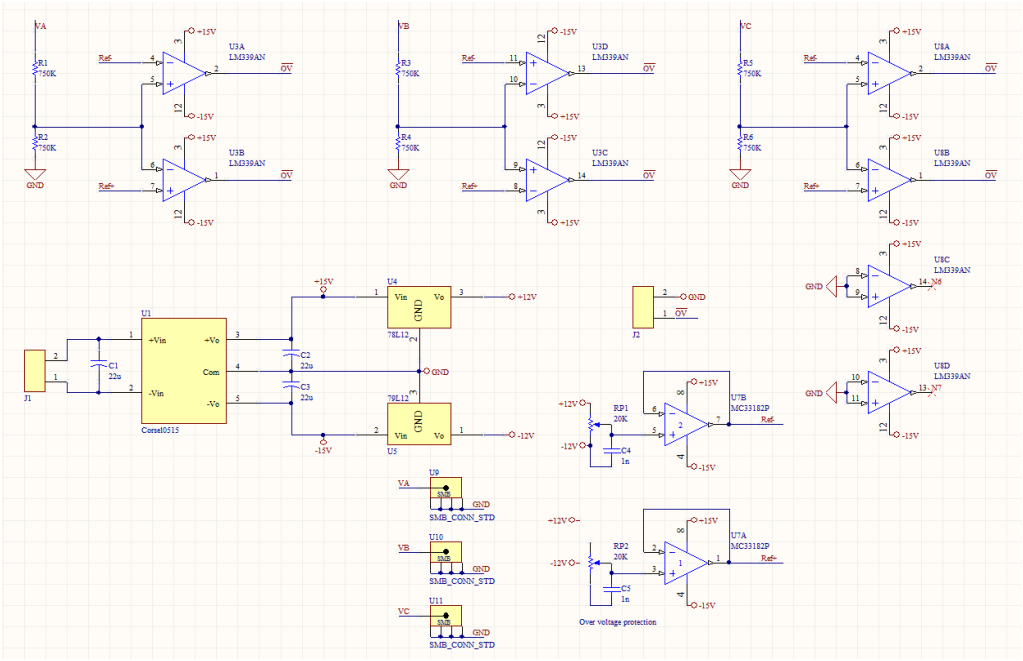

Fig. 3-5 Overvoltage protection board

On the board, bipolar op-amp is used to generate positive reference and negative reference. Three voltages across the transformers are sensed and input to this board. They are compared with the reference voltage limitation. If any of the three voltages goes out of limitation, the output signal OV will be locked high voltage to drive the relay. Until all the errors are cleaned, the board should be repowered up to clear the output high voltage.

3.3.2. Power up sequence fault

The system needs to be powered up in a correct sequence: the DSP codes of UC need to be run first, to give the correct references to the amplifiers. Then then amplifiers should be turned on and connected to the system bus. Finally the system can be turned on. If the off-state amplifiers are connected to the system bus with bus voltages, there is possibility for the amplifiers to blow up. Therefore power up sequence protection is very important.

The back panel of the amplifier is used for power up sequence protection, as shown in Fig. 3-6.

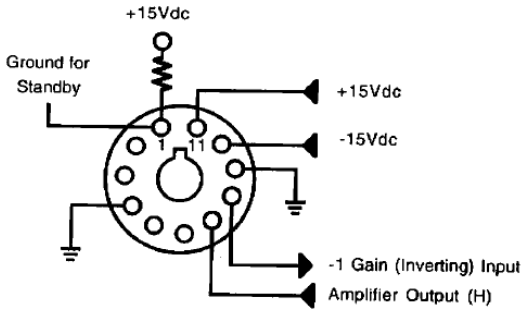

Fig. 3-6 Back control panel of Techron 7570 amplifier

If the amplifiers are powered up, Pin 11 will be +15VDC, Pin 10 will be -15VDC. These two signals are used to control the relay between amplifiers and system bus: without these DC voltage signals, the relay will always disconnect the amplifiers from the system bus.

If Pin 1 is grounded, the amplifier will enter standby mode and will not output the reference signal. Using this function, UC is programed to output a sinusoidal signal to control the output state of amplifier: if the DSP program is not running, the amplifiers will enter standby mode; if DSP program is running, the amplifiers will be in output mode.

The schematic of power up sequence protection board is shown in Fig. 3-7.

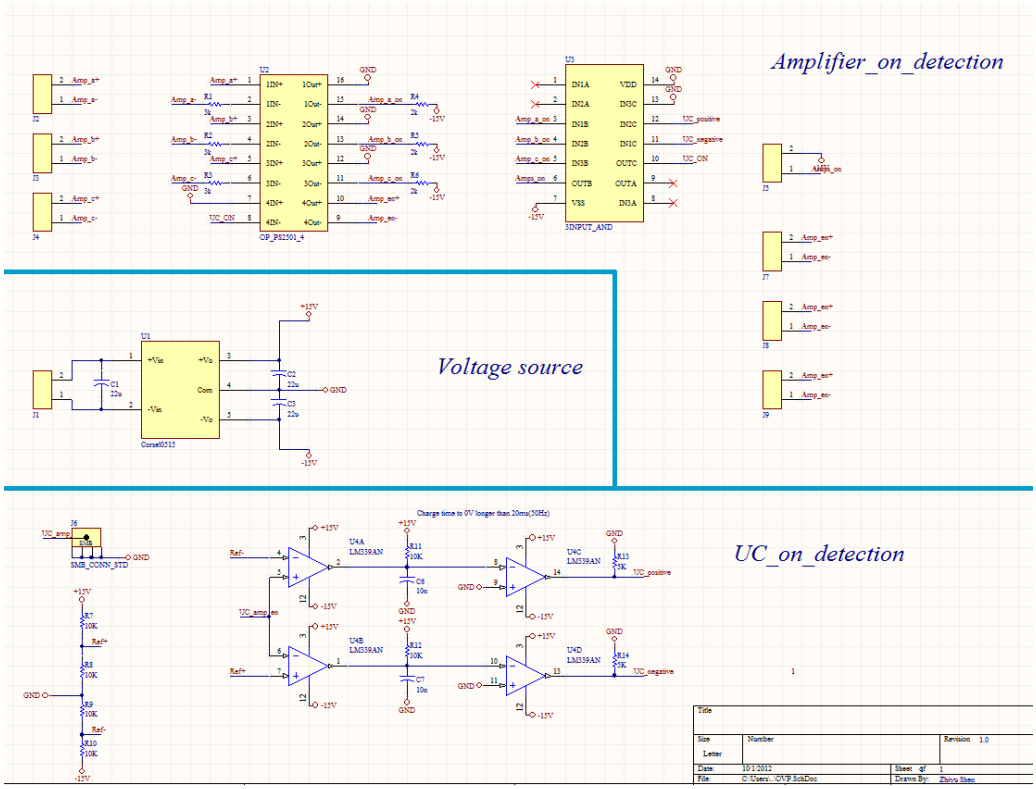

Fig. 3-7 Power up sequence protection board

This board is used to detect the state of the amplifiers and UC. Only when all the amplifiers are turned on, the board will trigger the relay to connect the amplifiers to system bus. Only when the DSP codes are running, the board will turn the amplifiers into output mode.

3.3.3. Summary of protection

The overview of protection for series voltage injection is shown in Fig. 3-8.

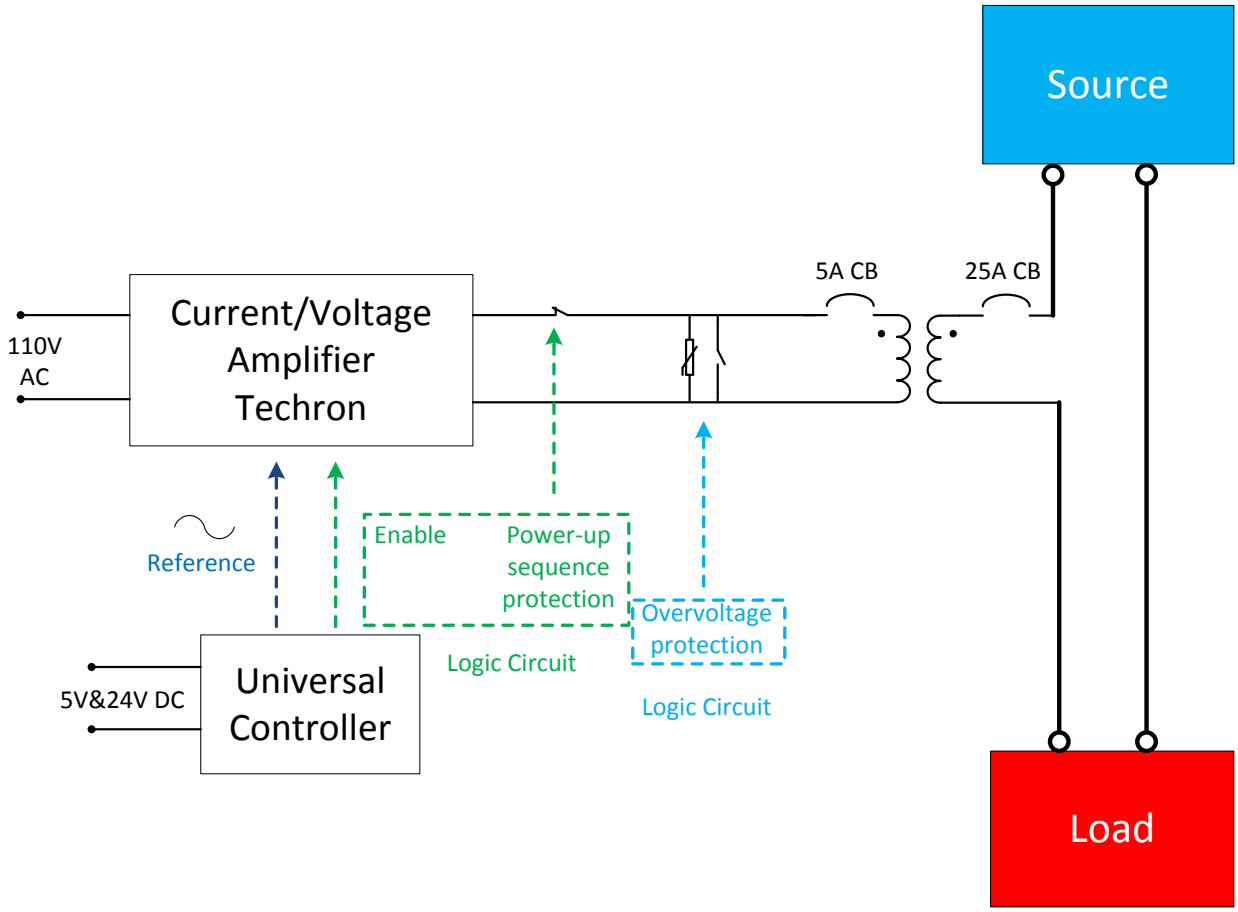

Fig. 3-8 Overview of protection for series voltage injection

The overview of protection for shunt current injection is shown in Fig. 3-9.

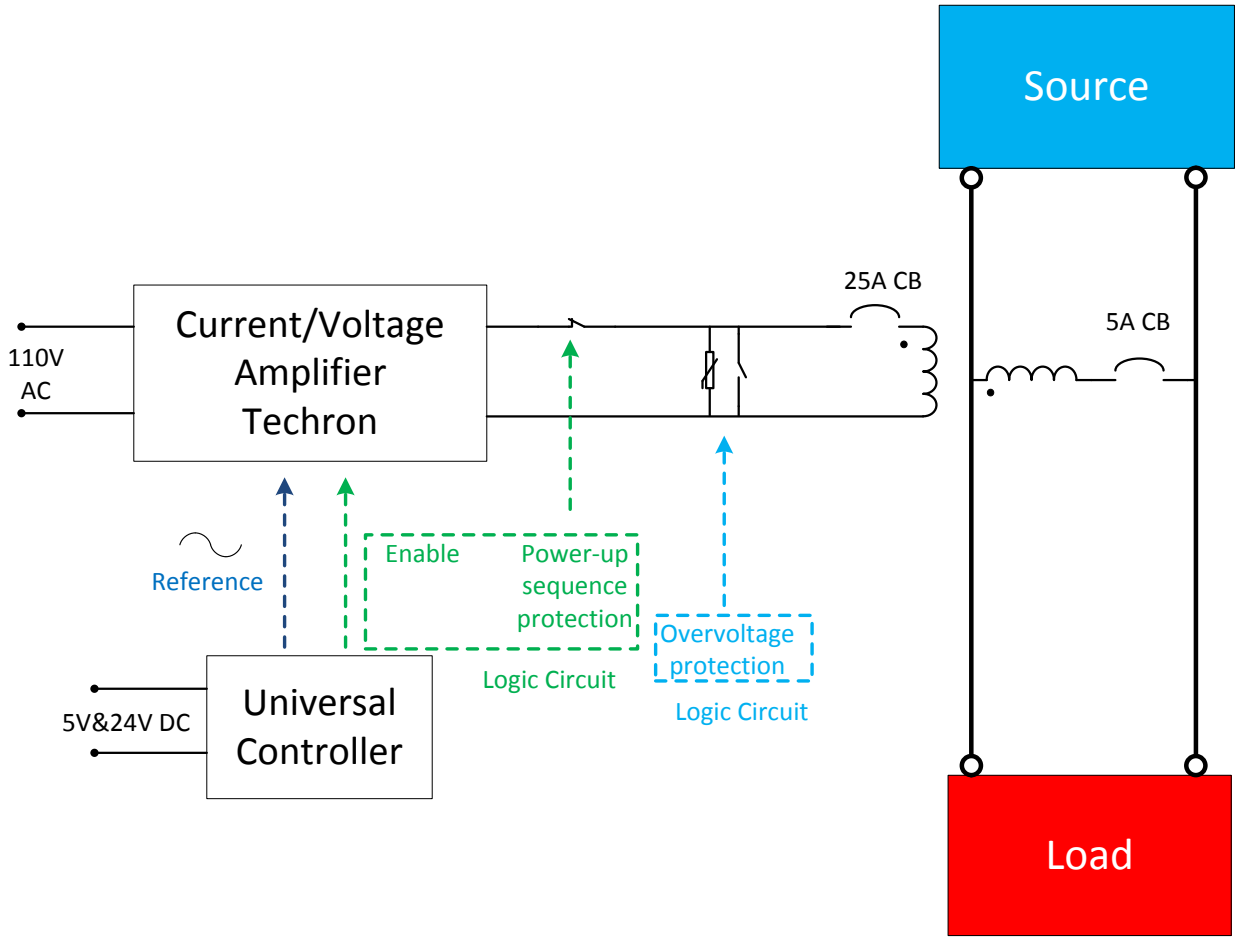

Fig. 3-9 Overview of protection for shunt current injection

3.4. Test results

3.4.1. Shunt current injection test

To verify the shunt current injection of impedance analyzer, a voltage source inverter is used as an example. The circuit diagram is shown in Fig. 3-10. The parameters are included in the figure.

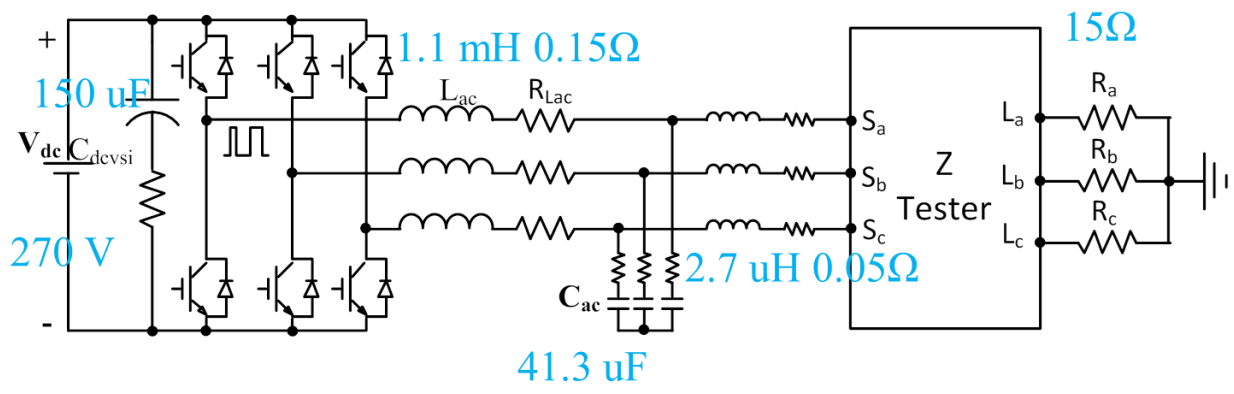

Fig. 3-10 VSI closed-loop output impedance measurement

The output impedance results are shown in Fig. 3-11 and compared with simulation results.

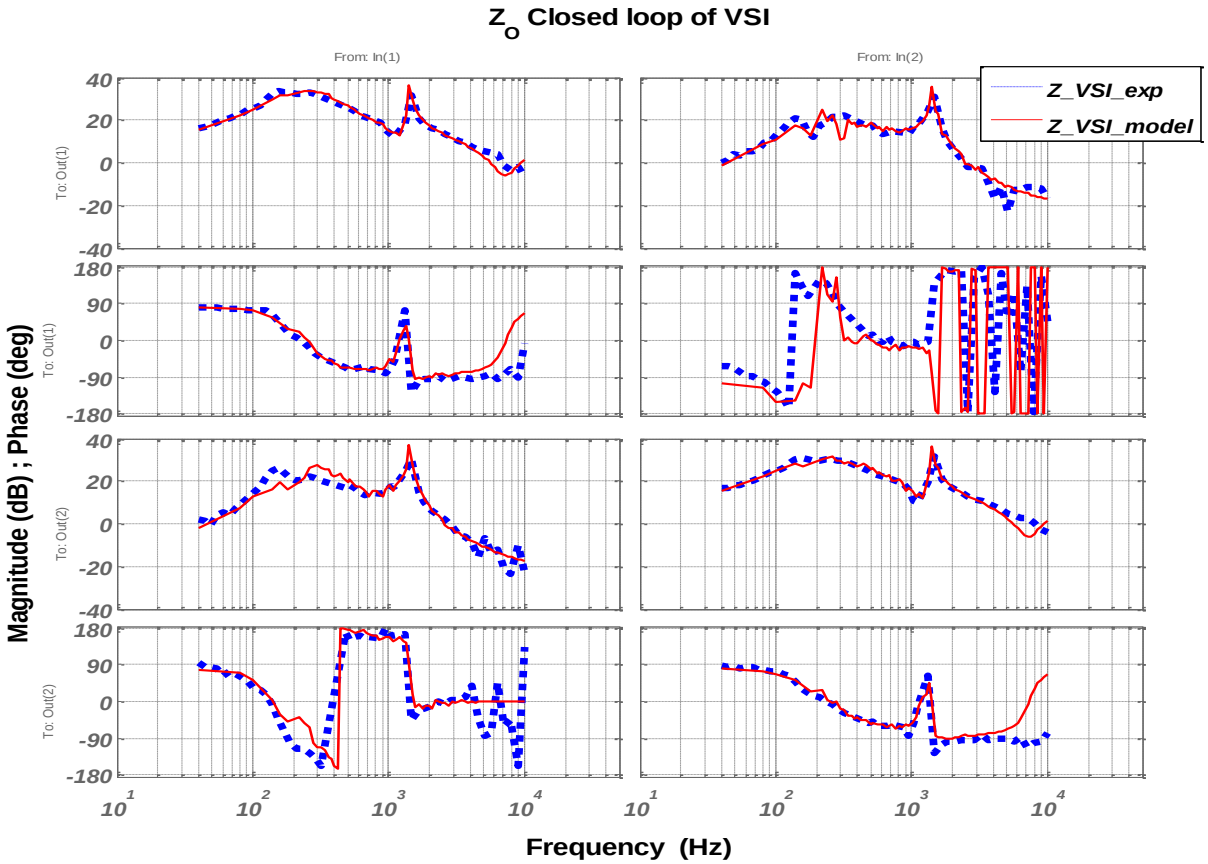

Fig. 3-11 VSI closed-loop output impedance

In the figure, the dotted line is from experimental measurement, the solid line is simulation result. From the result comparison, the experiment could match well with simulation result, which proves the effectiveness of impedance analyzer shunt current injection.

Chapter 4. THE APPLICATION OF MULTI-TONE APPROACH ON NONLINEAR LOAD

4.1. Introduction

The multi-tone approach is an important approach for STASU because it can greatly shorten the simulation time for impedance calculation, and has been verified to accurately measure the impedance of linear-time-invariant loads. However, for a non-linear load, such as a six-pulse diode rectifier, the multi-tone approach gives different results than the single-tone approach. This part explains the reason for this, and presents an algorithm to solve this problem.

The schematic of a six-pulse diode bridge rectifier is shown in Fig. 4-1, and its parameters are shown in Fig. 4-1.

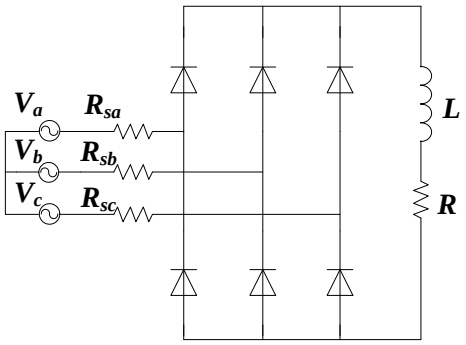

Fig. 4-1 Schematic of six-pulse diode bridge rectifier

Table 4-1 DIODE BRIDGE PARAMETERS

AC voltage amplitude	$V_a=V_b=V_c=110V$
Line frequency	$f_{line}=400Hz$
AC source resistor	$R_{sa}=R_{sb}=R_{sc}=2\ \Omega$
DC inductor	L=20mH
DC load resistor	R=100Ω

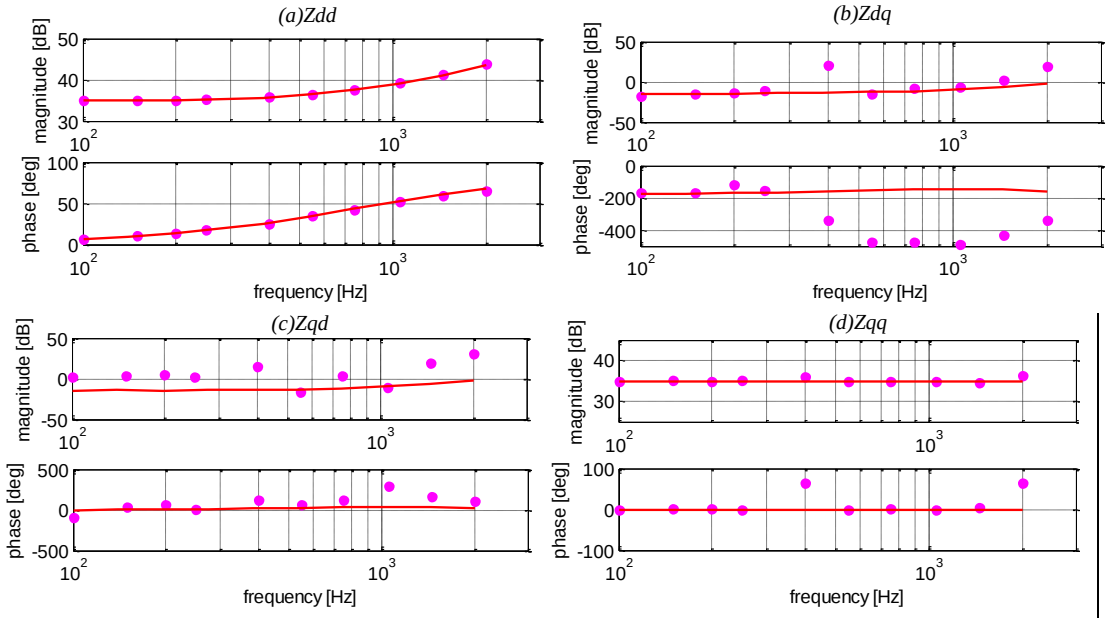

Fig. 4-2 Impedance results of the multi-tone and single-tone approaches (line: single-tone, dots: multi-tone)

Both multi-tone analysis and single-tone analysis are used to measure the input impedance of the rectifier. The results of both approaches are shown in Fig. 4-2 Impedance results of the multi-tone and single-tone approaches (line: single-tone, dots: multi-tone), which includes the frequency range from 100Hz to 2000Hz. Ten frequency points are measured. The line represents the results from the single-tone approach, and the dots represent the results from the multi-tone approach. In Z_{dq}, Z_{qd} and Z_{qq}, a difference in results between the two approaches can be observed. The following section analyzes the reason for the difference in results.

4.2. Harmonic transfer study

Since FFT is applied on the AC side to calculate impedance in the *d-q* frame, it is necessary to analyze the AC spectrum to understand the problem. As presented in [31], due to the line-commutated behavior of diode bridge rectifier, the harmonics of the AC side and DC side will be transferred to each other. Including the transfer of harmonics, the process of impedance calculation is shown in Fig. 4-3.

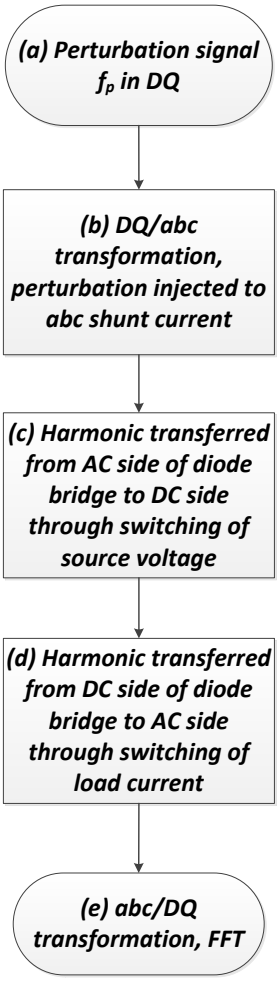

Fig. 4-3 Flowchart of impedance calculation process for diode bridge rectifier

When the frequency of the perturbation signal is defined as f_p, the amplitude of the perturbation current is I_p, and the line frequency is f_{line}:

4.2.1. Harmonic from d-q to abc

In (a), the perturbation signal of frequency f_p in *d-q* frame is generated. Assume the perturbation signals are defined as:

$$i_{pd} = I_p cos(2\pi f_p t + \varphi_d)$$
$$i_{pq} = I_p cos(2\pi f_p t + \varphi_q) \quad (4\text{-}1)$$

In (b), the perturbation signal is injected into the abc coordinate from the shunt current injector. After performing the Park transformation, the perturbation signals become:

$$\begin{bmatrix} i_{pa} \\ i_{pb} \\ i_{pc} \end{bmatrix} = T_{dq0/abc} = \begin{bmatrix} i_{pd} \\ i_{pq} \\ 0 \end{bmatrix} \tag{4-2}$$

where

$$T_{dq0/abc} = \sqrt{\frac{2}{3}} \begin{bmatrix} \cos(2\pi f_{line} + \varphi) & -\sin(2\pi f_{line} + \varphi) & \frac{1}{\sqrt{2}} \\ \cos(2\pi f_{line} + \varphi - \frac{2\pi}{3}) & -\sin(2\pi f_{line} + \varphi - \frac{2\pi}{3}) & \frac{1}{\sqrt{2}} \\ \cos(2\pi f_{line} + \varphi + \frac{2\pi}{3}) & -\sin(2\pi f_{line} + \varphi + \frac{2\pi}{3}) & \frac{1}{\sqrt{2}} \end{bmatrix}$$

The result of i_{pa} is shown in (4-2) as example:

$$\begin{aligned} i_{pa} = {} & k\cos\left[2\pi\left(f_p + f_{line}\right)t + \varphi_1\right] + k\cos\left[2\pi\left(f_p - f_{line}\right)t + \varphi_2\right] \\ & + k\sin\left[2\pi\left(f_p + f_{line}\right)t + \varphi_3\right] + k\sin\left[2\pi\left(f_p - f_{line}\right)t + \varphi_4\right] \end{aligned} \tag{4-3}$$

Where

$$k = \frac{\sqrt{6}}{6}, \varphi_1 = \varphi + \varphi_d, \varphi_2 = \varphi - \varphi_d, \varphi_3 = -\left(\varphi + \varphi_p\right), \varphi_1 = -\varphi + \varphi_p$$

In this step, a positive sequence harmonic $f_p + f_{line}$ and a negative sequence harmonic $f_p - f_{line}$ will be generated.

4.2.2. Harmonic transfer from AC to DC

In (c), due to the source impedance, the AC-side abc voltage has both positive-sequence and negative-sequence perturbation harmonics, which will be transferred to the DC side voltage.

The positive-sequence perturbation voltage harmonics could be defined as:

$$\begin{aligned} \mathrm{u}_a^+ &= U^+\cos\left[2\pi\left(f_p + f_{line}\right)t + \varphi^+\right] \\ \mathrm{u}_b^+ &= U^+\cos\left[2\pi\left(f_p + f_{line}\right)t + \varphi^+ - \frac{2\pi}{3}\right] \\ \mathrm{u}_c^+ &= U^+\cos\left[2\pi\left(f_p + f_{line}\right)t + \varphi^+ + \frac{2\pi}{3}\right] \end{aligned} \tag{4-4}$$

The negative-sequence perturbation voltage harmonics could be defined as:

$$\begin{aligned} \mathrm{u}_a^- &= U^- \cos\left[2\pi\left(f_p - f_{line}\right)t + \varphi^-\right] \\ \mathrm{u}_b^- &= U^- \cos\left[2\pi\left(f_p - f_{line}\right)t + \varphi^- - \frac{2\pi}{3}\right] \\ \mathrm{u}_c^- &= U^- \cos\left[2\pi\left(f_p - f_{line}\right)t + \varphi^- + \frac{2\pi}{3}\right] \end{aligned} \tag{4-5}$$

Assuming the commutation angle can be ignored. Therefore, the switching function of 6 pulse diode bridge rectifier can be expressed as:

$$\begin{aligned} \mathrm{s_a} &= \sum_{n=1}^{\infty} A_n cos(2n\pi f_{line} t) \\ \mathrm{s_b} &= \sum_{n=1}^{\infty} A_n cos\left(2n\pi f_{line} t - \frac{2\pi}{3}\right) \\ \mathrm{s_c} &= \sum_{n=1}^{\infty} A_n cos\left(2n\pi f_{line} t + \frac{2\pi}{3}\right) \end{aligned} \tag{4-6}$$

Where

$$A_n = \frac{4}{n\pi} \sin\frac{n\pi}{2} \cos\frac{n\pi}{6}$$

The DC voltage is given by:

$$u_{DC} = u_a s_a + u_b s_b + u_c s_c$$

The perturbation voltage transferred to the DC side could be calculated:

$$\begin{aligned} \mathrm{u}_{DC}^+ = \sum_{k=1}^{\infty} \frac{3U^+}{2} \{ & A_{6k-1} \cos\left[2\pi\left(f_p + 6kf_{line}\right)t + \varphi^+\right] \\ & + A_{6k+1} \cos\left[2\pi\left(f_p - 6kf_{line}\right)t + \varphi^+\right]\} \end{aligned} \tag{4-7}$$

$$u_{DC}^{-} = \sum_{k=0}^{\infty} \frac{3U^{-}}{2} \{A_{6k+1} \cos\left[2\pi(f_p + 6kf_{line})t + \varphi^{-}\right] + A_{6k-1} \cos\left[2\pi(f_p - 6kf_{line})t + \varphi^{-}\right]\}$$

where $u_{DC}^{+}$is the transferred positive-sequence harmonic, and u_{DC}^{-} is the transferred negative-sequence harmonic.

Thus the DC-side perturbation harmonic frequency is given by $f_p \pm 6kf_{line}(k = 0,1 \ldots \infty)$.

4.2.3. Harmonic transfer from DC to AC

In (d), due to the impedance on the DC side, the DC voltage perturbation harmonic will produce a current harmonic, which will be transferred to the AC side. As the perturbation frequency increases, the amplitude of the perturbation harmonic current $A_n = \frac{4}{n\pi} \sin\frac{n\pi}{2} \cos\frac{n\pi}{6}$ decreases. Thus the largest perturbation harmonic on the DC side is taken into consideration.

The DC side perturbation current can be defined as a DC current plus the major harmonic current:

$$i_{DC} = I_D + I_p \cos\left[2\pi f_p t + \varphi_{DC}\right] \tag{4-8}$$

The AC current is given by:

$$i_a = i_{DC} s_a$$
$$i_b = i_{DC} s_b$$
$$i_c = i_{DC} s_c$$

For simplicity only i_a is shown here:

$$i_a = \sum_{k=0}^{\infty} I_D A_{6k\pm1} \cos[2\pi(6k \pm 1)f_{line}t] + \sum_{k=0}^{\infty} \frac{I_p A_{6k\pm1}}{2} \cos\left\{2\pi\left[f_p + (6k \pm 1)f_{line}\right]t + \varphi_{DC}\right\} \tag{4-9}$$

$$+\sum_{k=0}^{\infty}\frac{I_p A_{6k\pm1}}{2}\cos\{2\pi[f_p-(6k\pm1)f_{line}]t-\varphi_{DC}\}$$

From (4-9), it is shown that the DC part of DC current I_D becomes $(6k\pm1)f_{line}$ harmonic when transferred to the AC side. The AC pert of DC current $I_p\cos[2\pi f_p t+\varphi_{DC}]$ becomes $f_p\pm(6k\pm1)f_{line}$ harmonic component when transferred to the AC side.

In sum, a perturbation harmonic on the AC side will be transferred to the DC side, then reflected back to the AC side. Equation (4-9) shows that if a perturbations signal of f_p is injected from *d-q* coordinates, it will split around the $(6k\pm1)^{th}$ $(k=0,1,2\ldots\infty)$ order line-frequency harmonic.

In the multi-tone approach, the perturbation signals of multiple frequencies are injected at the same time. In this case, the frequency components of the perturbation frequencies may overlap, which will affect the impedance results. For example, Fig. 4-4 shows the case in which two perturbation frequencies are injected at the same time. The line frequency is 400Hz, and the perturbation frequencies are 240Hz and 1360Hz. The spectrum shows that the 640Hz component is the overlap of two splitting frequencies (400+240Hz and 2000-1360Hz).

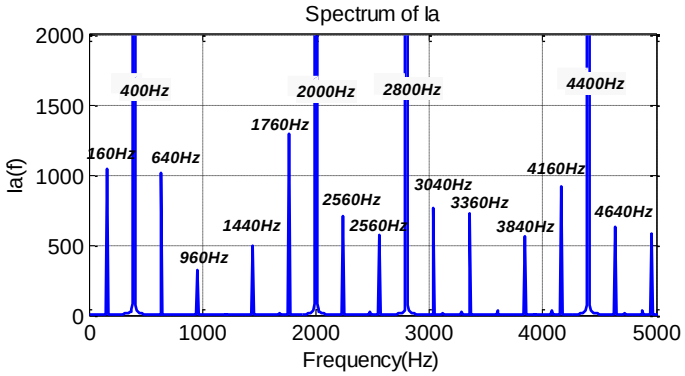

Fig. 4-4 Spectrum of line current (240Hz and 1360Hz perturbation frequencies)

When the FFT is applied to the AC side to extract the impedance, the effect of the perturbation frequencies overlapping will influence the final impedance result, which is the reason a difference in the results for the multi-tone and single-tone approaches.

It is obvious that one could limit the highest perturbation frequency to less than twice the value of f_{line} to avoid overlapping, but this would be a limitation for the frequency measurement range.

4.2.4. Frequency selection algorithm for nonlinear load

The following section proposes an algorithm to improve the multi-tone approach and enable it to measure above twice the value of f_{line}.

To get the same results from the multi-tone and single-tone approaches, the effect of overlapping perturbation frequencies should be avoided. If the measurement frequency range is lower than twice the value of f_{line}, it could be shown that there will be no overlapping, and the multi-tone approach could give the same results as the single-tone approach. If the measurement frequency range is not limited, it will be possible for the perturbation frequencies to overlap. In this paper, an iterative algorithm is developed to avoid this effect.

The parameters are defined in Table 4-2:

Table 4-2 Frequency parameter definitions

Perturbation frequencies	$f_{p1} < f_{p2} \dots < f_{pi} \dots < f_{pn}$
FFT Resolution frequency	$f_{resolutionh}$
Line frequency	f_{line}

If two perturbation frequencies overlap, for example f_{p1} and f_{p2}, from (4-9), it is shown that:

$$\begin{aligned} f_{p1} + f_{line} &= (6k \pm 1) f_{line} - f_{p2} \pm f_{resolution} \\ \rightarrow f_{p1} + f_{p2} &= (6k \pm 1) f_{line} - f_{line} \pm f_{resolution} \end{aligned} \tag{4-10}$$

Where $k = 0,1,2 \dots \infty$.

In the algorithm used in this report, the criteria for overlapping perturbation frequencies is defined as the sum of two perturbation frequencies as the multiple of the line frequency:

$$f_{p1} + f_{p2} = m f_{line} \pm f_{resolution} \tag{4-11}$$

Where $m = 0,1,2 \dots \infty$.

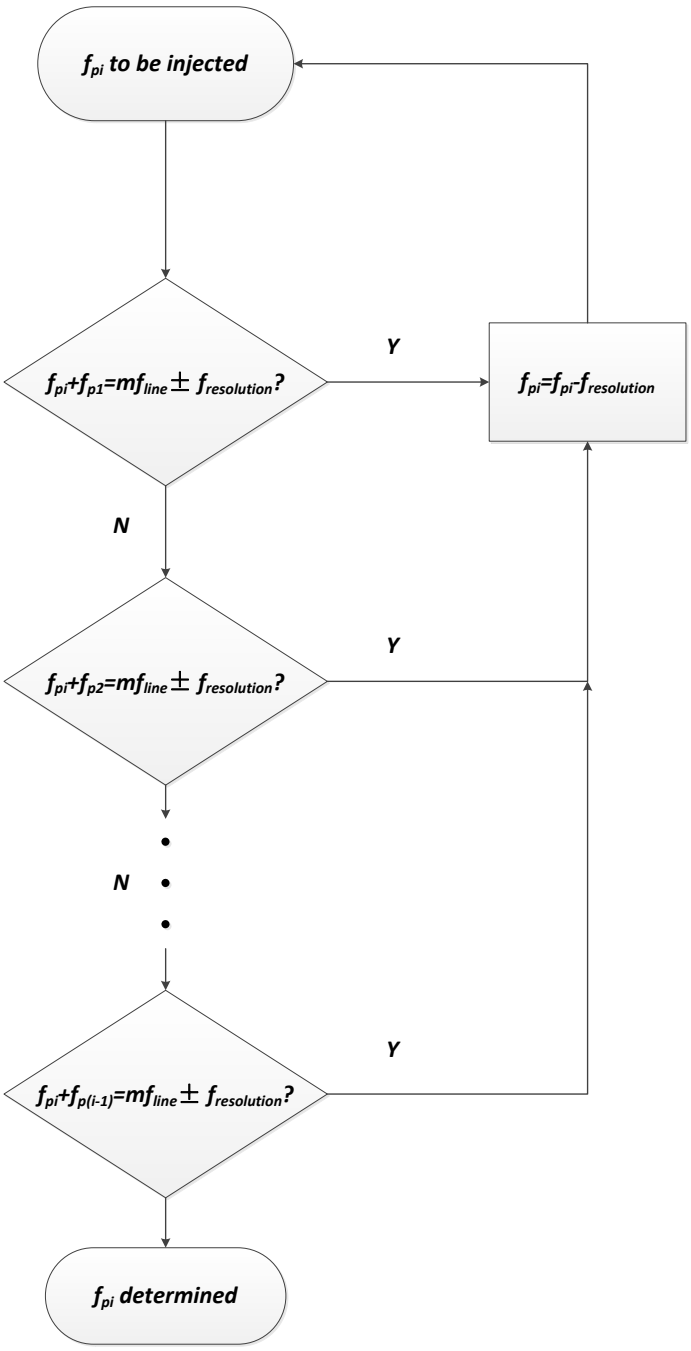

Fig. 4-5 Flowchart of algorithm to avoid perturbation frequencies overlapping

The flowchart of the algorithm is shown in Fig. 4-5. Before perturbation frequency f_{pi} is determined, it will be checked against the criteria along with all the perturbation frequencies lower than f_{pi}. If f_{pi} overlaps with any of the other perturbation frequencies, it will be adjusted by $f_{resolution}$, and this process will be repeated until no more perturbation frequencies overlap.

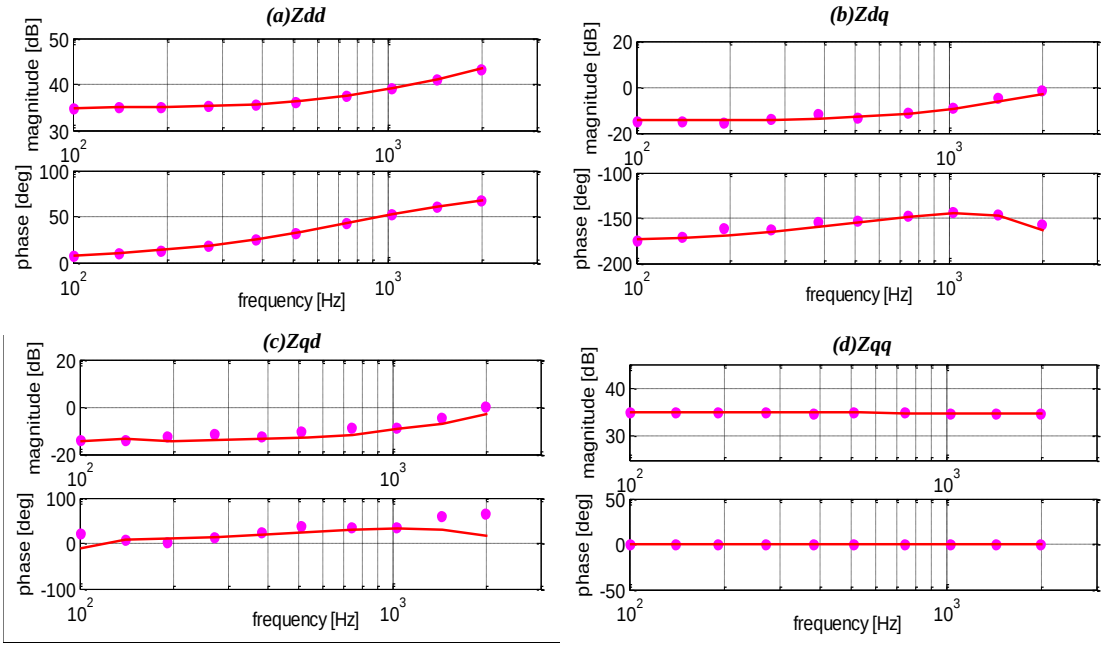

Fig. 4-6 Impedance result comparison of improved multi-tone and single-tone approach (line: single tone, dots: multi-tone)

With the improvement of this algorithm, the result of the multi-tone approach is compared again with single-tone approach, and the results are shown in Fig. 4-6. The frequency measurement range is from 100Hz to 2000Hz, and there are 10measured frequency points, which is the same as Fig. 4-2. Fig. 4-6 shows that by using the algorithm to avoid overlapping perturbation frequencies, the multi-tone approach can give the same results as the single-tone approach for a six-pulse diode-bridge application.

4.2.5. Other potentially applicable cases

The algorithm is derived from 6-pulse diode bridge rectifier. However it may be applicable for other nonlinear loads.

Other multi-phase diode rectifiers should have similar effects. For example 12-pulse diode rectifier, if we inject a perturbation signal f_p in d-q coordinate into a twelve pulse diode rectifier, on the AC side, $f_p \pm (12k \pm 1)f_{line}$ harmonic should be observed. Thus this algorithm should be able to work. This case will be shown in the following sections.

In [34][35], it is shown that dead time in a voltage source inverter will have voltage distortion effect on the DC side. Then back to the AC side, $(6k \pm 1)f_{line}$ harmonic could be observed in

the phase current. This behavior is similar as 6-pulse diode rectifier. Therefore the algorithm may be also working. VSI and AFE with significant dead time still need further study.

4.3. Simulation and experimental verification

4.3.1. Simulation verification

The simulation model is shown in Fig. 4-7.

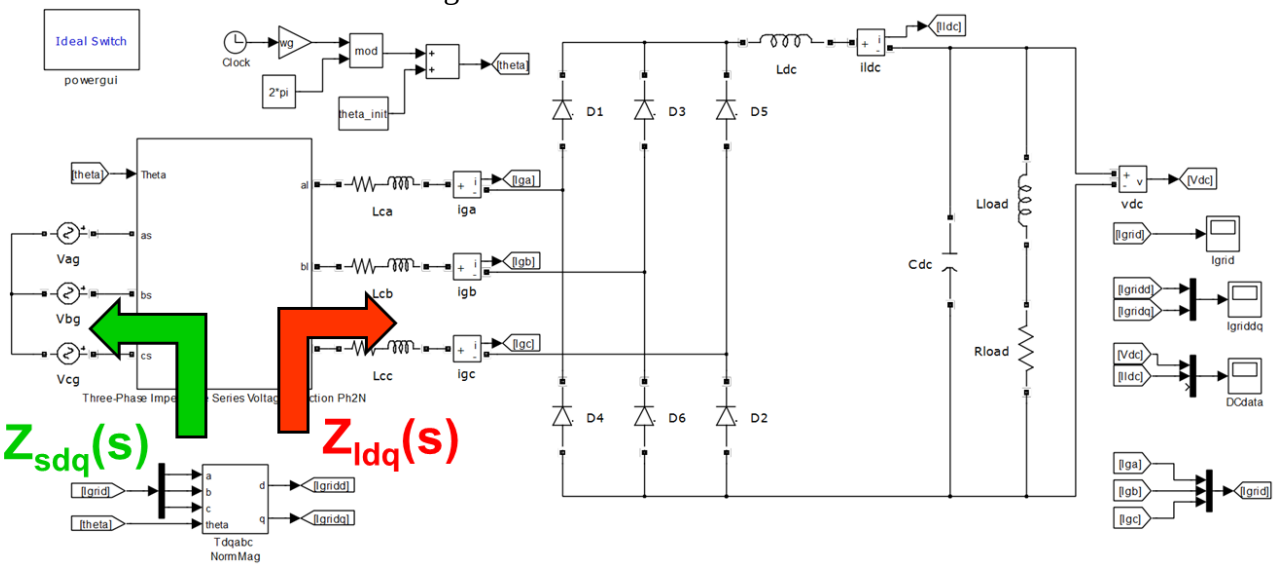

Fig. 4-7 6-pulse diode bridge rectifier impedance simulation measurement

This model includes commutation inductance at the AC side and LC filter at the DC side. The parameters are shown in Table 4-3.

Table 4-3 Parameters of 6 pulse diode rectifier simulation model

Source voltage rms	V_{grms}=120 V;	DC side inductance	L_{dc}=500 μH;
Source frequency	f_g=400 Hz;	DC side capacitance	C_{dc}=0.22mF;
AC side inductance	L_c=0.17 mH;	Load inductance	L_{load}=100 μH;
Diode parameters	V_d=0.9 V; R_d=3 mΩ;	Load resistor	R_{load}=14.5 Ω
Impedance measurement block	*Three phase mtone series voltage P2N*	Measurement range	*40Hz~1800Hz*

Number of points	*20*	Perturbation amplitude	*0.1V*

The input impedance is measured by three different methods: single-tone, multi-tone without algorithm compensation and multi-tone with algorithm compensation. The result is shown in Fig. 4-8.

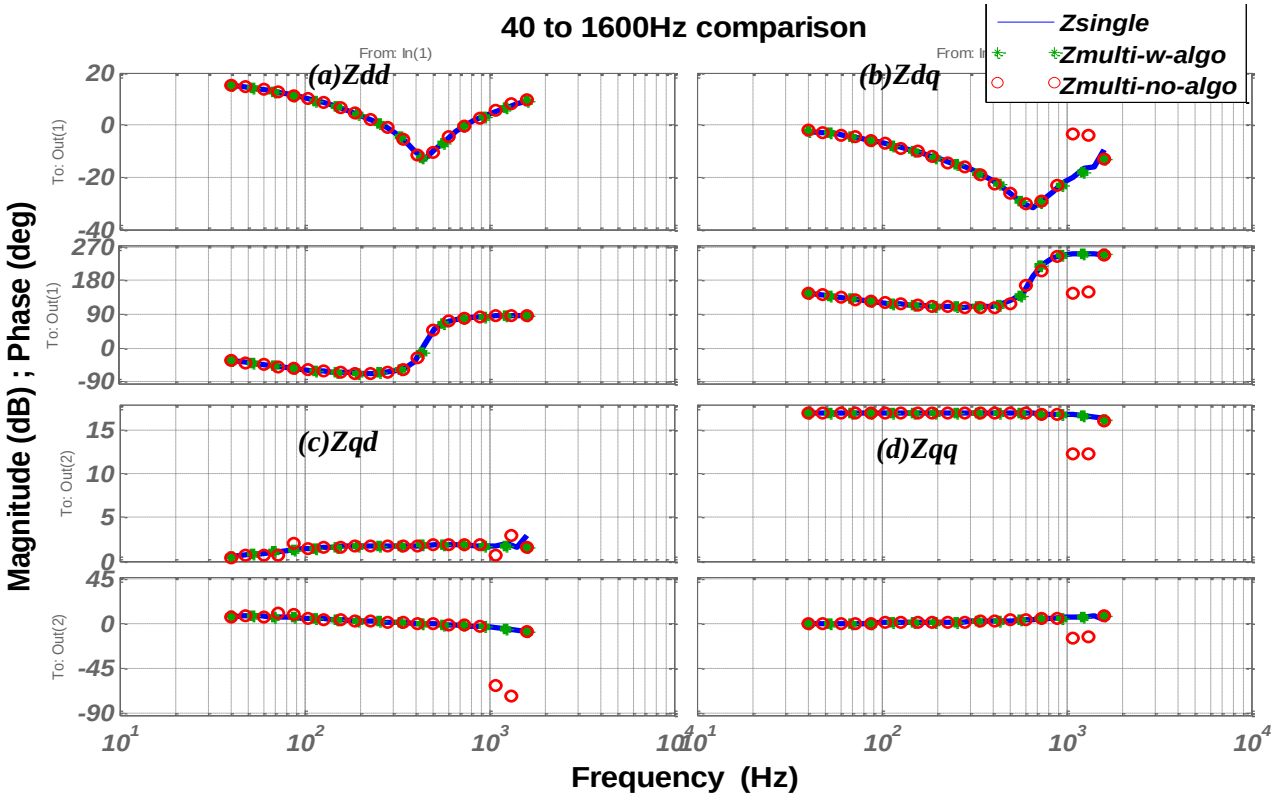

Fig. 4-8 Result comparison for 6-pulse diode bridge rectifier input impedance

The single-tone result is used here as reference. The dots are result from multi-tone with compensation. The circles are result from multi-tone without compensation. It is shown clearly that with algorithm compensation multi-tone approach could achieve same results with single-tone method.

4.3.2. Twelve-pulse diode bridge rectifier

Twelve-pulse diode bridge rectifier should also have the effect of side-band harmonics. Unlike six pulse diode rectifier, if we inject a perturbation signal f_p in *d-q* coordinate into a twelve pulse diode rectifier, on the AC side, $f_p \pm (12k \pm 1)f_{line}$ harmonic should be observed. This is also covered by the algorithm in 4.2.4. Therefore twelve pulse diode rectifier is tested with the frequency selection algorithm for nonlinear loads.

The simulation model for 12-pulse diode rectifier is shown in Fig. 4-9.

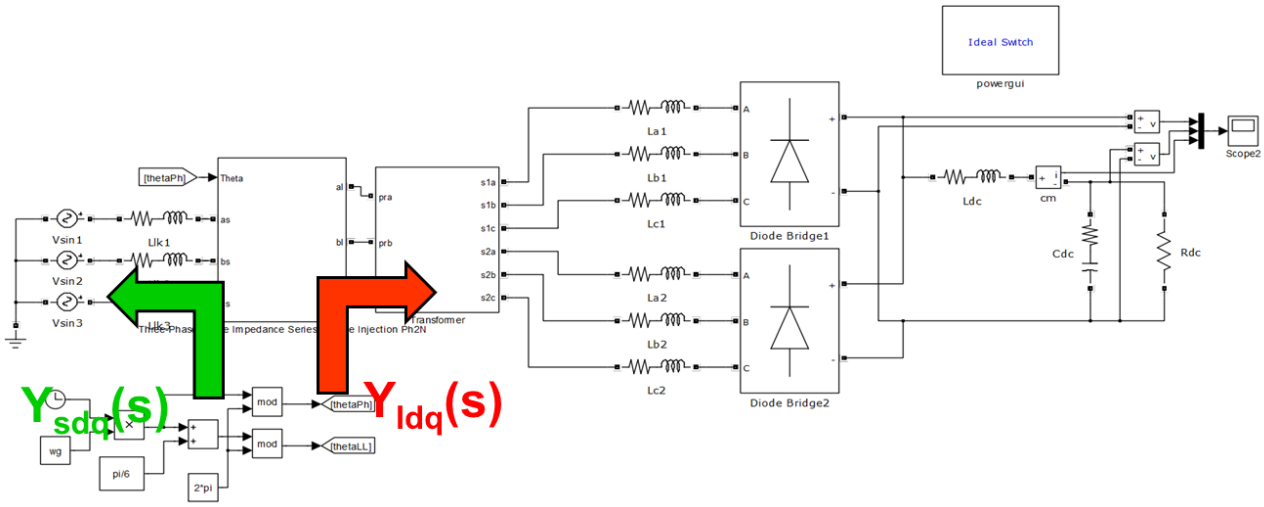

Fig. 4-9 12-pulse diode bridge rectifier impedance simulation measurement

The parameters are shown in Table 4-4.

Table 4-4 Parameters of 12-pulse diode rectifier simulation model

Source voltage rms	V_{grms}=120 V;	DC side inductance	L_{dc}=1.6 mH; R_{ldc}=60 mΩ;
Source frequency	f_g=60 Hz;	DC side capacitance	C_{dc}=1.05 mF; R_{cdc}=35 mΩ;
AC side inductance	L_c=220 μH; R_{lc}=30 mΩ;	Leakage inductance	L_{load}=80 μH;
Diode parameters	V_d=0.9 V; R_d=3 mΩ;	Load resistor	R_{load}=12.7 Ω
Impedance measurement block	*Three phase mtone series voltage P2N*	Measurement range	*10Hz~1000Hz*

Number of points	*40*	Perturbation amplitude	*0.05V*

The input impedance is measured by three different methods: single-tone, multi-tone without algorithm compensation and multi-tone with algorithm compensation. The result is shown in Fig. 4-10.

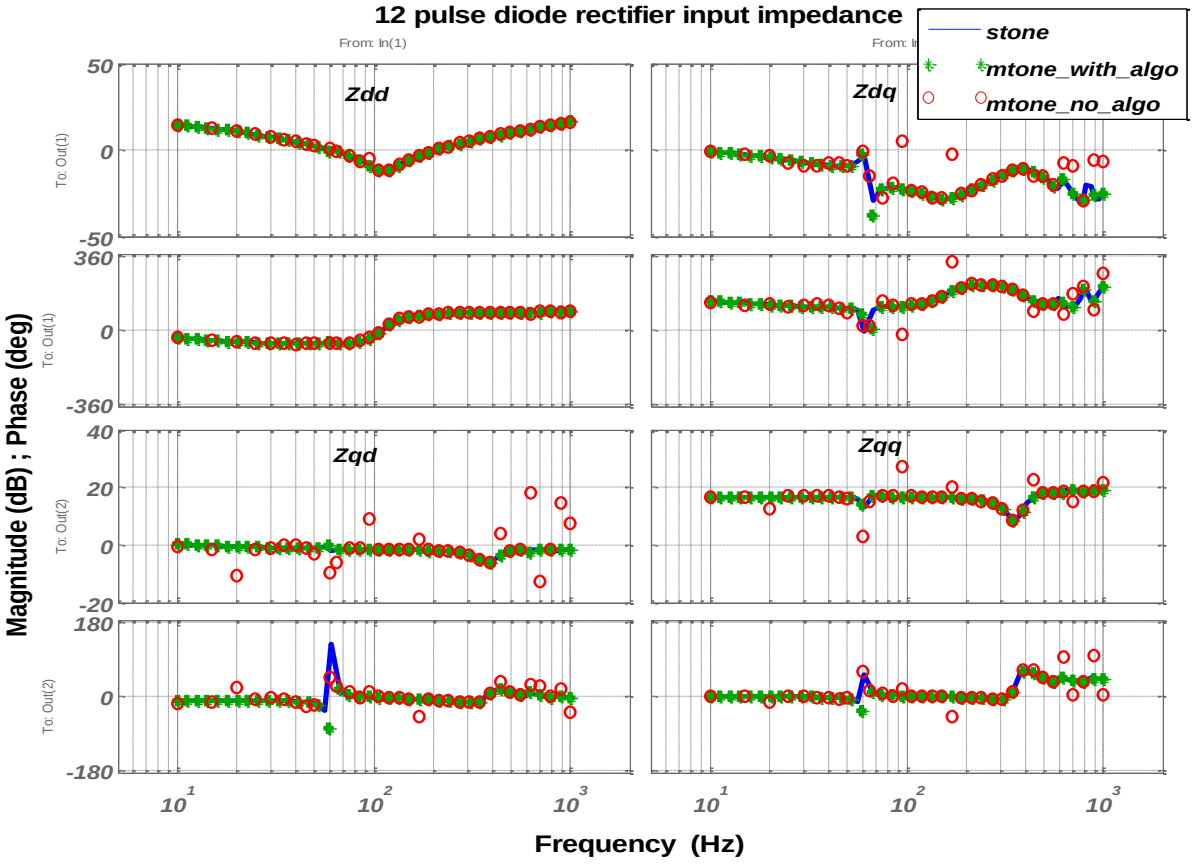

Fig. 4-10 Result comparison for 12-pulse diode bridge rectifier input impedance

The single-tone result is used here as reference. The dots are result from multi-tone with compensation. The circles are result from multi-tone without compensation. It is shown clearly that with algorithm compensation multi-tone approach could achieve same results with single-tone method

4.3.3. Experimental verification

The experiment setup is shown in Fig. 4-11.

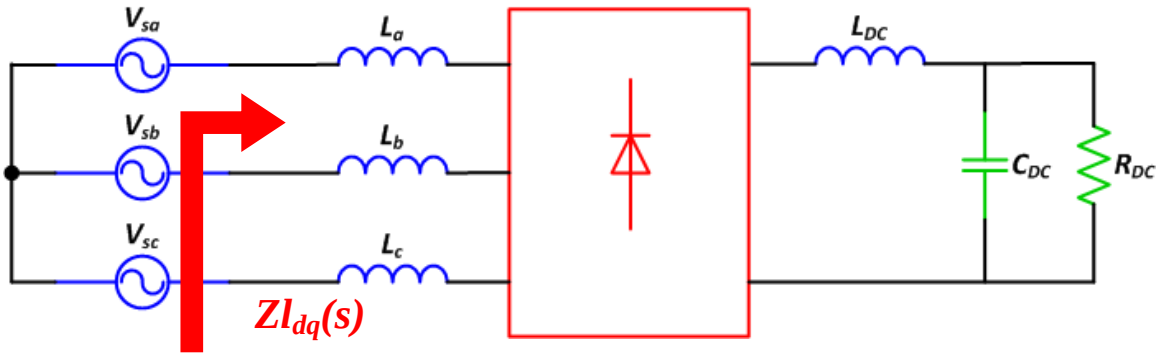

Fig. 4-11 6 pulse diode rectifier input impedance measurement setup

The parameters are shown in Table 4-5.

Table 4-5 Parameters of 6 pulse diode rectifier

Source voltage rms	V_s=60 V;	DC side inductance	L_{dc}=1.2 mH;
Source frequency	f_g=60 Hz;	DC side capacitance	C_{dc}=0.6 mF;
Source impedance	R_S=3 mΩ;	Load resistor	R_{load}=15 Ω
AC side inductance	L_c=0,22 mH;		

Multi-tone approach is used for two times. In the first measurement, 5 perturbation frequencies are arbitrarily chosen to have overlapping. In the second measurement, 5 perturbation frequencies are arbitrarily chosen not to have overlapping.

The perturbation frequencies of the first measurement are shown in Table 4-7. The highlighted frequencies have overlapping.

Table 4-6 Perturbation frequencies of the first measurement

$f_{pert}(Hz)$	20	**40**	**80**	**160**	**200**

The perturbation frequencies of the first measurement are shown in Table 4-7. The highlighted frequencies have overlapping.

Table 4-7 Perturbation frequencies of the second measurement

$f_{pert}(Hz)$	10	20	33	75	155

The results are compared with single-tone measurement, as shown in Fig. 4-12.

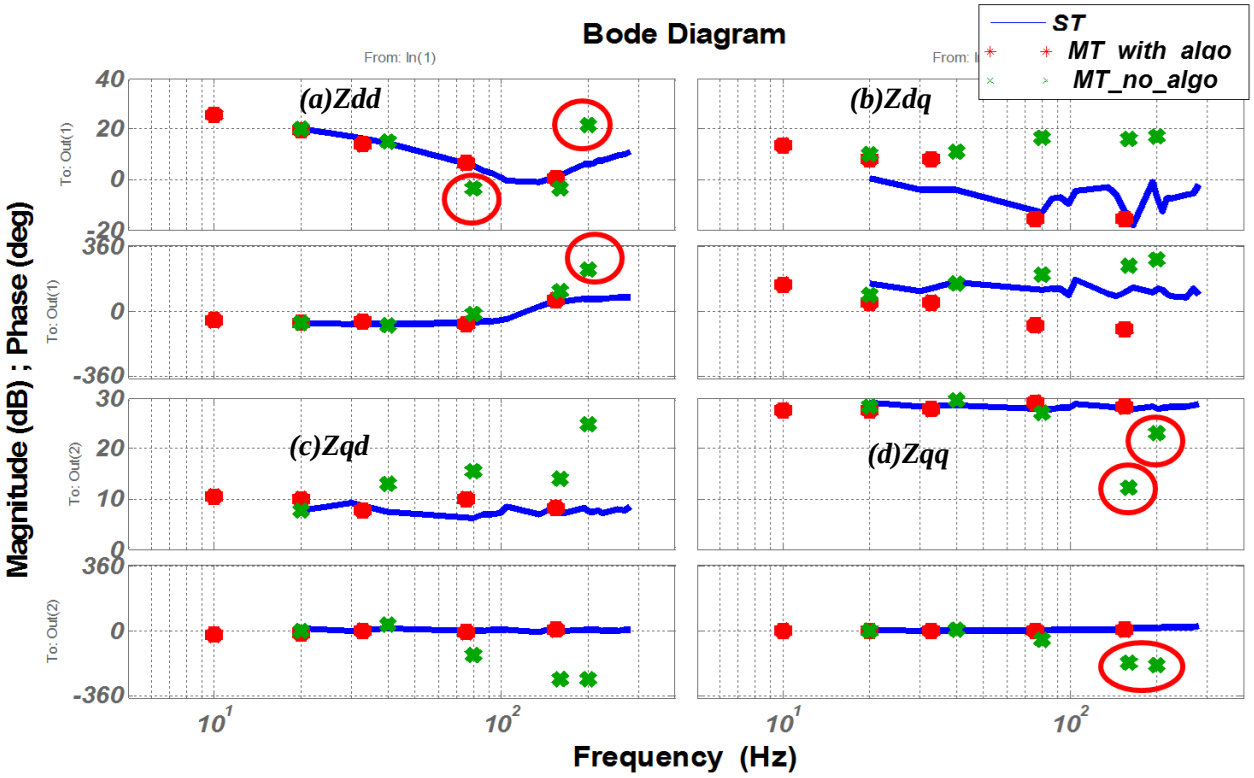

Fig. 4-12 Input impedance comparison for 6 pulse diode bridge rectifier

The single-tone result is used here as reference. The dots are result from multi-tone with compensation. The crosses are result from multi-tone without compensation. It is shown clearly that with algorithm compensation multi-tone approach could achieve much better results than without compensation: without algorithm compensation, the error in amplitude can be as large as 15dB.

4.4. Summary

When multi-tone is used to measure nonlinear loads such as 6 pulse diode bridge rectifier, it may give incorrect results because of the overlapping with side-band harmonics of perturbation frequencies. An algorithm is developed to overcome this problem. This algorithm has been verified by both simulation and experiment.

Chapter 5. SUMMARY AND FUTURE WORK

5.1. Summary

This thesis presents a comprehensive software suite for AC system stability analysis. A new perturbation method is proposed and verified.

In chapter 2, the impedance measurement theory is introduced. A few previous impedance measurement methods are reviewed. After that the design of STASU is discussed. Algorithm on how to select perturbation frequencies is discussed. In chapter 3, some efforts are made to recovery a low power impedance tester, and implement series voltage injection, which is a new capability of the system.

In order to save measurement time, multi-tone method is applied in AC system in chapter 4. This method has been implemented in STASU. It is experimentally verified with the measurement of passive loads. When it is applied on multi-pulse diode bridge rectifier, the multi-tone method may give inaccurate measurement results due to the overlapping of side-band harmonics. This phenomenon is studied and an algorithm is proposed to solve the problem. This algorithm is verified experimentally.

5.2. Future work

Multi-tone method has been experimentally verified to effectively measure the *d-q* impedances. This method has been implemented in STASU, and it is proved to save a lot of simulation time compared with single-tone method.

In the experiment verification of multi-tone method, the whole process needs manual operation. In the future, this method can be also implemented as an automated perturbation method in the impedance tester.

The frequency selection algorithm for nonlinear loads has been experimentally verified with 6-pulse diode rectifier. Due to the limited time, only a measurement of 5 frequency points is achieved. In the future it should be tested with more points. Moreover, the simulation results show that this algorithm also work for 12-pulse diode rectifier. The case of VSI and AFE with significant dead time has not been studied yet, which should be an important future work. After simulation study, these test cases should also be repeated by experiment.

Appendix A. STASU programmer's manual

A.1. Introduction

STability Analysis Suite (STASU) is a comprehensive software tool for DC and AC system impedance calculation and stability analysis. The tool is developed under Matlab/Simulink.

For impedance calculation, the impedance calculation blocks are implemented in "mylib.mdl", hence they can be directly inserted into SimPowerSystems switching models and extract impedances. Several m-files are developed to control the simulation process and calculate impedances from sampled data.

For stability analysis, all the functions are implemented in m-files, which are named corresponding to the functions.

A graphical user interface is developed in m-file, to provide the user a convenient access to the tool. The buttons of GUI are all connected with the STASU files. Once the user click on one button, the corresponding m-files will be called and run automatically.

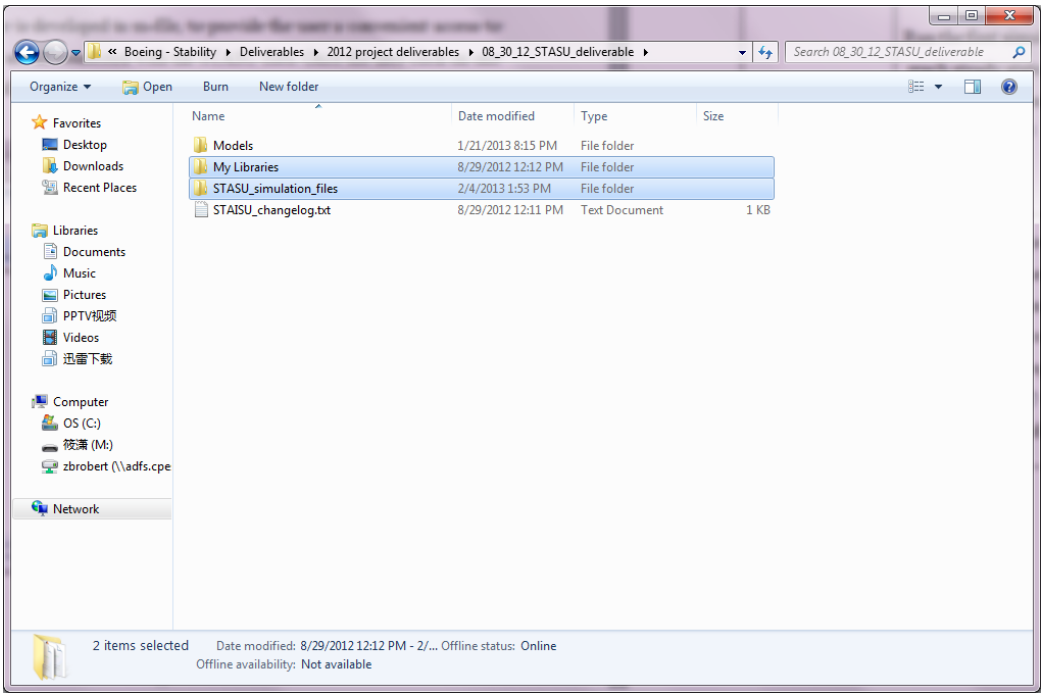

Fig_Apx. A-1 STASU file folders

As shown in Fig_Apx. A-1, the STASU package consists of 2 file folders. In "My Libraries", there is 1 mdl file containing all the impedance measurement blocks. In "STASU_simulation_files", there are all the m-files used in STASU.

The m-files and mdl file are classified and listed in Table_Apx. A-1.

Table_Apx. A-1 Summary and classification of STASU files

Type of the STASU file	Description	STASU file name
Graphical user interface	Provides a convenient access to control STASU	Stability_software_suite.m OnChangedSelTabs.m Stability.png VICTO.png
Impedance calculation	Run the first simulation to reach steady state, record line frequency and all the states	zac_mtone_sci_1.m, zac_mtone_svi_1.m, zac_stone_sci_1.m, zac_stone_svi_1.m, zdc_mtone_sci_1.m, zdc_mtone_svi_1.m, zdc_stone_sci_1.m, zdc_stone_svi_1.m.
	Select FFT window based on line frequency information from the 1st simulation, calculation perturbation frequency based on the FFT window and user's specification	zac_mtone_sci_2.m, zac_mtone_svi_2.m, zac_stone_sci_2.m, zac_stone_svi_2.m, zdc_mtone_sci_2.m, zdc_mtone_svi_2.m, zdc_stone_sci_2.m, zdc_stone_svi_2.m.

	Run the second simulation, inject perturbations, record voltage and current responses at the interface and calculate impedances	zac_mtone_sci_3.m, zac_mtone_svi_3.m, zac_stone_sci_3.m, zac_stone_svi_3.m, zdc_mtone_sci_3.m, zdc_mtone_svi_3.m, zdc_stone_sci_3.m, zdc_stone_svi_2.m.
	Impedance calculation blocks library	mylib.mdl
Stability analysis	Plot GNC or simplified GNC for AC stability analysis, plot SISO Nyquist Criteria for DC stability analysis, and over-plot impedance data to check interaction. The autoZplot function is to automatically plot impedance when the user specifies the impedance file. Smooth is to provide the user an option to use smoothed data (moving averaged data) or raw data for analysis.	GNC_plot.m SNC_plot.m SISO_plot.m Multiple_impedace_plot.m AutoZplotL.m AutoZplotS.m Smooth.m

A.2. Flowcharts

In this part, the flowcharts for different kinds of STASU m-files are listed. The flowcharts and the annotations in the m-files can provide sufficient information for a programmer about STASU.

The flowchart of GUI is shown in Fig_Apx. A-2.

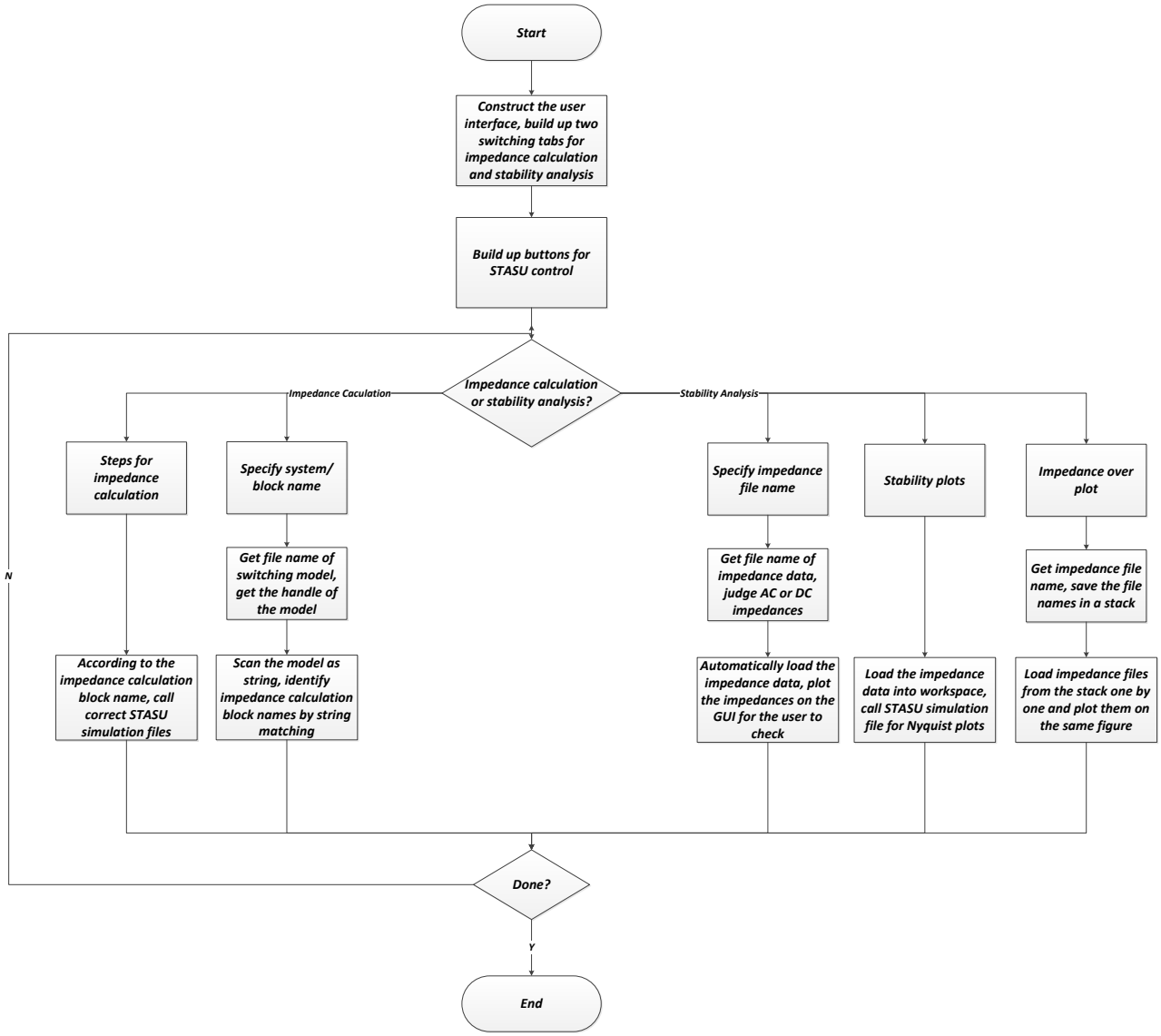

Fig_Apx. A-2 Flowchart of GUI

Virtual impedance calculation consists of 3 steps: 1, run the first simulation to reach steady state; 2, calculate perturbation frequencies and FFT window; 3, run the second simulation with perturbation and calculate impedance.

The flowchart of the first step is shown in Fig_Apx. A-3.

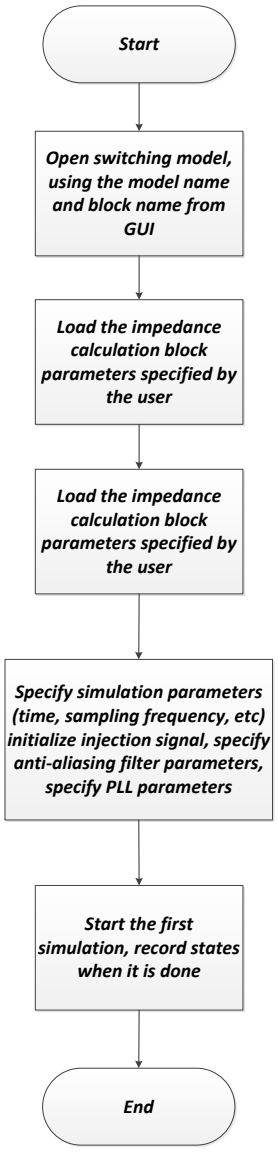

Fig_Apx. A-3 Flowchart of 1st step of impedance calculation

The flowchart of the second step is shown in Fig_Apx. A-4.

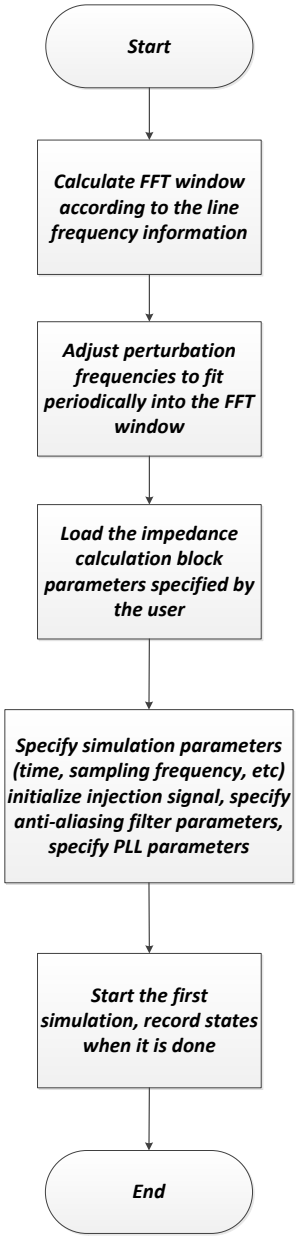

Fig_Apx. A-4 Flowchart of 2nd step of impedance calculation

The flowchart of the third step is shown in Fig_Apx. A-5.

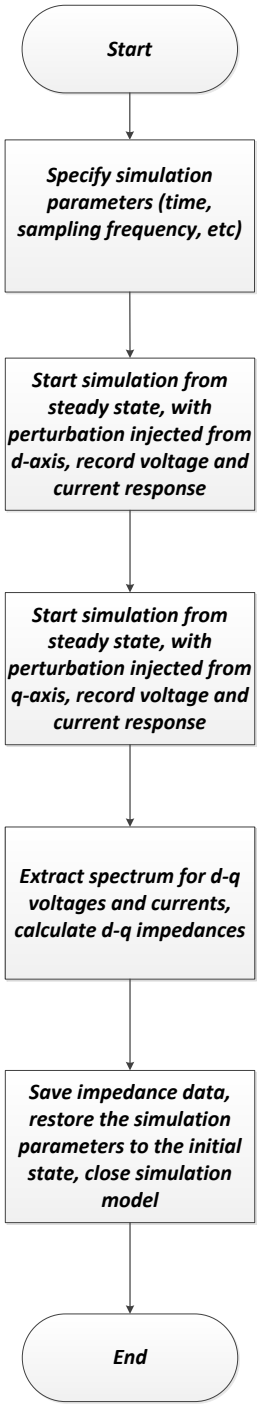

Fig_Apx. A-5 Flowchart of 3rd step of impedance calculation

The flowcharts of virtual impedance calculation have been shown above. Detailed explanation of the m-files is included in the annotation of the codes.

For stability analysis, the flowcharts have been shown in Fig_Apx. A-6. There is code annotation in the m-files too.

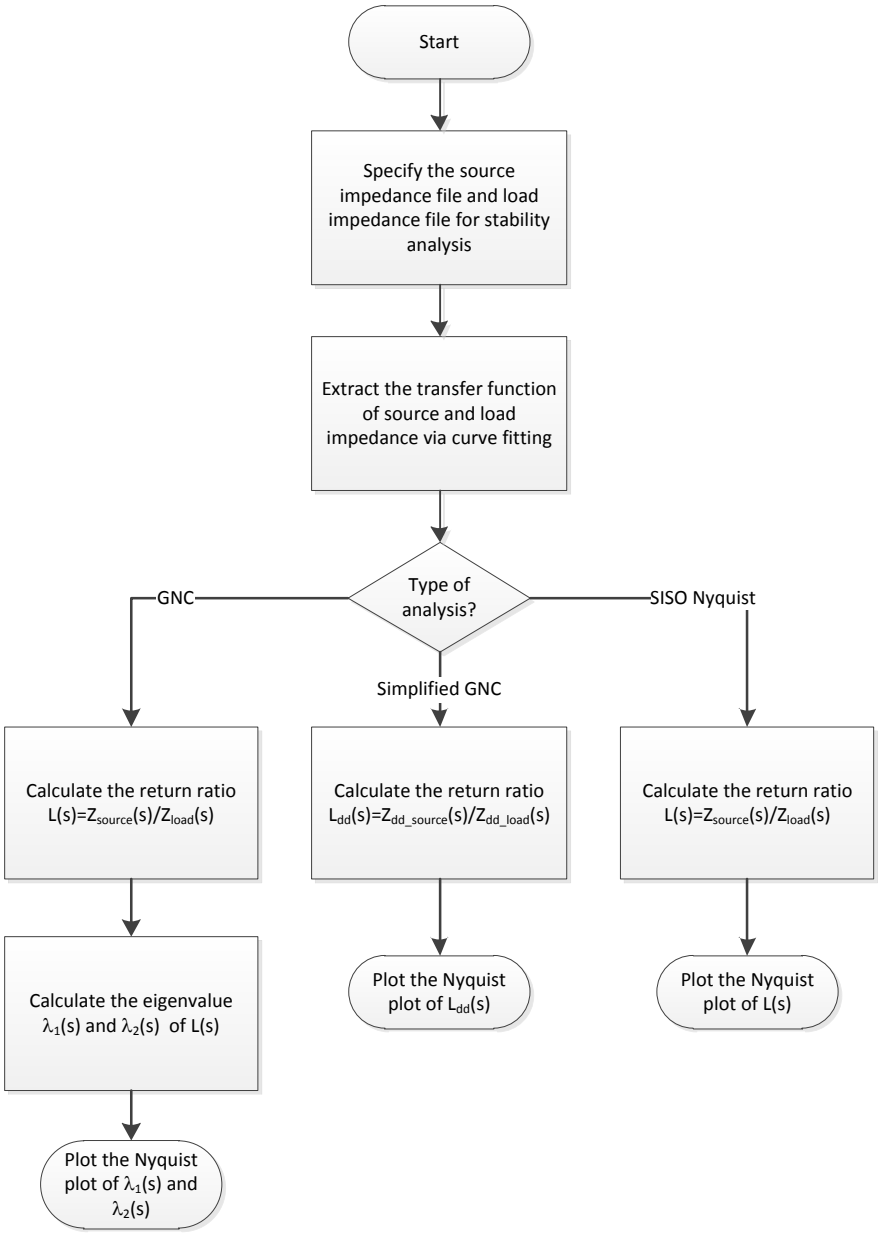

Fig_Apx. A-6 Flowchart of stability analysis

A.3. Impedance calculation blocks

Besides the m-files, the other important component for STASU is the impedance calculation blocks library. This library is implemented with SimPowerSystems Toolbox and Simulink Toolbox. In this section, a Shunt Current block will be taken as an example, to explain how the library is implemented.

Fig_Apx. A-7 shows an overview of impedance calculation blocks library mylib.mdl. To do any modifications on the library, the library needs to be first unlocked, by clicking on Edit-> Unlock Library.

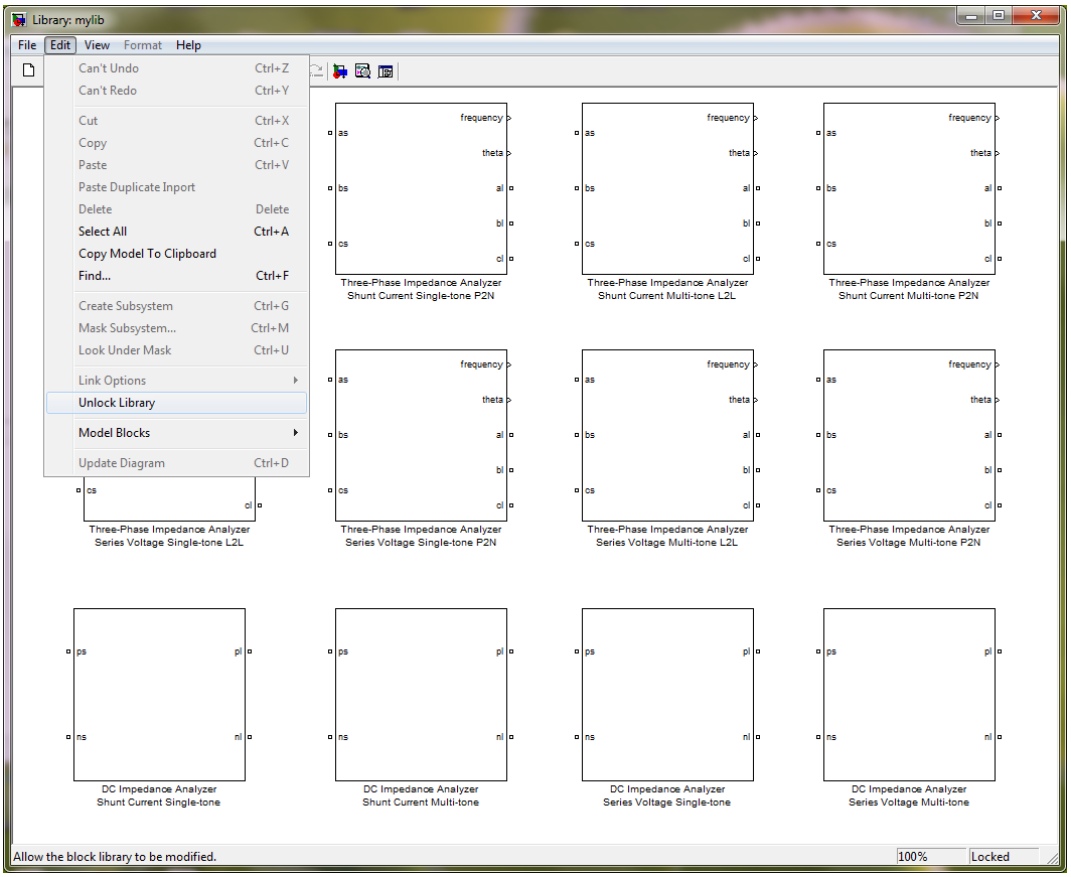

Fig_Apx. A-7 Overview of impedance calculation blocks

Let's take the "Three-Phase Impedance Analyzer Shunt Current Multi-tone P2N" block as an example, to illustrate how the impedance measurement blocks are implemented and what is the structure.

There are several block parameters which the user could specify to control the simulation. In order to add/delete/edit these parameters, the programmer could right click the block and choose "Edit Mask". It is shown in Fig_Apx. A-8.

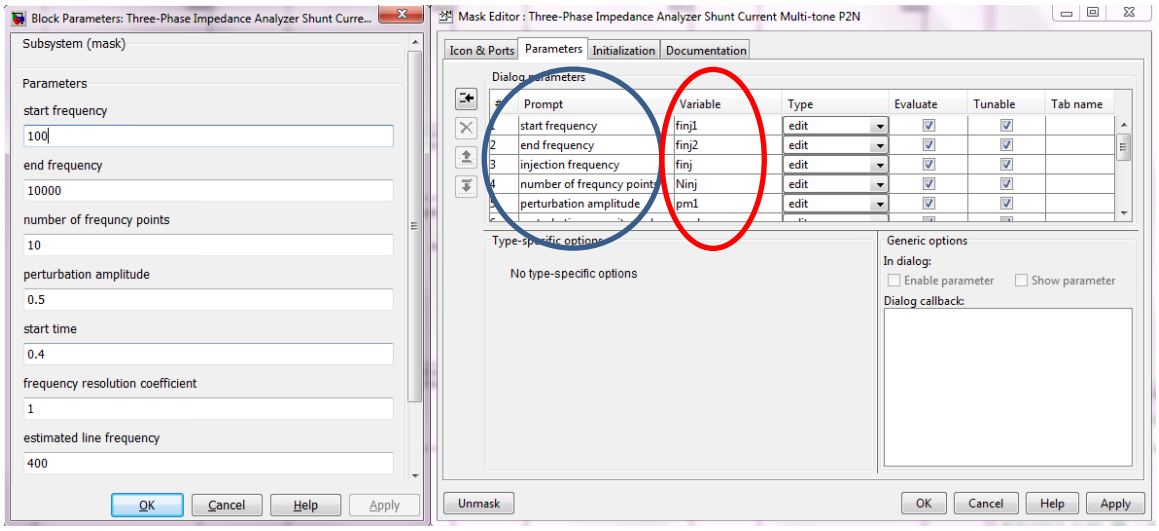

Fig_Apx. A-8 Block mask editing

The "Prompt" stands for the variable names shown as block parameters. The "Variable" is the specific variable in the workspace, which will be used by the STASU m-files.

Under the mask, the impedance measurement block is implemented with SimPowerSystem library components. It is shown in Fig_Apx. A-9.

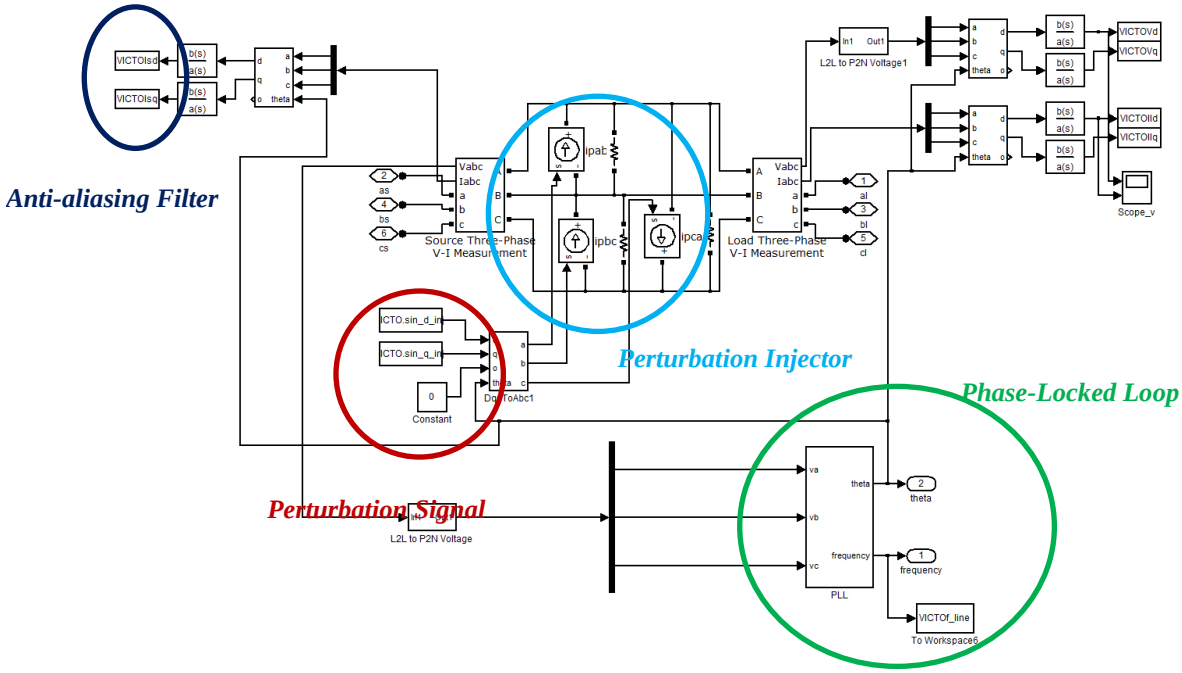

Fig_Apx. A-9 Impedance calculation block implementation

As shown above, at the AC interface, three controlled current source is connected as injector. The voltage and currents at the interface are sensed by the "V-I Measurement" block. The line-to-line voltages are transferred to phase-to-neutral voltages and sent to PLL for system angle tracking. The perturbation signals are generated in MATLAB workspace. All the voltages and currents are passed through anti-aliasing filters and stored in MATLAB workspace, which is shared with STASU m-files. The parameters for PLL and anti-aliasing filters are all specified by the STASU m-files.

A.4. Summary

In this appendix, the flowcharts of all the m-files for STASU have been provided. The implementation of impedance calculation blocks has been explained. With this information, STASU could be modified and enhanced for future use.

Appendix B. Impedance Analyzer

B.1. Introduction

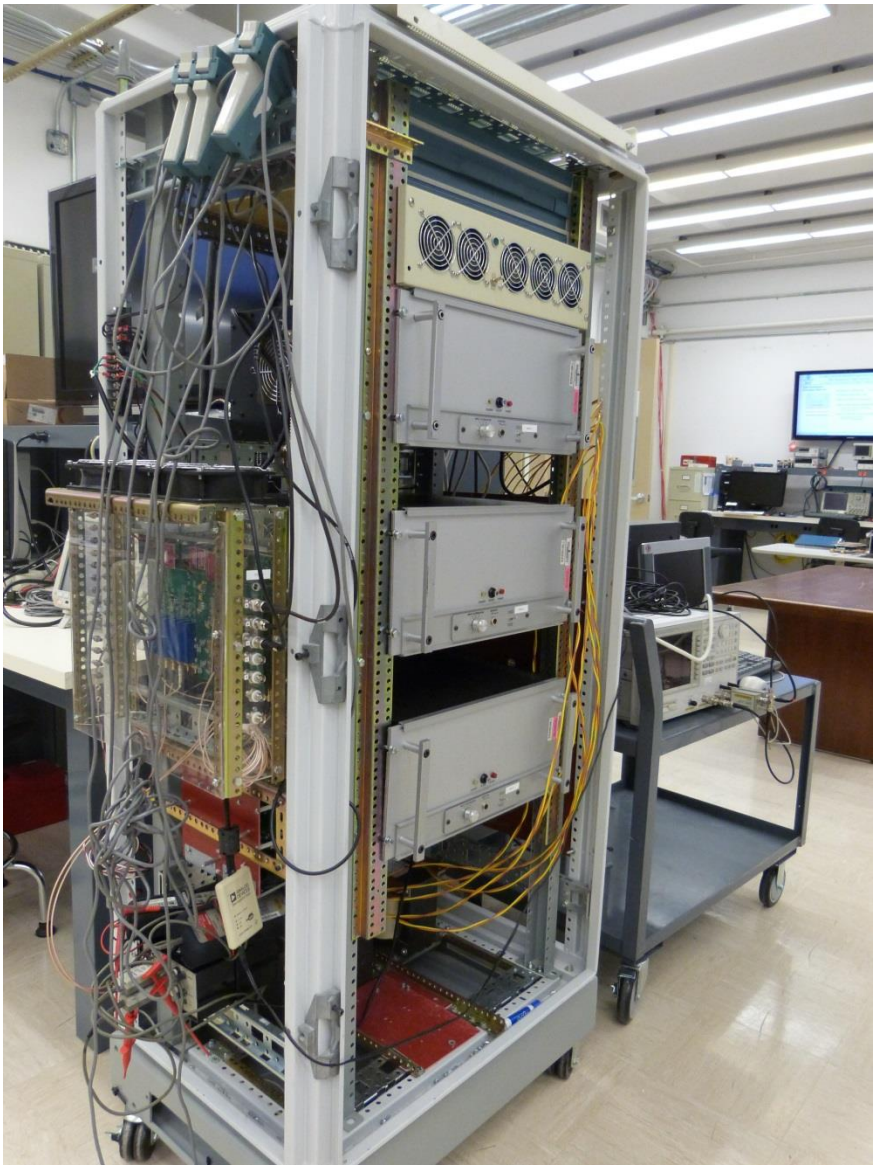

Fig_Apx. B-1 Low-power impedance analyzer

The low-power impedance analyzer is built to measure d-q impedances of three phase AC systems. It can be configured to inject either perturbation currents or perturbation voltages. In this section, the instruction for the low-power impedance analyzer will be given.

B.2. Instrument specs

B.2.1. Power amplifier AE7570 specs

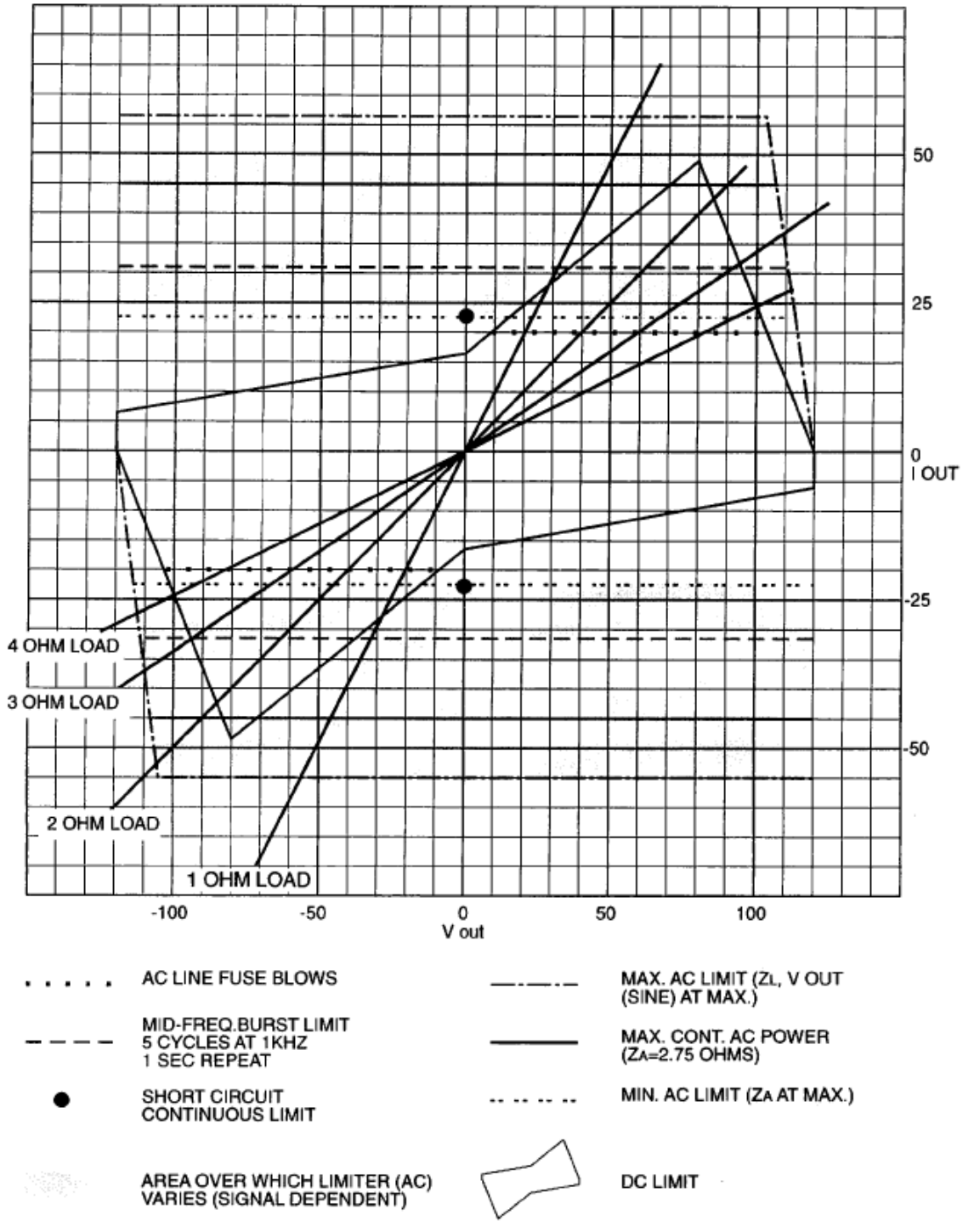

Fig_Apx. B-2 Output specs of AEtechron 7570

The power rating of AEtechron 7570 amplifier is 1kW.

As shown in Fig_Apx. B-2. The maximum output AC voltage (RMS) can be 120V, the maximum output AC current can be 20A (AC line fuse limit).

B.2.2. Transformer specs

Fig_Apx. B-3 POWERTRAN transformer

The transformer is a 1:5 AC transformer from POWERTRAN, rated at 3kVA.

For the high voltage side, the max AC RMS voltage is 600V, the max current is 5A. For the low voltage side, the max voltage is 120V, the max current is 25A.

B.2.3. Impedance analyzer specs

B.2.3.1. Shunt Current Configuration

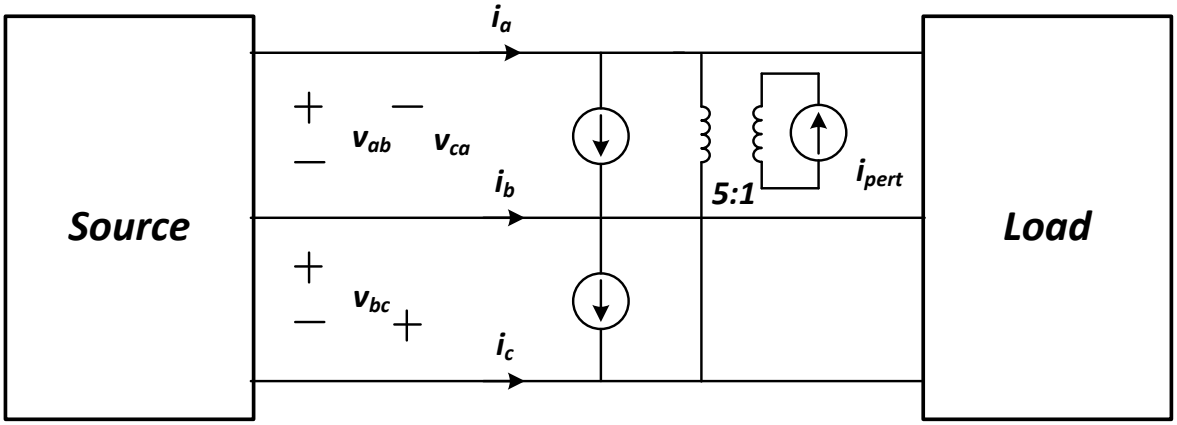

Fig_Apx. B-4 Shunt current configuration

In this configuration, the amplifier is switched into controlled current source. It is connected to the AC bus through the transformer. The high voltage side of the transformer is connected to the bus, and the low voltage side to the amplifier.

The max AC line-to-line voltage allowed is 600V RMS (600V line-to-line voltage on the system side and 120V on the amplifier side). It can measure the typical 220V and 110V three-phase AC systems. There is no critical limitation on system current.

For 220V system, the line-to-line system voltage is 381V. The voltage on the amplifier side is 76.2V. The amplifier can inject up to 20A perturbation current. The perturbation current on the system side is up to 4A. Suppose the injection power is 10% of the system power. The system current can be 40A, and the system power rating is 25kW in this case.

There are breakers in series with the transformer for over-current protection. 25A breakers are on the low-voltage side and 5A on the high-voltage side.

B.2.3.2. Series Voltage Configuration

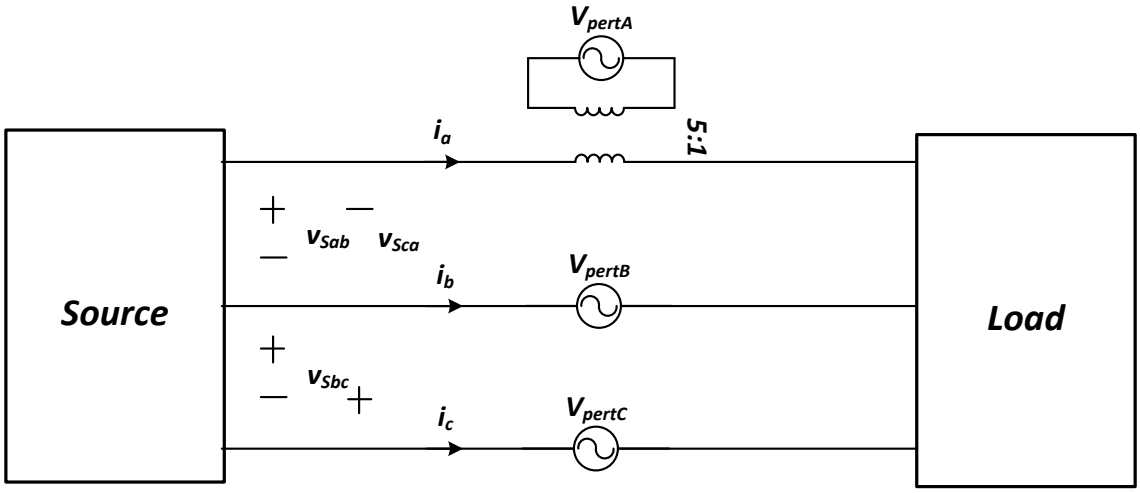

Fig_Apx. B-5 Series voltage configuration

In this configuration, the amplifier is switched into controlled voltage source. It is connected to the AC bus through the transformer. The low voltage side of the transformer is connected to the bus, and the high voltage side to the amplifier.

The max AC phase current allowed is 25A RMS (limited by the circuit breaker). There is no critical limitation on system voltage.

If the system phase current is 25A. The current on the amplifier side is 5A. The amplifier can inject up to 110V perturbation voltage. The perturbation voltage on the system side is up to 22V.

Suppose the injection power is 10% of the system power. The system phase-to-neutral voltage can be 220V, and the system power rating is 16.5kW in this case.

B.3. Wiring Diagram

In this part, the wiring diagrams of impedance analyzer will be illustrated. The connection of AC bus and the connection of signal cables will be respectively

B.3.1. Bus connections

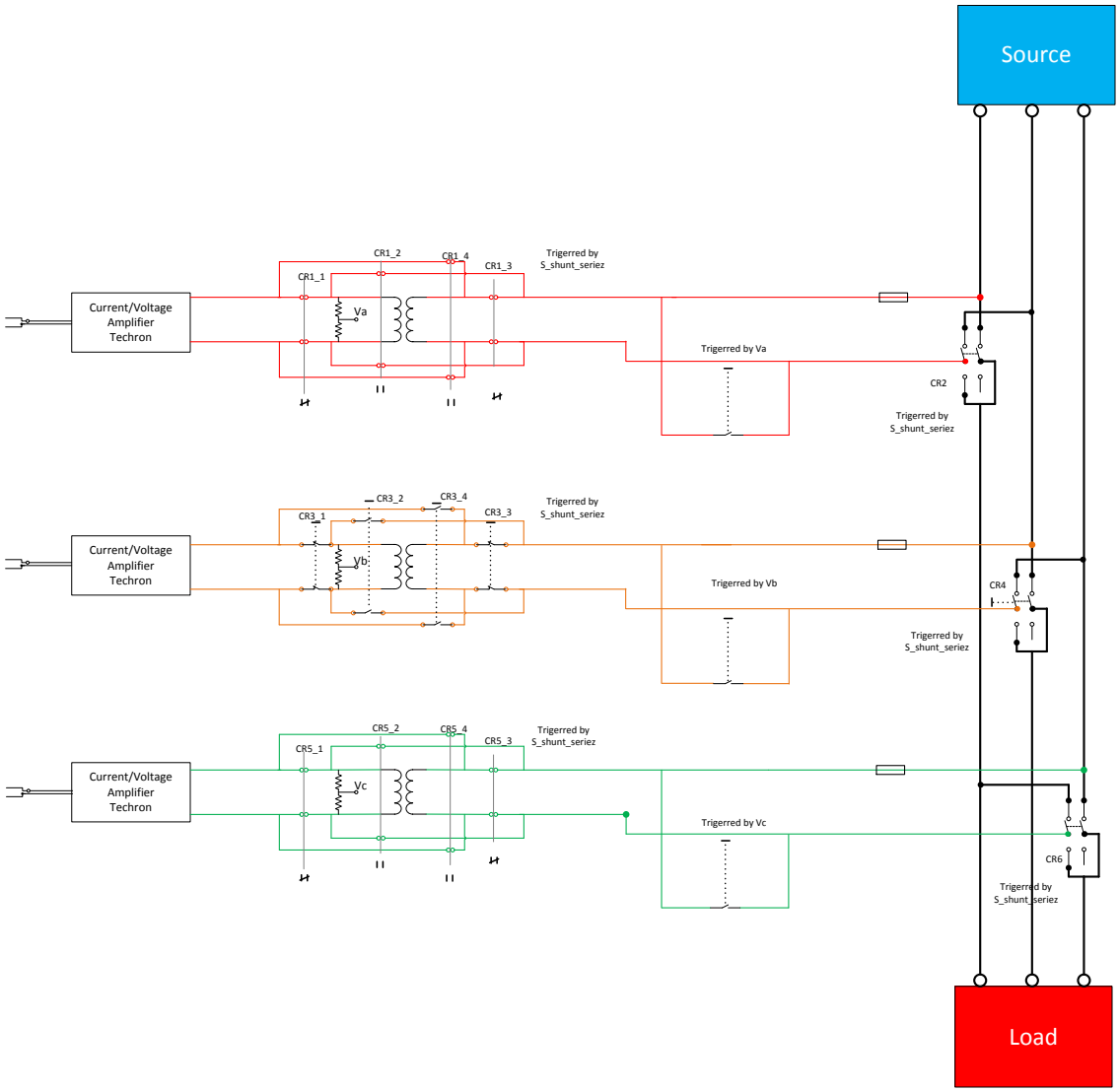

Fig_Apx. B-6 Bus connection diagram

The wiring diagram for impedance analyzer is shown in Fig_Apx. B-6. The amplifiers are connected to the bus through the transformers.

There are 3 DPDT relays on the bus, to switch the connection of transformers, between shunt current and series voltage. There are 6 DPDT relays, to turn over the high voltage side and low voltage side of the transformers, when the shunt current/ series voltage configuration changes.

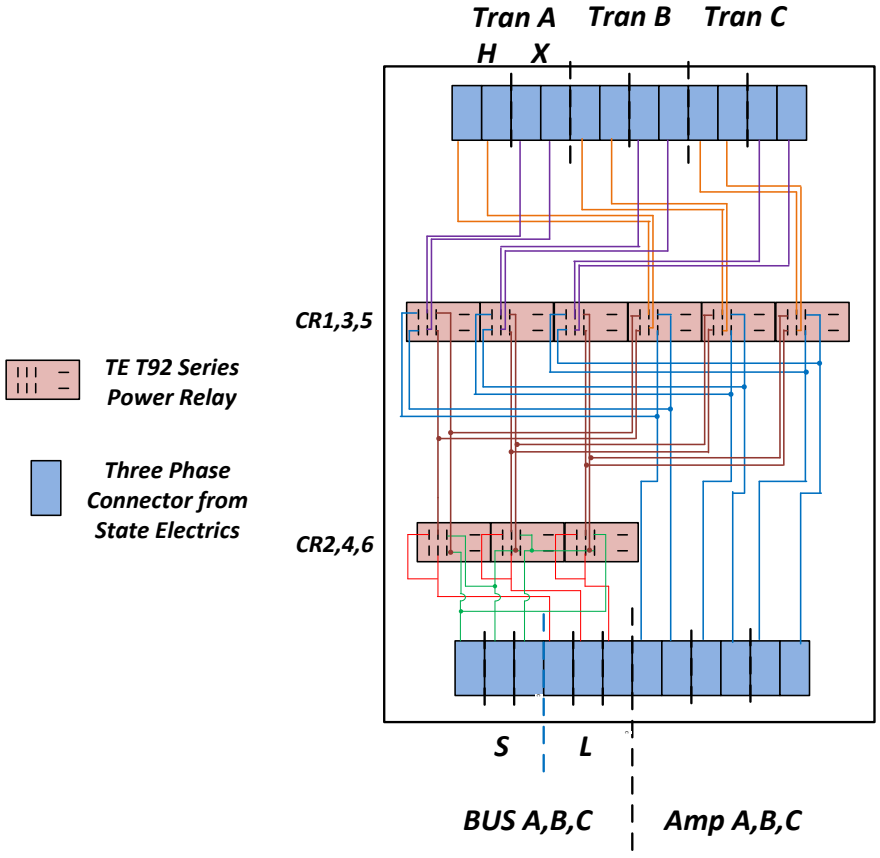

Fig_Apx. B-7 Wiring diagram for relay board

The DPDT relays are all rated at 30A, controlled by 110V AC voltage. They are mounted on a single board. The diagram is shown in Fig_Apx. B-7. On the top left of this board, there is a switch to control the bus configuration (shunt or series).

B.3.2. Signal connections

For signal connections, there are three parts to be interconnected: Network Analyzer (NA), Personal Computer (PC), and digital controller (UC and signal board).

PC is connected with NA via GPIB-USB cable.

PC is connected with UC via USB cable.

NA is connected with UC via two BNC cables.

All the sensors are connected to the UC.

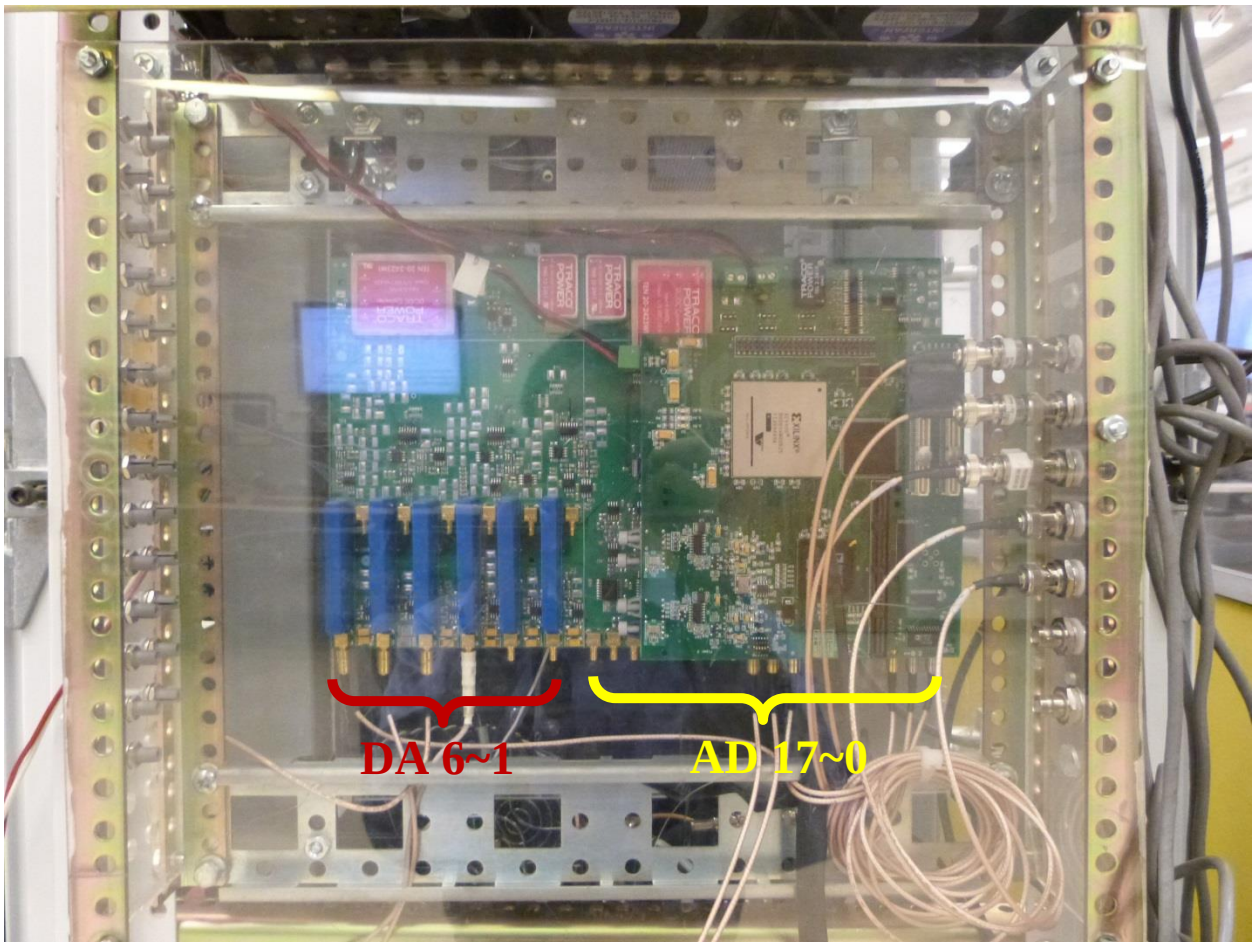

Fig_Apx. B-8 Signal channels of UC

As shown in Fig_Apx. B-8. UC has 6 DA channels and 18 AD channels. The function of the channels used in impedance analyzer are listed in Table_Apx. B-1.

Table_Apx. B-1 Signal channels discription

Channel	Function
AD 0	Sensed current I_a
AD 1	Sensed current I_b
AD 2	Sensed current I_c
AD 7	Input perturbation signal from NA
AD 8	Sensed voltage V_a

AD 9	Sensed voltage V_b
AD 10	Sensed voltage V_c
DA 3	Reference signal to amplifier A
DA 4	Reference signal to amplifier B
DA 5	Reference signal to amplifier C
DA 6	Output signal to NA

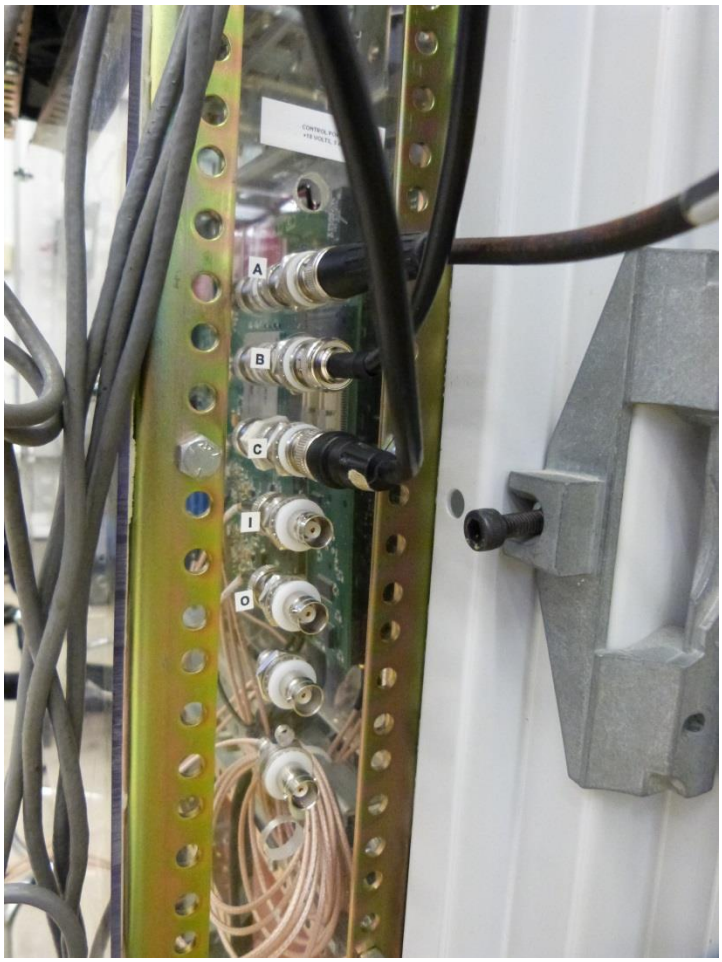

Fig_Apx. B-9 BNC connector panel

As shown in Fig_Apx. B-9, there is a BNC connector panel, for the BNC connection with instruments outside the cabinet. The “A,B,C” labeled ports are connected with corresponding

current sensors. The “I” is connected with the “R” port of NA. The “O” is connected with the “A” port of NA.

B.4. Protection

B.4.1. Introduction

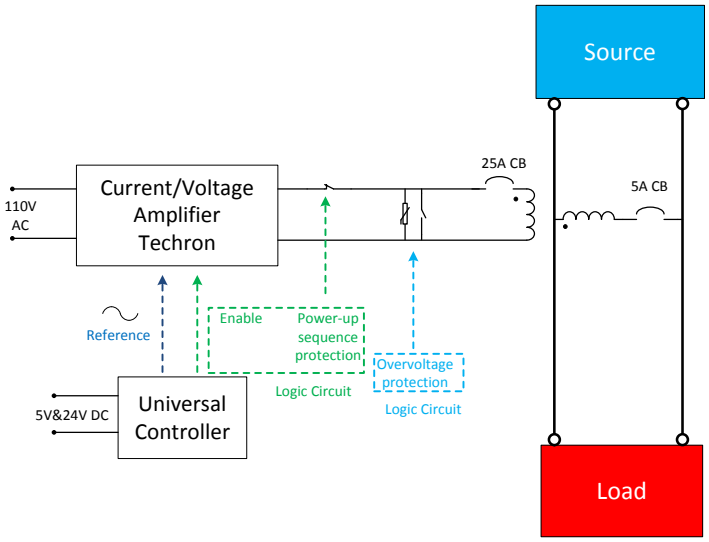

(a)

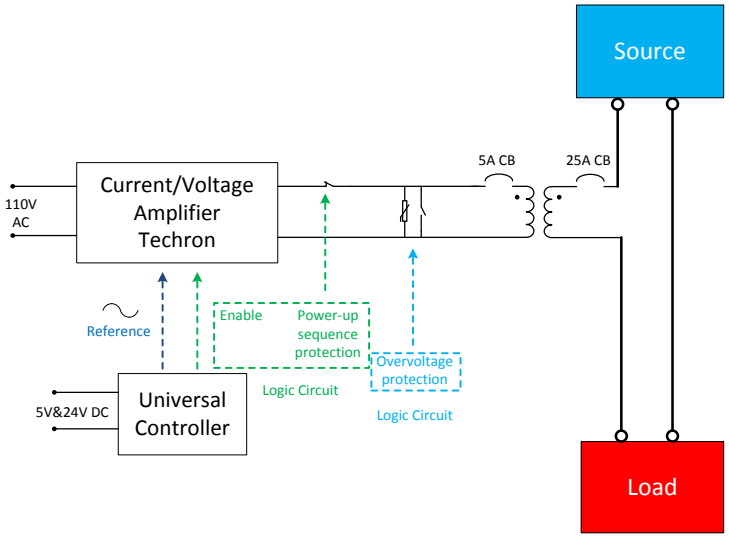

(b)

Fig_Apx. B-10 Summary of impedance analyzer protection

The summary of protection for shunt current configuration and series voltage configuration is shown in Fig_Apx. B-10. There are three protections:

1. Over-current protection : implemented with circuit breaker
2. Power-up sequence protection : connect the amplifiers to the bus only when all the amplifiers are on, enable the output of the amplifiers only when digital controller is running
3. Overvoltage protection: mainly used in series voltage configuration, short the amplifiers' output when the voltage stress is too high

B.4.2. Power up sequence protection

The power up sequence protection (PUS) is implemented with a circuit board and a solid state relay Crydom D53TP50C.

The picture, the schematic and the PCB of the PUS board is shown in Fig_Apx. B-11.

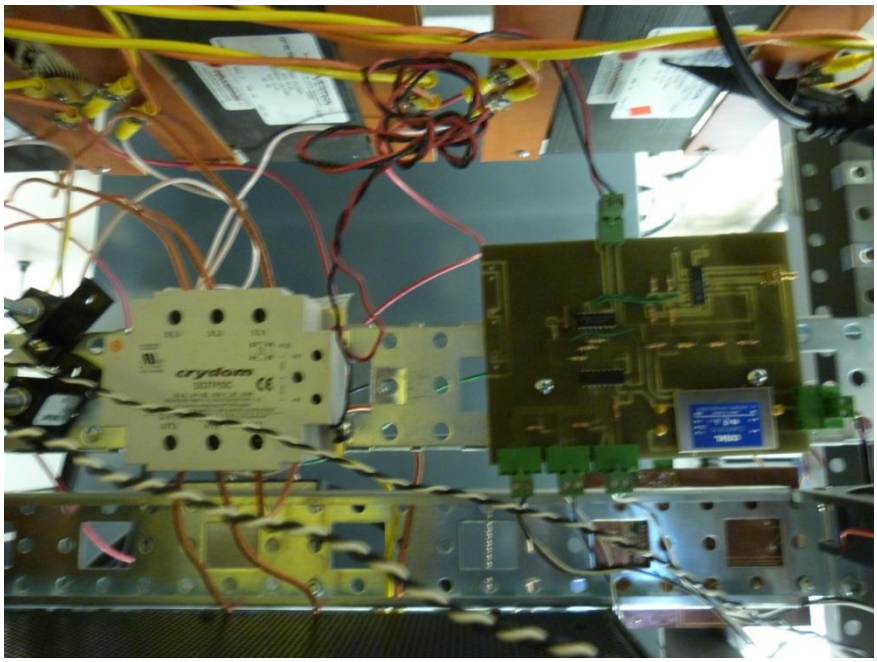

(a)

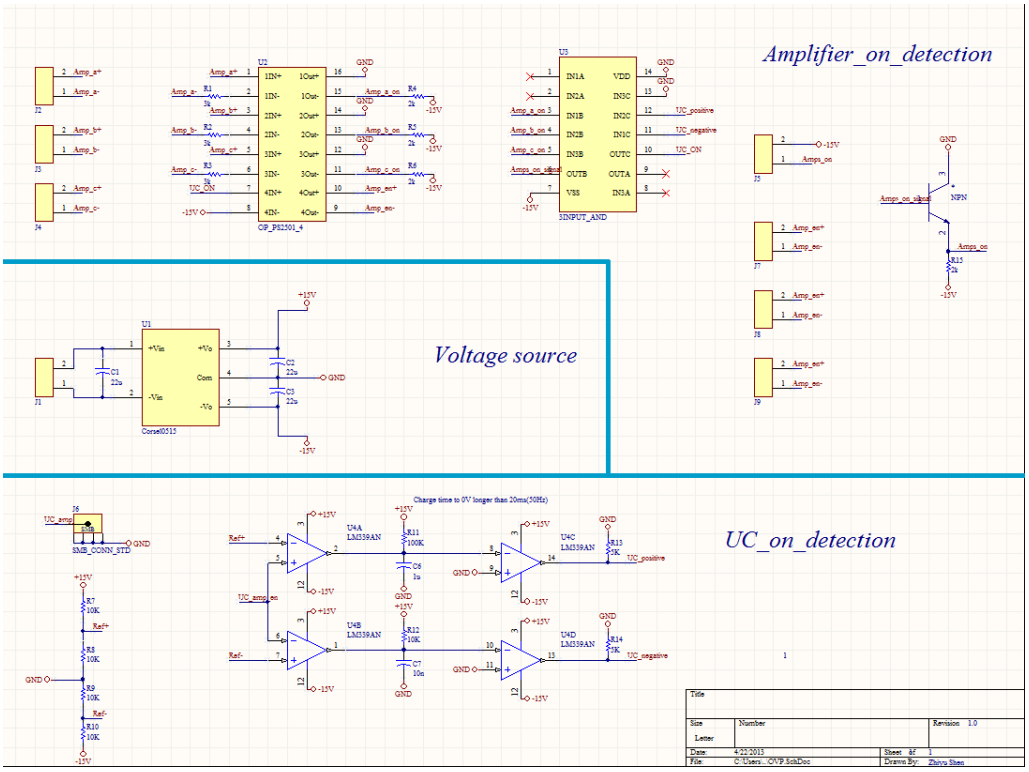

(b)

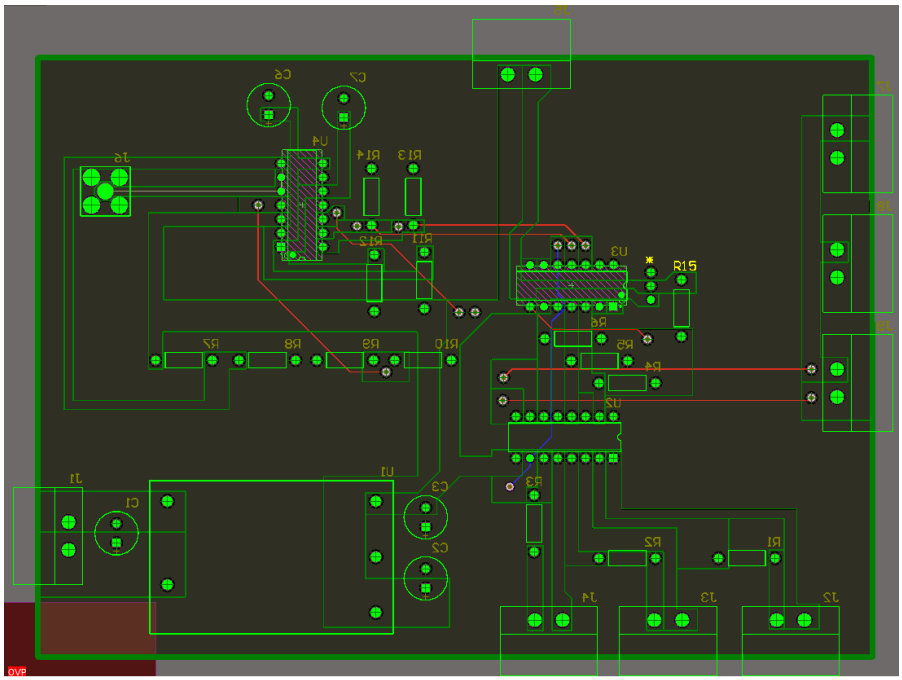

(c)

Fig_Apx. B-11 Power up sequence protection board

In the amplifier on detection, the 3 inputs are from the back panels of the 3 amplifiers. When the amplifier is on, the input will be 15V, otherwise the input is 0V. After an opto-coupler stage, the input signals are sent to an AND gate to get the output signal, which is the control signal for the relay.

In the UC on detection, the input is from the DA output of UC. When UC is outputting a sinusoidal signal, the amplifier enabling signal will be high and the amplifiers will be enabled.

B.4.3. Overvoltage protection

The overvoltage protection (OVP) is implemented with a circuit board, a solid state relay Crydom D53TP50D and varistors. The max turn-on time for the relay is 0.02ms. The varistor is ERZ-V20D101 from ZNR, rated at 100V, 50J.

The picture, the schematic and the PCB of the OVP board is shown in Fig_Apx. B-12.

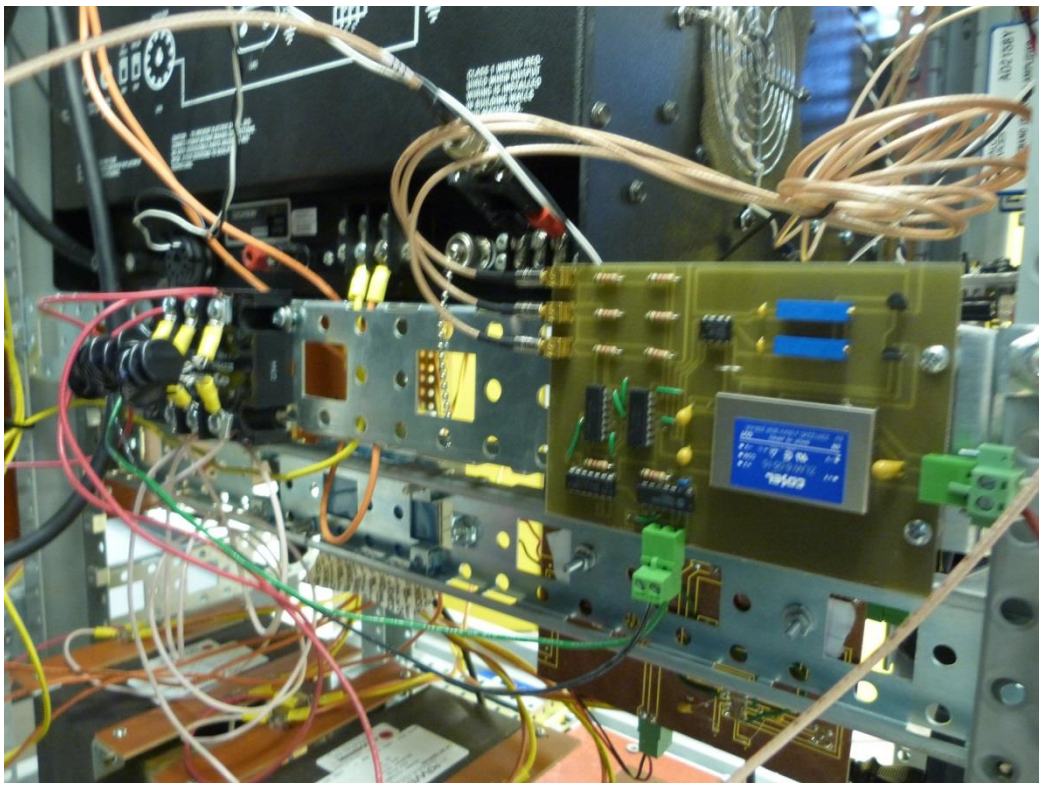

(a)

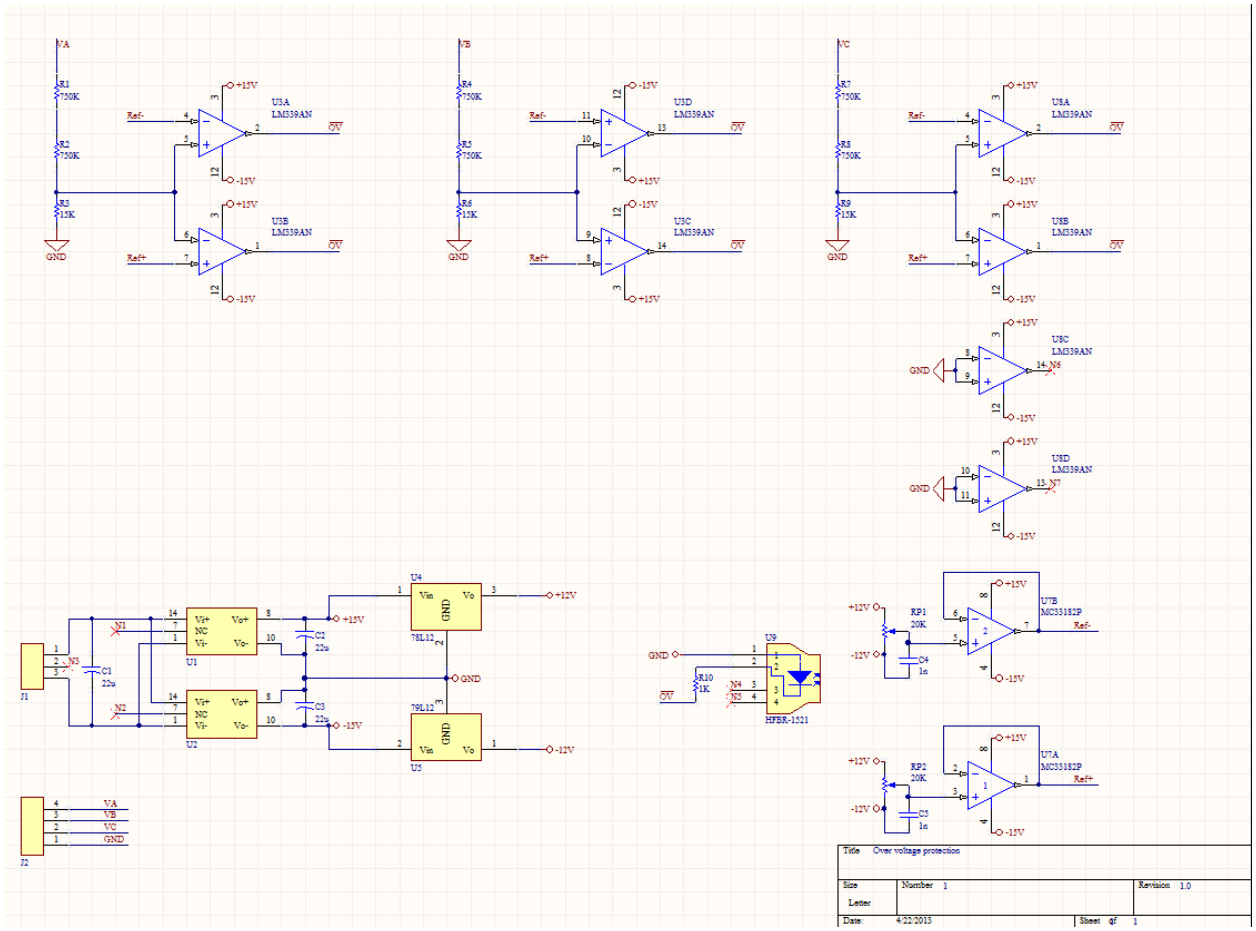

(b)

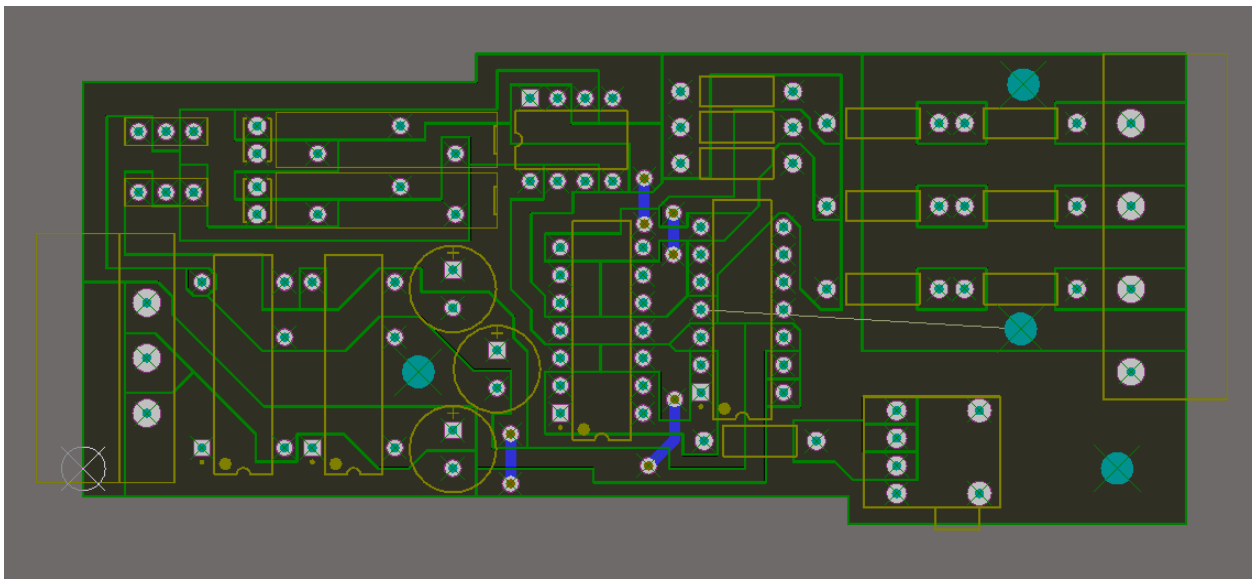

(c)

Fig_Apx. B-12 Over-voltage protection board

The inputs are three sensed voltages across the amplifiers. They are compared with upper limit and lower limit. If any of these voltage are over the limitation, the output signal with be high and the relay will be triggered and short the output of the amplifiers.

B.5. Operation procedure

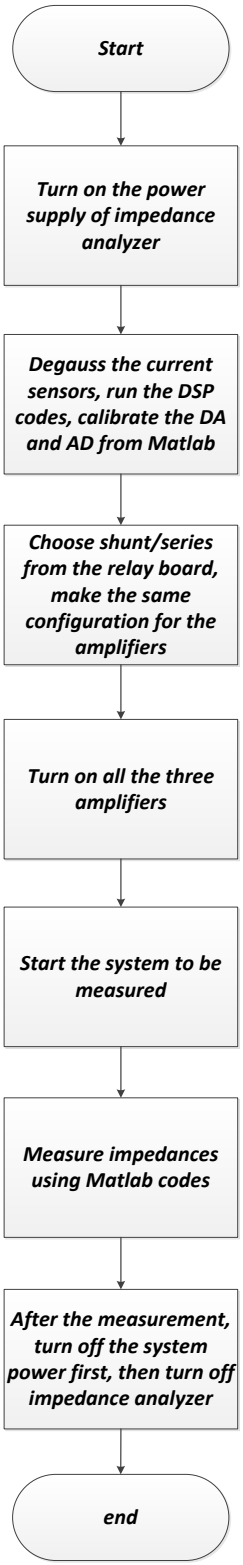

Fig_Apx. B-13 Flowchart for operation procedure

The correct operation procedure is shown in Fig_Apx. B-13. The impedance analyzer should always be turned on before the system is powered up, although there is power up sequence protection. After the measurement, the system should be shut down before the impedance analyzer is turned off.

B.6. Summary

In this appendix, guidance for the operation of impedance analyzer has been provided. The impedance analyzer is able to inject both shunt current perturbation and series voltage perturbation. The detailed implementation has been explained. The protection for impedance analyzer has been illustrated.

REFERENCES

[1] N. Sokal, "System oscillations from negative input resistance at power input port of switching-mode regulator, amplifier, dc/dc converter, or dc/ac inverter," in IEEE PESC '73, pp. 138-140.

[2] M. Belkhayat, R. Cooley, and E. H. Abed, "Stability and dynamics of power systems with regulated converters," *1995 Ieee International Symposium on Circuits and Systems, Vols 1-3*, pp. 143-145, 1995.

[3] M. Belkhayat, R. Cooley, and A. Witulski, "Large signal stability criteria for distributed systems with constant power loads," *Pesc 95 Record - 26th Annual Ieee Power Electronics Specialists Conference, Vols I and II*, pp. 1333-1338, 1995.

[4] M. Belkhayat, "Stability criteria for AC power systems with regulated loads," West Lafayette, IN: Purdue University, 1997.

[5] R.D. Middlebrook, "Input filter considerations in design and application of switching regulators," in IEEE IAS '76, pp. 366-382.

[6] R.D. Middlebrook, "Design Techniques for Preventing Input-Filter Oscillations in Switched-Mode Regulators", *Proceedings of PowerCon 5, the Fifth National Solid State Power Conversion Conference*, May 1978.

[7] Jang, Yungtaek, and Robert E. Erickson, "Physical Origins of Input Filter Oscillations in Current Programmed Converters", IEEE Transactions on Power Electronics, Vol. 7, No. 4, October 1992, pp. 725-733.

[8] C. M.Wildrick, F. C. Lee, B. H. Cho, and B. Choi, "A method of definingthe load impedance specification for a stable distributed power system,"IEEE Trans. Power Electron., vol. 10, pp. 280–284, May 1995.

[9] X. Feng, Z. Ye, K. Xing, F. C. Lee, and D. Borojevic, "Individual loadimpedance specification for a stable DC distributed power system," in Proc. IEEE Applied Power Electronics Conf., 1999, pp. 923–929.

[10] A. G. J. MacFarlane, "The generalized Nyquist stability criterion and multivariable root loci," *International Journal of Control*, vol. 25, pp. 81–127, 1977.

[11] Mohamed Belkhayat, "Stability Criteria for AC power Systems with Regulated Loads", PhD Dissertation, Purdue University, 1997.

[12] R. Burgos, D. Boroyevich, F. Wang, K. Karimi, and G. Francis, “Ac stability of high power factor multi-pulse rectifiers,” in *Energy Conversion Congress and Exposition (ECCE), 2011 IEEE*, 2011, pp. 3758-3765.

[13] X. Feng and F. C. Lee, “On-line measurement on stability margin of DC distributed power system,” in Proc. IEEE Applied Power Electronics Conf., 2000, pp. 1190–1196.

[14] J. Liu, X. Feng, F. C. Lee, and D. Borojevich, “Stability margin monitoring for DC distributed power systems via current/voltage perturbation,” in Proc. IEEE Applied Power Electronics Conf., 2001, pp. 745–751.

[15] X. Feng, Z. Ye, C. Liu, R. Zhang, F. C. Lee, and D. Boroyevich, “Fault detection in DC distributed power systems based on impedance characteristics of modules,” in Conf. Rec. IEEE IAS Annu. Meeting, 2000, pp. 2455–2462.

[16] G. Francis, “An Algorithm and System for Measuring Impedance in *d-q* Coordinates,” Virginia Tech, Blacksburg, 2010.

[17] J. Huang, K. A. Corzine, and M. Belkhayat, "Small-Signal Impedance Measurement of Power-Electronics-Based AC Power Systems Using Line-to-Line Current Injection," *IEEE Transactions on Power Electronics*, vol. 24, pp. 445-455, Jan-Feb 2009.

[18] Y. L. Familiant, K. A. Corzine, J. Huang, and M. Belkhayat, "AC Impedance Measurement Techniques," in *Electric Machines and Drives, 2005 IEEE International Conference on*, 2005, pp. 1850-1857.

[19] V. Valdivia, A. Lazaro, A. Barrado, P. Zumel, C. Fernandez, and M. Sanz, “Black-box modeling of three phase voltage source inverters based on transient response analysis,” *Applied Power Electronics Conference and Exposition (APEC), 2010 Twenty-Fifth Annual IEEE*, 2010, pp. 1279-1286.

[20] V. Valdivia, A. Lázaro, A. Barrado, P. Zumel, C. Fernández, and M. Sanz, “Impedance Identification Procedure of Three-Phase Balanced Voltage Source Inverters Based on Transient Response Measurements,” *Power Electronics, IEEE Transactions on*, vol. 26, no. 12, pp. 3810-3816, 2011.

[21] SABER: *www.synopsys.com/saber*

[22] PSIM: *http://www.powersimtech.com/*

[23] PLECS: *http://www.plexim.com/*

[24] Matlab: *http://www.mathworks.com/*

[25] SIMPLIS: *http://www.simplistechnologies.com*

[26] D'Antona, Gabriele, Ferrero, Alessandro, “Digital signal processing for measurement systems: theory and applications”, Springerlink.

[27] C. Fernandez, A. Fernandez-Herrero, P. Zumel, A. Lazaro, A. Barrado, “Measuring bode plots of switching power converters from a single simulation in the time domain: Application to a digital control implemented on an FPGA,” in Control and Modeling for Power Electronics (Compel), 2010, pp. 1-7.

[28] C. Fernandez, P. Zumel, A. Fernandez Herrero, M. Sanz, A. Lazaro, A. Barrado, “Frequency response of switching DC/DC converters from a single simulation in the time domain,” in proc of IEEE 2011 Applied Power Electronics Conference, 2011, pp. 1846-1851.

[29] S. Boyd, “Multitone signal with the low crest factor,” IEEE Transactions on Circuits and Systems, vol. 33, no. 10, pp. 1018-1022, Jan. 1986.

[30] M. Friese, “Multitone signals with low crest factor,” IEEE Transactions on Communications, 1997, vol. 45, no. 10, pp. 1338-1344, Oct. 1997.

[31] L. Hu, R. Yakamini, “Harmonic transfer through converters and HVDC links,” Power Electronics, IEEE Transactions on, vol. 7, pp. 514-525, 1992.

[32] W. Bo, D. Boroyevich, P. Mattavelli, S. Zhiyu, B. Rolando, “Experimental Verification of the Generalized Nyquist Stability Criterion for Balanced Three-phase Ac Systems in the Presence of Constant Power Loads”, in *Energy Conversion Congress and Exposition (ECCE), 2012 IEEE,* 2012, pp. 3926-3933.

[33] G. Grandi, J. Loncarski, “Analysis of Dead-Time Effects in Multiphase Voltage Source Inverters,” proc. of 6th IET Conf. on Power Electronics, Machines and Drives, PEMD 2012, Bristol (UK), march 27-29, 2012

[34] G. Grandi, J. Loncarski, “Space Vector Analysis of Dead-Time Voltage Distortion in Multi-phase Inverters”, accepted for EPEPEMC, ECCE Europe Conference, Novi Sad (RS), Sept. 4-6, 2012.

[35] R. Burgos, et. al, "Modeling Considerations and Stability Analysis of Aerospace Power Systems with Hybrid AC/DC Distribution," in SAE Power Systems Conference, 2006

[36] L. Harnefors, M. Bongiorno, and S. Lundberg, “Stability analysis of converter-grid interaction using the converter input admittance,” in Power Electronics and Applications, 2007 European Conference on, 2007, pp. 1-10.

[37] R. Burgos, D. Boroyevich, F. Wang, K. Karimi, and G. Francis, “On the Ac stability of high power factor three-phase rectifiers,” in *Energy Conversion Congress and Exposition (ECCE),* 2010 IEEE, 2010, pp. 2047-2054.

[38] G. Francis, R. Burgos, D. Boroyevich, F. Wang, and K. Karimi, “An algorithm and implementation system for measuring impedance in the D-Q domain,” in *Energy Conversion Congress and Exposition (ECCE),* 2011, pp. 3221-3228.

[39] Jian Sun and K. J. Karimi, “Small-signal input impedance modeling of line-frequency rectifiers,” *Aerospace and Electronic Systems, IEEE Transactions on*, vol. 44, no. 4, pp. 1489-1497, 2008.

[40] Zhonghui Bing, K. J. Karimi, and Jian Sun, “Input Impedance Modeling and Analysis of Line-Commutated Rectifiers,” Power Electronics, IEEE Transactions on, vol. 24, no. 10, pp. 2338-2346, 2009.

[41] Justin S. Walraven, “Design of an Arbitrary Waveform Generator for Power System Perturbation,” Virginia Tech, Blacksburg, 2011.